SURFACE MODIFICATION OF NANOPARTICLES FOR BIOLOGICAL APPLICATIONS

THESIS SUBMITTED TO

THE UNIVERSITY OF PUNE

FOR THE DEGREE OF

DOCTOR OF PHILOSOPHY

IN

CHEMISTRY

BY

HRUSHIKESH M. JOSHI

PHYSICAL CHEMISTRY DIVISION
NATIONAL CHEMICAL LABORATORY
PUNE 411 008
INDIA

OCTOBER 2006

Dedicated to my parents, teachers and those soldiers who gave their supreme sacrifice during the war and fight against terrorism

DECLARATION

I hereby declare that the work presented in the thesis entitled **"SURFACE MODIFICATION OF NANOPARTICLES FOR BIOLOGICAL APPLICATIONS"** submitted for the degree of Doctor of Philosophy in Chemistry to the University of Pune, has been carried out by me at the Physical Chemistry Division of National Chemical Laboratory, Pune under the supervision of Dr. Murali Sastry. Such material as has been obtained by other sources has been duly acknowledged in this thesis. The work is original and has not been submitted in part or full by me for any other degree or diploma to other University.

Date: Hrushikesh M Joshi

Place: Pune (Research Student)

CERTIFICATE

This is to certify that the work presented in the thesis entitled **"SURFACE MODIFICATION OF NANOPARTICLES FOR BIOLOGICAL APPLICATIONS"** by **HRUSHIKESH M. JOSHI**, for the degree of Doctor of Philosophy in Chemistry was carried out under my supervision at the Physical Chemistry Division of National Chemical Laboratory, Pune. Such material as has been obtained by other sources has been duly acknowledged in this thesis. To the best of my knowledge, the present work or any part thereof has not been submitted to any other University for the award of any other degree or diploma.

Date:

Place: Pune

Dr. Murali Sastry

(Research Guide)

Acknowledgements

During the last four years of doctoral work, I had very close interaction with many people without whom this work was impossible. It is a great pleasure for me to thank all of them for their guidance, patience, direct and indirect help.

I take this opportunity to express my deep sense of gratitude to my research guide, Dr. Murali Sastry for his constant support, guidance, fruitful discussions and encouragement during the course of my research work. I am greatly impressed by his passion, hard work, speed and discipline in research. His constant support was invaluable and helped me in the completion of this thesis.

I would like to express my sincere respect towards my Mother, Father, Uncle, Aunty, Brothers and Sister in law for their love, blessings, constant extraordinary moral support to me during the hard times in my research work.

My special thanks to Dr. Varsha Pokharkar, Poona College of Pharmacy, Bharati Vidyapith, Pune for her valuable guidance, technical support, and making all the facilities available for animal studies. I thank Dr. Kalpana Joshi from School of Health Sciences, University of Pune for useful discussions. I would like to thank Dr. K.N. Ganesh, Former Head of Organic Chemistry Division, National Chemical Laboratory for his valuable suggestions and making the ITC instrument available. It gives me great pleasure to thank Dr. S.D. Prasad, Physical Chemistry Division, National Chemical Laboratory for his suggestions, discussions, guidance and helping me in analyzing the ITC data.

I would like to acknowledge Dr. Pravin Shirude, Ms. Devika Bhumkar and Dr. Rajendra Srivastava, without whom this work would not have been possible.

I express my gratitude towards Mrs. Suguna Adyanthaya for her constant help and for TGA measurements of the samples. I wish to give special thanks to Mrs. Renu Pasricha for her support, valuable help and making TEM facility available for nanoparticles characterization. Dr. Patil and Dr. Mandale are greatly acknowledged for their help in XPS measurements.

I would like to take this opportunity to thank Dr. Absar Ahmad, Dr. Asmita Prabhune, Dr. Pundle, Dr. M.I. Khan, Dr. Bhonde, Dr. Ashish Lele, Dr. Satish Ogale, Dr. B.L.V. Prasad and Dr. Pankaj Poddar for their direct / indirect help and making available characterization facilities.

I am thankful to Dr. Sourav Pal, Head of Physical Chemistry Division for his moral support, help and allowing me to work in Physical Chemistry Division, National Chemical Laboratory.

I wish to thank Dr. S.K. Date, Dr. S.R. Sainkar, former Heads and Dr. Mohan Bhadbhade, present Head of Center for Material Characterization, for allowing me to work in CMC and making special instruments available for characterization.

I am grateful to Dr. S. Sivaram, Director, National Chemical Laboratory for giving me opportunity to work in NCL and making most of the facilities available for research work.

I would like to extend my sincere gratitude to my senior colleagues Dr. Ashavani Kumar, Dr. Saikat Mandal, Dr. Sumant Phadtare, Dr. Debabrat Rautray Dr. Anita Swami, Dr. Sushma Pethkar, Dr. P. Madhu Kumar, Mr. PR. Selvakannan, Mr. S. Shiv Shankar for their valuable help as well as time to time discussions.

I would like to take this opportunity to acknowledge Ambarish, Akhilesh, Tanushree, Manasi, Amit, Atul, Sourabh, Vipul, Prathap, Sanjay, Deepti, Ritwik, Minakshi, Sujatha, Ravi, Ruchi, Dr. P. Senthil Kumar, Virginia, Umesh, Sudrsan, Priyanka, Rammya, Imran, Anil, Boishakhi, Dr. Bapurao, Anuja, Sheetal, Sayan Dev, Gayatri, Raghini, Anie, Milind, Ajay, Amol, Chinmay, Sushrut, Amar, Abhirup, Avisek, , Tushar, Vivek, Mugdha, Avinash, and Dr. Ankamwar for company, help and discussions. Very special thanks to all my labmates who helped me to complete this thesis.

I would like to express my appreciation to my friends Pankaj, Paresh, Amit, Yogesh, Ashish, Shoukat, Rameshwar, Sanket, Mandar, Bhagyashree, Girish, Shekhar, Deepali, Rohit, Shankar, Dr. Kala, Gouri Shankar, Shailesh, Vinod, Arohi, Anamika, Sachin, Induvadana, Nachiket, Subhendu, Prashant, Sasanka, Niranjan, and Deepak Jori for their company.

The co-operation I received from other faculty members and support staff of Physical Chemistry Division is gratefully acknowledged. I would like to acknowledge the library staff and administrative and security staff of NCL for their timely help.

My thanks are duly acknowledged to Department of Science and Technology, Government of India for financial assistance.

Hrushikesh M. Joshi
Pune, India

Contents

Declaration

Certificate

Acknowledgements i

List of abbreviations vii

Chapter 1: Introduction

1.1 Introduction 2
1.2 Different methods for synthesis of nanoparticles 4
1.3 Properties of nanomaterials 6
1.4 Surface modification of nanoparticles 10
1.5 Applications of nanoparticles 16
1.6 Objective and outline of the thesis 21
References 22

Chapter 2: Characterization techniques

2.1 Introduction 39
2.2 UV- Visible absorption spectroscopy 39
2.3 Fourier transform infrared spectroscopy 40
2.4 X-ray photoelectron spectroscopy 44
2.5 Isothermal titrations calorimetry 46
2.6 Inductive coupled plasmon spectrometry 49
2.7 Transmission electron microscopy 51
2.8 Thermo gravimetric analysis 52
2.9 Electrophoresis 53
References 54

Chapter 3: The energetics of the binding of amino acids to gold nanoparticles

3.1	Introduction	58
3.2	Synthesis of amino acid-capped gold nanoparticles	59
3.3	UV-Visible spectroscopic analysis	60
3.4	Transmission electron microscopic analysis	61
3.5	Isothermal titration calorimetric analysis	62
3.6	X-ray photoelectron spectroscopy measurements and analysis	66
3.7	Electrophoresis measurements	69
3.8	Thermo gravimetric analysis	71
3.9	The integral heat mode of isothermal titration calorimetry	73
3.10	Conclusion	87
	References	88

Chapter 4: Gold nanoparticles for efficient transmucosal insulin delivery

4.1	Introduction	94
4.2	Synthesis and surface modification of nanoparticles	98
4.3	UV-visible spectroscopy measurements	99
4.4	Fourier transform infrared spectroscopy measurements and analysis	100
4.5	Transmission electron microscopy measurements	102
4.6	In-vivo insulin delivery studies	103
4.7	Inductively coupled plasmon measurements and insulin levels in the blood	109
4.8	Conclusion	111
	References	111

Chapter 5: Phase transfer of platinum nanoparticles from aqueous to organic medium and its catalytic applications

5.1 Introduction 118
5.2 Phase transfer of platinum nanoparticles from aqueous phase to organic phase 120
5.3 Thermo gravimetric studies 121
5.4 Fourier transform infrared spectroscopy studies 123
5.5 X-ray photoelectron spectroscopy studies 124
5.6 Catalytic activity studies 126
5.7 Transmission electron microscopy studies 127
5.8 Conclusion 129
References 130

Chapter 6: Conclusion

6.1 Summery of the work 135
6.2 Scope of the future work 135

List of Publications

List of Abbreviations

ODA……Octadecylamine

TEM …….Transmission Electron Microscopy

FTIR ……...Fourier Transform Infrared Spectroscopy

DRS……..……Diffuse reflectance mode

HATR ……..Horizontally attenuated total reflectance mode

ITC…….. Isothermal Titration Calorimetry

UV-Vis ……...….Ultra violate-Visible

XPS…….. X-ray Photoelectron Spectroscopy

TGA ……..Thermo Gravimetric Analysis

ICP…… …….Inductive Coupled plasmon Spectrometry

GOD…….. Glucose Oxidase

POD…….Peroxidase

CHAPTER I

Introduction

This chapter emphasizes importance of surface modification of nanoparticles and its applications. The different protocols used for synthesis of nanoparticles and properties of nanomaterials have been discussed. This chapter also describes the various protocols used for surface modification of nanoparticles and its advantages for various practical applications. Comparison has been made between inorganic nanoparticles with other drug carriers. Catalytic applications of nanoparticles are also described.

1.1 *Introduction*

Nanoscience and nanotechnology deal with the manipulation of materials at a nanoscale. It is an interdisciplinary field of science, where concepts derived from physics, chemistry, biology and engineering are used to synthesize nanomaterials for different applications. At nanoscale dimensions, inorganic and organic components exhibit unique physical and chemical properties which can be useful for a wide range of practical applications in conventional and prospective fields which would have direct and indirect impact on the life style of human beings [1].

One nanometer is a billionth part of meter i.e. 10^{-9}m. Materials having at least one dimension in the range between 1 to 100 nm, show unusual properties when compared with bulk counterparts. Nanometer scale is a size range of matter where transition of properties takes place from atomic level to bulk level. The small size of nanomaterials provides huge surface area which enables more functionality with improved performance in the given space [2]. The change in the properties is due to the increased surface to volume ratio which in turn dictates the surface properties and interactions [3]. Fundamental properties of nanomaterials such as electrical and thermal conductivity, band gap, density of states, electron affinity, mechanical, magnetic and optical properties etc. are a strong function of size and shape of the particles for a given composition of the nanomaterial [3]. Nanomaterials have applications in catalysis [4-6], medicine [7], sensors [8], information storage devices [9], optoelectronic devices [10], textiles [11], food technology [12] etc.

Synthesis and surface modification of nanoparticles for specific application constitutes an important branch of nanoscience and nanotechnology. Top-down [13] and bottom-up [14-16] approaches are widely used for the synthesis and surface manipulations of nanoparticles. As shown in Fig. 1.1, the top-down approach, bulk materials are physically or chemically sliced till a desired size is acquired. Below certain size range, synthesis of nanoparticles by the top-down approach becomes costly and laborious. This approach can also produce surface defects, internal stresses and

contamination due to harsh conditions at the time of synthesis of nanoparticles [2], which may affect surface and physical properties of the nanomaterials. Therefore, top-down approach reaches its practical and theoretical limits resulting from the above mentioned disadvantages.

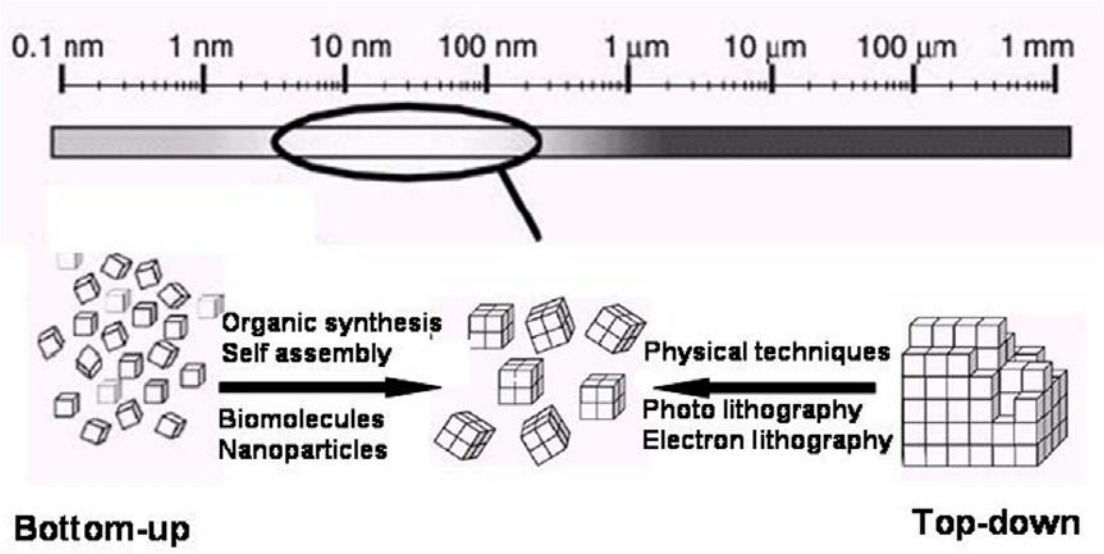

Figure 1.1: *Different approaches to achieve desired size and shape of nanomaterials [17, 18].*

On the other hand, the bottom-up approach has been used to synthesize nano or micro sized materials by assembling atoms or molecules on molecular or supramolecular templates. Though different micelles structures are commonly used as templates, biomolecules such as proteins [19] and nucleic acids [20] are also receiving great interest as templates due to their functionality. These templates can be controlled through their specific recognition, conformation, and configuration to generate self assembled structures. This can be achieved by using different biomolecular interactions ranging from van der Waals forces to hydrogen bonding. These forces allow two-and three-dimensional nanostructured architectures [19, 20]. Biomolecules can be easily attached to metal nanoparticles. These hybrid materials can act as basic building blocks for construction of nano and micro devices. The bottom-up approach permits better chance to synthesize nanomaterials with less defects, more homogeneous chemical composition and better short and long range ordering. The bottom up approach is

mainly driven by reduction in Gibbs free energy and hence materials synthesized by this approach are closer to thermodynamic equilibrium state [2]. This thesis describes the study of surface modification of metal nanoparticles and their applications in drug delivery systems and catalysis. The following sections concentrate on different types of synthesis of nanoparticles, their properties, stability and methods of surface modification. It also includes various methods of drug delivery and nano catalysis.

1.2 Different methods for synthesis of nanoparticles

Metal nanoparticles can be synthesized in many ways. Important criteria for the synthesis of nanoparticles are control over size, shape, surface functionalities and various properties of nanoparticles. However choice of method is mainly selected from the application point of view. The methods for nanoparticle synthesis are mainly divided in three different types.

1.2.1 Physical methods

Different physical methods are used for synthesis of nanoparticles. In evaporation methods such as physical vapor deposition (PVD) [21], nanometer thicknesses of metal films are produced by heating metal in an electrical heating boat under high vacuum. In chemical vapor deposition (CVD) [22], where carrier gasses containing the elements of desired compound are passed over appropriately heated surfaces resulting in decomposition of carrier gas causing the deposition of atoms/ molecules on the surface. Solvated metal atom deposition (SMAD) [23] involves heating of bulk metal till it starts evaporating under vacuum and co-condensation of its vapors with solvents to form nanoparticles in solution. In the laser ablation method [24-26], intense laser pulses are focused on metal targets immersed in solvent containing surfactant. Due to high temperature resulting from intense laser pulses, metal atoms are vaporized and solvated by surfactant molecules to form nanoparticles in solution. In the sonochemical method, gas bubbles in given liquid medium are forced to oscillate in the presence of acoustic field caused by ultrasonic waves. It leads to growth and collapsing of bubbles followed by generation of micro streaming in the liquid, thereby

generating mass transport within same medium. Collapsing of bubbles results in high temperature thus causing local heating. Due to extreme conditions, solvent and solute molecules decompose into reactive radicals. In aqueous systems, radicals generated by ultra sonication have been used for reduction of metal ions to synthesize nanoparticles in bulk medium [27, 28]. In radiolytic methods, solvated electrons or free radicals produced by radiolysis are used to reduce metal ions in the presence of donor ligands to synthesize nanoparticles [29]. However cost of production and hence scaling up of nanoparticles in larger quantities are major drawbacks of the physical routes.

1.2.2 Chemical methods

Chemical route of synthesis is the most popular and easy route to synthesize nanoparticles. In this route, metal precursors are reduced by suitable reducing agents such as citrate reduction [30], sodium borohydride [31], trisodium citrate [32], amino acids [33, 34], etc. Temperature, concentration of precursor and reducing agents may affect the size and shape of the nanoparticles [35]. Easy manipulation in chemical reactivities of reactants, better control over reaction conditions during synthesis of nanoparticles, and ease in surface functionalization of nanoparticles are the most attractive features of this route. It allows synthesis of nanoparticles in different solvent mediums; for example, synthesis of nanoparticles in aqueous medium [31-34.], organic medium [36], ionic liquids [37] and in supercritical fluids [38]. This particular feature is important with respect to the use of nanoparticles in different applications, which are mainly dependent on the use of medium or solvent; for example, catalysis in aqueous as well as organic medium and biological applications in aqueous medium etc. Chemical route also facilitates freedom to synthesize and assemble nanoparticles at various interfaces such as at air-water interfaces [39] and liquid-liquid [40] interfaces with the help of different chemical functionalities, which allow reduction and controlled growth of nanoparticles and facilitates 2-D arrangement of nanoparticles. Since the chemical route can be used to synthesize nanoparticles with minimum resources and with easy control on their shape and size of the nanoparticles, this route can be used to produce nanoparticles in larger quantities for various industrial applications.

1.2.3 Biological methods

Biological route for synthesis of nanoparticles involves direct synthesis by living cells, biomolecules such as enzymes and biological templates. It uses micro-organisms such as fungi and bacteria for the synthesis of nanoparticles [41- 44]. Heavy metal ions are toxic to biological systems; micro organisms detoxify these ions by reducing them into metal atom [43, 44]. During this process, formation of nanoparticles takes place and these nanoparticles are stabilized by biomolecules. Medicinal plant extracts are also used as reducing agents for synthesis of nanoparticles. Recently, Sastry and co-workers showed efficient way of synthesis of gold nanoparticles with better control on size and morphology with help of medicinal plant extracts [45-47].

In this thesis, the chemical reduction method is used to synthesize metal nanoparticles since they are comparatively easy, economical and less time consuming than the other methods.

1.3 Properties of nanomaterials

1.3.1 Optical properties

Figure 1.2: *Size dependent optical properties of gold nanoparticles [48].*

Metal nanoparticles show different optical properties from their bulk form (Fig. 1.2) [49]. These properties are dependent on composition, size, shape and surrounding medium of the nanoparticles [50]. It varies from visible region to NIR region depending on the size and shape of the nanoparticles [51]. This effect appears due to interaction of electromagnetic radiation with the electron cloud present on the surface of metal

nanoparticles. Gold, silver and copper nanoparticles are known to exhibit unique optical properties in visible and in NIR region within certain size limit of particles [49].

1.3.1A) Surface plasmon resonance

Large number of atoms present on the surface of nanoparticles contributes electron cloud on the surface of nanoparticles. As shown in the Fig. 1.3, the movement of these free electrons under the influence of the electric field vector of the incoming light leads to a dipole excitation across the particle. This induces positive polarization charge on cationic lattice. This charge acts as a restoring force, and brings back electron cloud to its original position, thus causing the oscillations of the electron cloud.

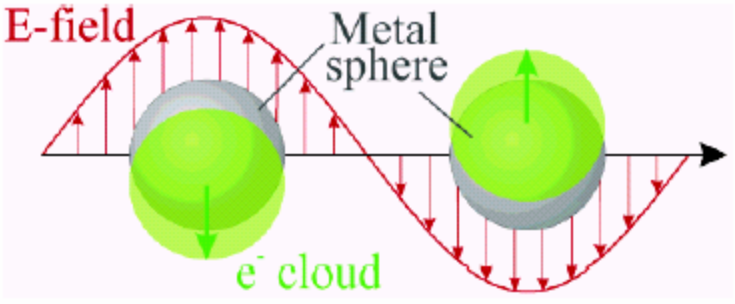

Figure 1.3: *Schematic of plasmon oscillation for a sphere, showing the displacement of the conduction electron charge cloud relative to the nuclei [49].*

Thus, the electron density within a surface layer, the thickness of which is about equal to the screening length of a few angstroms, oscillate, whereas the density in the interior of the particle remains constant. This phenomenon is called surface plasmon resonance, and has been explained by Mie in 1908, based on the Maxwell's equation of scattering [52]. The absorption spectrum of particles in a given solvent can be calculated from optical constants of the bulk metal. The absorption spectrum of spherical particles of sizes between 3 to 20 nm does not strongly depend on particle size. This is because the particles are below the size at which higher order term in the Mie formulae for the absorption constant becomes significant. Thus, one has to regard only the dipole term, which depends only on the total metal concentration in the solution and not on particle size. The absorption coefficient α is calculated from equation given below

$$\alpha = \frac{18\pi}{\ln 10}\frac{10^5}{\lambda}\frac{Mn_0^3}{\rho}\frac{\varepsilon_2}{(\varepsilon_1 + 2n_0^2) + \varepsilon_2^2} \quad \text{.....(1.1)}$$

where, λ is the wavelength of light in nanometers, M and ρ are the molecular weight and density of the metal, n_o is the refractive index of the solvent and ε_1 and ε_2 are the real and imaginary parts of the dielectric constant of the metal. When the size of the particles becomes smaller than the mean free path of the electrons, the absorption bands are broadened; this is accounted for by using size-corrected values of ε_2. [49, 53]

$$\varepsilon_2 = \varepsilon_{2(bulk)} + \left(\frac{\omega_p^2}{\omega^2}\right)\left(\frac{V_F}{R}\right) \quad \text{..... .....(1.2)}$$

where, ω is the light frequency, ω_p the plasmon frequency, v_F the electron velocity at the Fermi level and R the particle radius (R/v_F, mean time of the free movement of the electrons). From the equation 1.1, resonance with the incident light reaches at the wavelength where the negative value of ε_1 of the metal is equal to twice the dielectric constant of the medium. In other words, any changes in the electron density near surface of nanoparticles will lead to changes in the plasmon absorption. This surface sensitivity of colloidal nanoparticles has been used to study adsorption/chemisorption of biomolecules etc.[36, 54-59]. Several applications are emerging based on the surface plasmon resonance properties of nanoparticles.

Applications based on optical properties in the visible region are receiving considerable scientific interest due to its promising technological development. In plasmonics, transfer of the electromagnetic energy from one place to another has been shown efficiently with the help of nanoparticles arrays. Nanoparticles arrays in these cases are used as wave guide [10].

Since the optical properties of metal nanoparticles are sensitive to surface modifications and environment around it, cross linking of antibody/ antigen/thiolated DNA functionalized silver / gold nanoparticles exhibit dramatic change in the optical

properties due to overlap of dipole resonance from neighboring nanoparticles. This forms the basis for colorimetric technique for following molecular recognition events [60]. On these guidelines, biotin-avidin molecular recognition was demonstrated [61], in which thiolated biotin modified gold nanoparticles were used for the avidin induced cross linking process. DNA tagged gold nanoparticles were studied extensively for DNA base pair sequence recognition and genetic disorder, which occurs primarily due to base imperfections in DNA molecule [60].

Due to the poor scattering cross section of the molecules, Raman scattering generally produces weak signals for analyte molecules. When the analyte is subjected to intensified electromagnetic fields generated by localized surface plasmon resonance of nanoscale roughness featured on silver, gold, or copper substrate, the magnitude of the induced dipole increases, and accordingly, the magnitude of intensity of the inelastic scattering increases with order of 10^{10}-10^{13}. This enhanced scattering process is known as Surface Enhanced Raman Scattering (SERS) [62]. Such large enhancement in the magnitude of scattering is able to detect even single molecule present on the surface of nanoparticles [63]. Due to extreme sensitivity of SERS, it has tremendous potential applications in biodiagnostics and in molecular detections [62].

1.3.2 Electronic properties

Metal nanoparticles show different electronic properties below certain size limit. There will be change in electronic distribution in metal which may transform some metal into semiconductor at nanometer scale. For example, gold nanoparticles act as quantum dot below certain size range [64]. Coulomb blockade is important and interesting effect that occurs when nanoparticles embedded between metal-insulator-metal junctions show charging of differential capacitance or charging at low temperature even at zero bias. This effect is a result of extremely small capacitance of the metal nanoparticles [65].

1.3.3 Melting point

Metal nanoparticles below 100 nm of size have low melting point than its bulk form. Number of surface atoms increases with decrease in the size of nanoparticles. Since it decreases the co-ordination number of atoms, atoms on the surface can be easily rearranged than those atoms present inside nanoparticles, thus melting process starts at lower temperature leading to decrease in melting point [66].

1.3.4 Magnetic properties

Ferromagnetic particles form single domains with large single magnetic moments at nanoscale. It changes magnetic properties drastically. Under thermodynamic equilibrium, magnetization behaviour of these nanoparticles is similar as that of atomic magnetization but with large magnetic moment. Below certain size, ferromagnetic particles become super-paramagnetic in nature [67]. These particles do not show hysteresis in magnetization, since there is only one domain per particle.

1.3.5 Mechanical properties

Mechanical strength of the material depends on several parameters such as impurities, dislocations etc. More defects in materials lead to less mechanical strength. Thus, due to small cross sections and less number of imperfections, nano materials such as nano wires and nano rods show enhanced mechanical strength. Since imperfections are thermodynamically more energetic, small size of nanomaterials eliminates imperfections in the crystal and acquires better mechanical strength [68].

1.4 Surface modification of nanoparticles

Surface modification of nanoparticles is a very important factor for stability and designed functionality. Atoms on the surfaces posses less co-ordination number than the bulk atoms. Thus, it experiences inward force and tries to achieve maximum co-ordination number. It results in smaller bond length with its immediate atomic layer than bulk atoms. As the nanoparticle size decreases, more and more atoms are exposed to surface, leading to decrease in the bond length with its next layer of atoms. Since at

such a small scale, large numbers of atoms are present on the surface, as a consequence of this, lattice parameters of nanoparticle changes [2]. Energy required to bring back these atoms to its original position is nothing but surface energy. As the particle size of the nanoparticles decreases their surface energy increases significantly. Increase in the surface energy also results into increase in Gibbs free energy. According to the laws of thermodynamics, every system always tries to attain minimum Gibbs free energy [69]. As a result of this thermodynamic property of matter, nanoparticles have a tendency of agglomeration to attain minimum Gibbs free energy, therefore it loses its "nanoness" and exotic properties related to it. Hence it is very important to stabilize the nanoparticles against aggregation. There are many ways by which nanoparticles can be stabilized.

1.4.1 Electrostatic stabilization

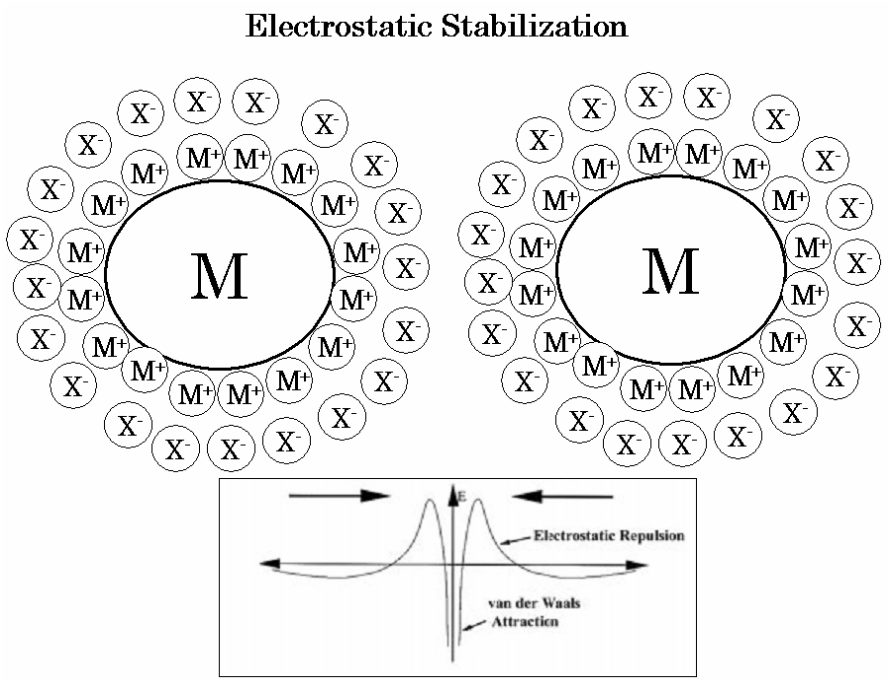

Figure 1.4: *Scheme illustrating the stabilization of metal nanoparticles by electrostatic interactions [70].*

During the synthesis of noble metal nanoparticles specifically, the particles formed are surrounded by electric double layer due to adsorption of reactant ions on the

surface of nanoparticles. Simultaneously, there are two forces acting on nanoparticles, 1) van der Waals force of attraction and, 2) electrostatic force of repulsion (potential energy) due to charged ions on the surface. Stability of nanoparticles is dependant on the combination of these two forces [70].

Fig. 1.4 shows the graph of potential energy versus distance between the nanoparticles. At far distance electrostatic repulsion and van der Waals force of attraction are zero. At zero distance, there is a deep minimum in the potential energy curve due to strong dominating van der Waals force of attraction. As nanoparticles go away from each other electrostatic force start dominating the force of attraction resulting in a maxima in the potential energy diagram. This maxima is the repulsion energy barrier between two nanoparticles. Potential barrier depends on the thickness of double layer formed around the nanoparticles. Greater the thickness of the double layer higher is the potential energy barrier. If this barrier is greater than a certain value, nanoparticle solution remains stable [2]. Electrostatic stabilization is kinetic stabilization process and it is useful only in the case of dilute solutions. Addition of electrolytes screens the double layer charge leading to aggregation. It is not applicable in the case of multiphase systems.

1.4.2 Stability of nanoparticles by capping agents

Capping of nanoparticles with suitable ligands can overcome the above-mentioned disadvantages. As mentioned earlier, lithographic technique can be used for the synthesis of two-as well as three-dimensional nanostructures. But these techniques have inherent limitation of two dimensionality of lithographic step. Surface modification of nanomaterials gives freedom of controlling the interactions around its surface, which can be used to build three dimensional structures. Capping agents also minimize surface energy of the nanoparticles and prevent uncontrolled growth of the nanoparticles.

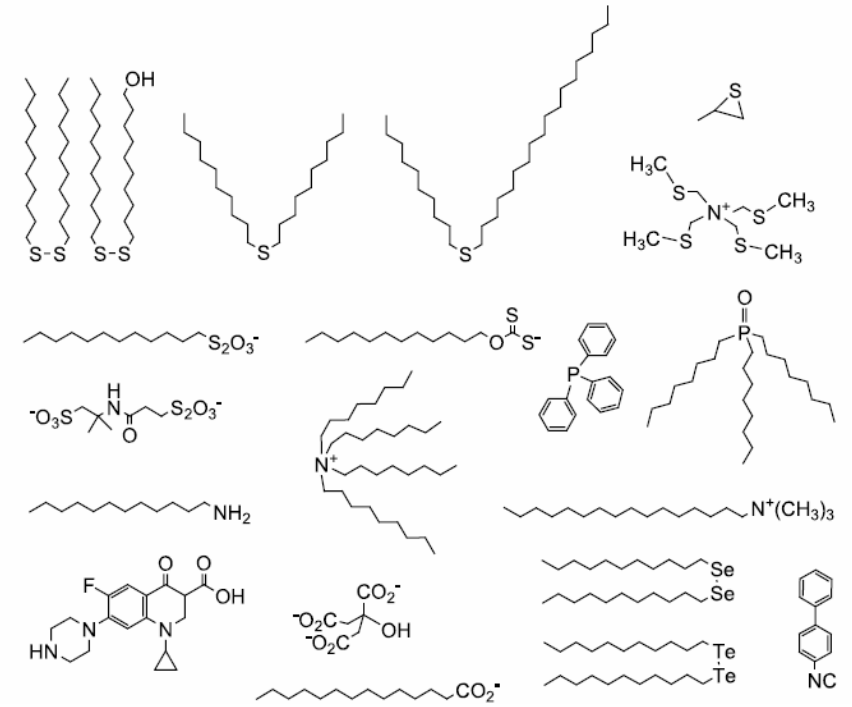

Figure 1.5: *Various organic compounds used for the protection of metal nanoparticles [69].*

As shown in Fig. 1.5, various electron rich ligands such as amines, thiols, phosphates, carboxylates have been used for capping of nanoparticles. Charge on the surface, reactivity, specificity, nature of the surface i.e. hydrophobicity can be easily induced in the nanoparticles with the help of different capping agents. Various strategies have been used to modify the surface of nanoparticles, for example, coupling of biomolecules like amino acids, enzymes, proteins and monolayer, mixed monolayer protection of molecules to metal clusters (MPC, MMPC) [71] etc.

In the case of nanoparticle dispersions in organic medium, where electrostatic effects are less significant, stability of the nanoparticles comes from steric interactions by physical or chemical adsorption of amphiphilic molecules (Fig 1.5). The head group of these molecules binds with metal nanoparticles surface while hydrocarbon chain prevent aggregation sterically as shown in Fig. 1.6. Due to these steric interactions, the nanoparticles are found to be stable in the form of powder even after complete evaporation of solvent.

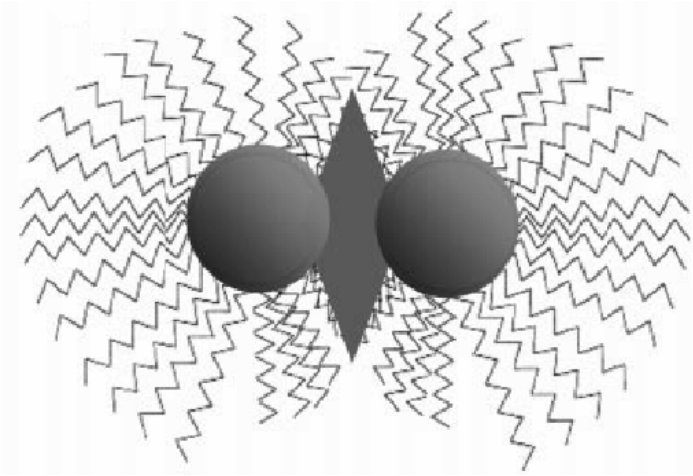

Figure 1.6: *Scheme illustrating the stabilization of nanoparticles by steric interactions [71].*

Biomolecules such as enzymes, proteins, oligonucleotides have been used to modify the surface of nanoparticles. The main idea behind coupling of large biomolecules with nanoparticles is to use their specificity and reactivity for different biological applications. In these cases, generally metal nanoparticles are reduced in the presence of labile stabilizing agent which can be easily exchanged with biomolecules. This method is used for surface modification of nanoparticles with different proteins, enzymes, thiolated DNA [72, 73]. When nanoparticles are stabilized with anionic ligands such as citrates, biomolecules often couple through electrostatic interactions. Electrostatic coupling is done through opposite charges on the nanoparticles and biomolecules [74, 75]. Another approach is the use of various capping agent such as thiols, phosphates containing ligands which have carboxyl, amino, or maleimide as terminal groups. These terminal groups can be used for coupling of nanoparticles with biomolecules by simple organic reactions such as carbodiimide mediated esterification, amidation or reactions with thiol groups [76, 77]. Such surface modification of nanoparticles can be utilized to make them more biocompatible and environment friendly.

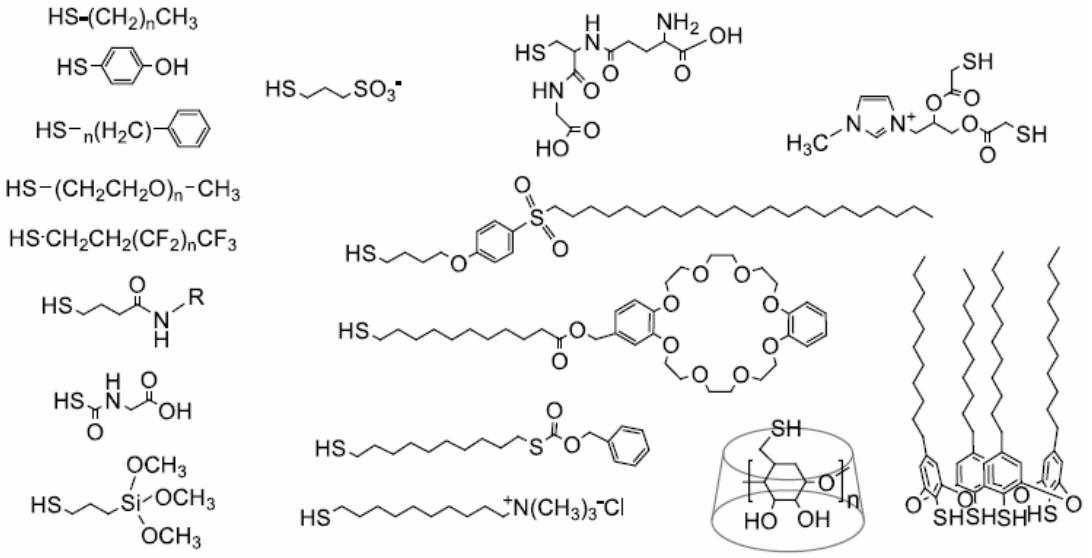

Figure 1.7: *Various thiols used for the generation of monolayer-protected gold nanoparticles [69].*

Monolayer and mixed monolayer of different molecules having different functionalities at both ends have been used to functionalize gold nanoparticles (Fig. 1.7). In these methods, reduction of metal ions by weak reducing agent, was performed in the presence of capping molecules. During the synthesis of the nanoparticles, size of nanoparticles depends on the stoichiometric ratio of metal ion to capping ligand concentration. It can be further modified by different functional molecules with the help of ligand exchange reactions [78]. Many times, surface modified nanoparticles may loose stability due to ionic strength of solution and strong intermolecular interactions between capping agents. To overcome this problem, new capping molecules with different amino acid sequences have been developed which mimic the principles of naturally existing non aggregating proteins [79]. These capping ligands readily attach to the surface and form well packed passivating surface with hydrophilic terminus, which makes it soluble and stable even in the presence of salt in aqueous phase. This ability to control properties of surfaces of nanoparticles can be used to assemble nanoparticles. Use of MPC and MMPC has been shown in various applications such as solution based sensors, electronic devices and drug delivery

systems. Surface modification has two advantages, it protects nanoparticles from agglomeration and provides various functionalities to nanoparticle surface [80].

Apart from these strategies, other capping agents have also been investigated such as, polymers [81] and silica [82]. However, from the above discussion, it is clear that surface modification with suitable ligands is preferable over electrostatic stabilization for following reasons,

1) It gives thermodynamic stability

2) It can be stored with high concentration without aggregation

3) It can be used in multiphase systems

4) It is not electrolyte sensitive [2]

1.5 Applications of nanoparticles

1.5.1 Nanoparticles as carrier for drug delivery

In last few decades different carriers have been developed to deliver biological molecules. Viral vectors [83], cationic lipids [84], and bio-degradable polymeric nanoparticles [85] are some such carriers.

Viral vectors such as adenovirus [86], retrovirus [87], and adeno associated viruses [88] have been mainly used because of their high efficiency in delivering biomolecules. In viral vectors, part of the original genes segment is replaced by required gene of interest and delivered. Though viral vectors can attain transfection efficiency of 80-90%, they induce inflammatory response, which can cause many side effects ranging from mild edema to multi system organ failure [89].

In order to overcome problems related to viral vector, non-viral vectors have been used for transfection of biological molecules. Carriers consisting of cationic compounds such as cationic lipids [90-92], cationic polysaccharides [93, 94] have been used in which positive charge of protonated amine group is utilized as driving force. Though efficiency of non viral vectors is about 40-50%, they are advantageous due to

low immune response that enables repeated administration and the capability of large production with acceptable cost. But toxicity is a major disadvantage of these non-viral vectors. It may cause toxic changes in the cell including shrinkage of cell, reduced number mitosis etc. Certain proteins in the body may also be affected because of cationic amphiphiles [95].

In parallel, due to advances in polymer science, there is considerable interest in developing polymeric nanoparticles as drug carriers. Polymeric nanoparticles are solid, colloidal particles consisting of macromolecular substances that vary in size from 10 nm to few hundred nanometers. In general practice, drug is dissolved, adsorbed, attached or encapsulated in the polymeric nanoparticles matrix. Depending on the method of preparation of nanoparticles, nanocapsules can be obtained with different properties and release characteristics for encapsulated therapeutic agents [96]. They can be used to provide targeted delivery of drugs, peptides, genes for intravascular delivery, and improve the stability of therapeutic agents like proteins, peptides and nucleic acids against enzymatic degradations. Small size of these particles allows crossing of barriers, ameliorates tissue tolerance and improves cellular uptake as well as transport. It enables efficient delivery of therapeutic agents to the target sites like liver, brain and solid tumors. It also permits drug accumulation at a target site. Due to flexibility in modifying the surface of polymeric nanoparticles, they have potential in tackling problems like low oral bioavailability and suboptimal therapeutic response associated with delivery of poorly water soluble drugs [96, 97]. In spite of this, polymeric nanoparticles can be toxic to biological systems due to the side products of these polymeric nanoparticles after degradation process in the body.

Technological advances in nanoscience offer synthesis of inorganic nanoparticles for drug delivery applications. There is much current interest in inorganic nanoparticles as carrier for delivery of DNA [98], proteins [99] etc. Many inorganic nanoparticles such as gold [100], calcium phosphate [101], silica nanoparticles [102] and iron oxide nanoparticles [103-105] have been studied in this respect. They show low toxicity and controlled release property and present a new class of carriers other

than viral, non-viral vectors or polymeric nanoparticles. They also offer rich functionality, biocompatibility, potential capability of targeted delivery and controlled release of carrier drugs [106].

In normal drug administration protocols, there is no specificity for drug molecules to recognize targeted cells upon administration, which decreases the effectiveness of drug molecules to large extent. In such cases, nanoparticles with certain functionalities can be used to increase the possibility to interact with targeted cells. For example, in drug-positively charged nanoparticles formulations, positive charge of the nanoparticles can be used as driving force to approach negatively charged cellular membrane via electrostatic complexation [107]. Targeted delivery of drug-nanoparticles formulation can be made possible by attaching it to site specific antibodies. Many groups have already shown the use gold particles for DNA transfection [108]. Gadolinium is known for its high neutron capture cross section and photon emission. Oyewumi et al. demonstrated recognition, internalization and retention of surface modified gadolinium nanoparticles in tumor cells, indicating potential for enhancing the efficiency in tumor destruction by neutron capture therapy [109-111]. Bimetallic nanoparticles have also been investigated for internalization of the molecules into the cell [112].

Similarly, oxide nanoparticles have been used for different therapeutic applications due to their versatile physicochemical properties, facile surface functionalization, low cost and biocompatibility. Kneuer et al. demonstrated successful cellular uptake of SiO_2-DNA by COS-1 cells [113].

Iron oxide nanoparticles have also been investigated for their low toxicity and superparamagnetic nature [114]. Superparamagnetic nature of magnetite nanoparticle has been used to concentrate drug-nanoparticles formulations at specific target site by external magnetic field. Magnetite nanoparticles are also used for hyperthermia of cancer [114]. Thus, inorganic nanoparticles are gaining considerable importance for drug delivery and therapeutic applications. Gold nanoparticles as carrier for biological

molecules have been discussed in chapter 4. In chapter 4, we have demonstrated, gold nanoparticles as efficient carrier for transmucosal insulin delivery.

1.5.2 Nanocatalysis

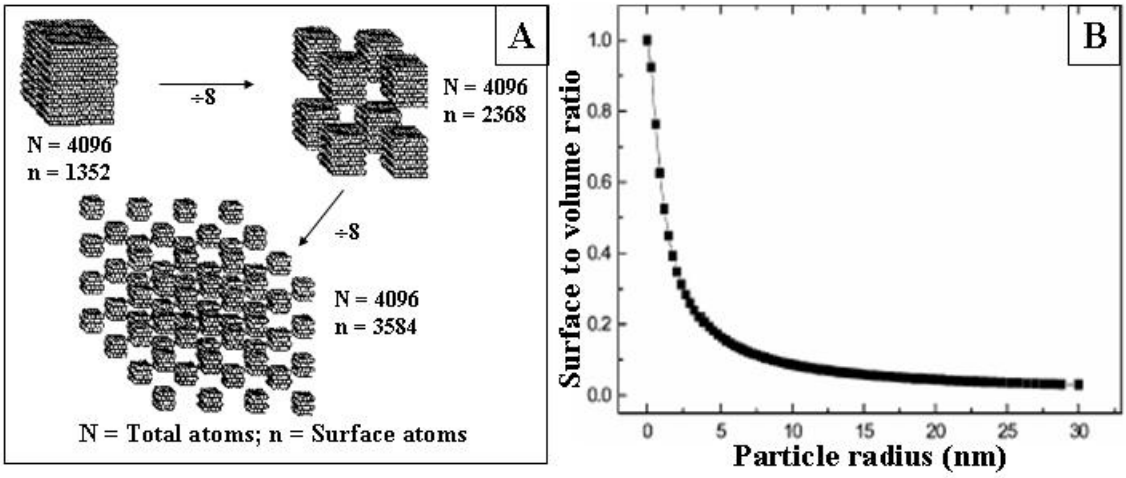

Figure 1.8: *Decrease in the particle size leads to increase in surface to volume ratio of the nanoparticles [50,116].*

As shown in Fig. 1.8, because of the smaller size of nanoparticles, large numbers of atoms are available on the surface. It also provides huge surface area to catalyze chemical reaction. Particles in the nanometer range make surface to reactant interaction stoichiometric because of the large number of atoms offered by nanoparticles, which allows excellent atom economy in surface-gas, surface-liquid, surface-solid reactions and also enhanced intrinsic chemical reactivity as size get smaller [115]. This makes nanoparticles highly attractive candidate for catalytic reactions. As the particle size gets smaller and smaller, anion / cation vacancies become prevalent. Different sizes of metallic nanoparticles exhibit different catalytic activities. This is mainly due to electronic effects, support effect and shape effects. Electronic effect affects the reactivity because of change in the electron density with respect to size of nanoparticles. Small size of nanoparticles makes it possible to use nanoparticles in homogenous as well as heterogeneous catalysis.

Many metals show excellent catalytic activity at nanoscale; for example, gold in bulk phase does not exhibit any catalytic properties but gold nanoparticles can be excellent low temperature catalysts. In homogeneous catalysis, many types of chemical reactions have been catalyzed using transition metal nanoparticles, which include cross coupling, electron transfer, hydrogenation and oxidations reactions. In the case of cross coupling reactions, Heck and Suzuki cross coupling reactions has been catalyzed with the help of palladium, copper and ruthenium nanoparticles [117-121]. In electron transfer reactions, platinum nanoparticles were used to catalyze the reactions [122]. Catalytic activity as function of shape and size of the platinum nanoparticles has been also studied in the case of electron transfer reactions [123-125]. In hydrogenation reactions, platinum, rhodium, iridium, and palladium nanoparticles demonstrated excellent catalytic activity [126-130], while silver nanoparticles have been reported to catalyze oxidation reactions [131, 132]. In the case of heterogeneous catalysis, generally metal nanoparticles are supported on substrates to catalyze the reaction. Catalytic activity of metal nanoparticles changes when it is bound to metal oxide surface [133]. This is because the electron density of metal particles changes when it is supported on metal oxides (Lewis acids or bases). Oxides such as alumina, titania and silica have been extensively used to support metal nanoparticles [133-135]. Heterogeneous catalysis supports various chemical reactions same as in the case of homogenous catalysis which includes oxidation and hydrogenation reactions [136-139]. Heterogeneous catalysis is also used in fuel cells, reduction and decomposition reactions. In fuel cells, metal nanoparticles supported on carbon are used to catalyze the oxidation reaction of methanol [140,141]. Alumina supported platinum has been used for NO reduction reaction [142]. Palladium supported on oxidized diamond and on titania has been used as catalyst to decompose methane, formic acid respectively [143, 144]. In this thesis, simple process has been developed in which platinum nanoparticles were synthesized in aqueous phase and transferred in organic phase. Resulting hydrophobized nanoparticles show excellent catalytic activity for hydrogenation reactions.

1.6 Objective and outline of the thesis

The main objective of this thesis is to understand the interaction of metallic nanoparticles with amine group containing ligands and their application in drug delivery and catalysis. This thesis consists of six chapters; other than the introduction, it consists of the following chapters.

Chapter 2 describes the different experimental characterization techniques used in nanotechnology/materials science such as UV-visible Spectroscopy, Fourier Transform Infrared Spectroscopy (FTIR), X-ray photoelectron spectroscopy (XPS), Transmission Electron Microscopy (TEM), Isothermal Titration Calorimetry (ITC), Electrophoresis technique, Inductive Coupled Plasmon (ICP), Thermo Gravimetric Analysis technique (TGA) etc. The physical principles involved in these techniques make them versatile for nanoparticle characterization.

Chapter 3 deals with the surface modification of gold nanoparticles with amino acids and understanding their binding mechanism with the gold nanoparticles. Isothermal titration calorimetry technique has been used to study the binding kinetics and interaction between amino acids and gold nanoparticles. The binding of one basic amino acid, lysine (pI ~ 9.4) and an acidic amino acid, aspartic acid (pI ~ 2.77) with aqueous gold nanoparticles has been studied at physiological pH. Calorimetric studies show that aspartic acid binds strongly with gold nanoparticles while weak binding is observed in the case of lysine at physiological pH. This result is validated by X-ray photoelectron spectroscopy and thermo gravimetric analysis. The pH dependant charge on amino acid modified gold nanoparticles was determined by gel electrophoresis. Detailed thermodynamic analysis of the binding of aspartic acid with gold nanoparticles was done with the help of ITC titrations at different concentrations.

Chapter 4 deals with the binding of the hormone insulin with bare gold nanoparticles and aspartic acid capped gold nanoparticles and their efficient oral and transmucosal delivery for the treatment of diabetes mellitus. Insulin binds to bare gold nanoparticles by co-ordinate and weak electrostatic bonds while in the case of aspartic

acid capped gold nanoparticles, the binding is via weak hydrogen bonds with aspartic acid, making it more facile for the release of insulin in-vivo. Both formulations were administered orally and intranasally to diabetic Wistar rats and blood glucose levels were monitored for 5 h. These studies were compared with subcutaneous administration of insulin. Our principle observations are that there is a significant reduction in the blood glucose levels (postprandial hyperglycemia) when insulin is delivered using gold nanoparticles as carriers by the transmucosal route in diabetic rats. Control of postprandial hyperglycemia by the intranasal delivery protocol is comparable to that achieved using the standard subcutaneous administration used for Type I diabetes mellitus.

Chapter 5 deals with the synthesis of platinum nanoparticles in aqueous medium and their phase transfer to organic medium. The phase transfer was accomplished by vigorous shaking of the biphasic mixture of platinum nanoparticles in aqueous medium and octadecylamine (ODA) in hexane. Aqueous platinum nanoparticles interact with amine groups of the ODA molecule in hexane during the phase transfer process. This process makes the nanoparticles surface hydrophobic. The nature of binding of ODA to platinum nanoparticles was characterized by thermo gravimetric analysis, transmission electron microscopy, X-photoelectron spectroscopy and fourier transform infrared spectroscopy. High catalytic activity of ODA-stabilized platinum nanoparticles was demonstrated during the hydrogenation of styrene to ethylbenzene and cyclohexene to cyclohaxane.

Chapter 6 summarizes the work presented in the thesis. It also discusses the scope of research for current and future developments in this field of research.

References

[1] Khomutov, G. B. " Interfacially formed organized planar inorganic, polymeric and composite nanostructures" *Adv. Colloid Interface Sci.*, **2004**, *111*, 79.

[2] Cao, G. "Nanostructures & Nanomaterials, synthesis, properties and application" imperial college press **2004.**

[3] Khomutov, G. B.; Koksharov, Y. A. "Effects of organic ligands, electrostatic and magnetic interactions in formation of colloidal and interfacial inorganic nanostructures" *Adv. colloid interface sci.* (in press).

[4] Haruta, M.; Kobayashi, T.; Sano, H.; Yamada, N. "Novel gold catalysts for the oxidation of carbon monoxide at a temperature far below 0 °C" *Chem. Lett.,* **1987**, 405.

[5] Haruta, M.; Yamada, N.; Kobayashi, T.; Ijima, S. "Gold catalysts prepared by coprecipitation for low-temperature oxidation hydrogen and of carbon monoxide" *J. Catal.,* **1989**, *115*, 301.

[6] Haruta, M. "Size- and support-dependency in the catalysis gold" *Catal. Today,* **1997**, *36*, 153.

[7] Whitesides, G. "The right size in nanobiotechnology" *Nat. Biotechnol.*, **2003,** *21*, 1161.

[8] Matejivic, E., **"**Production of monodispersed colloidal particles" *Annu. Rev. Mater. Sci.,* **1985**, *15*, 483.

[9] Matejivic, E. "Fine Particles: science and technology" *MRS bulletin*, **1989**, *14*, 18.

[10] Maier, S.A.; Brongersma, M.L.; Kik, P.G. Meltzer, S.; Requicha, A.A.G. Atwater, H.A. **"**Plasmonics - a route to nanoscale optical devices" *Adv. Mater*., **2001,** *13*, 1501.

[11] Qian, L.; Hinestroza, J. P. "Application of nanotechnology for high performance textiles" *JTATM*, **2004,** *4*, 1.

[12] Sanguansri, P.; Augustin M.A. "Nanoscale materials development -a food industry perspective" *Trends Food Sci. Tech.*, **2006**, 1.

[13] Scientific American, September issue **2001.**

[14] Whitesides, G. M.; "Nanoscience, nanotechnology and chemistry" *Small*, **2005**, *1*, 172.

[15] Fendler, J.H.; Meldrum, F.C. "The colloidal chemical approach to nanostructured materials" *Adv. Mat.,* **1995**, *7*, 607.

[16] Schmid, G. "Large clusters and colloids- metals in the embryonic state" *Chem. Rev.*, **1992**, *92,* 1709.

[17] Niemeyer, C.M. "Nanoparticles, Proteins, and Nucleic Acids:Biotechnology Meets Materials Science" *Angew. Chem. Int. Ed*., **2001**, *40,* 4128 .

[18] Reverchon, E.; Adami, R. "Nanomaterials and supercritical fluids" *J. Supercrit. Fluids,* 2006, *37*, 1.

[19] Mertig, M.; Kirsch, R.; Pompe, W.; Engelhardt, H. "Fabrication of highly oriented nanocluster arrays by biomolecular templating" *Eur. Phys. J. D,* **1999**, *9*, 45.

[20] Alivisatos, A.P.; Johnsson, K.P.; Peng, X.; Wilson, T.E.; Loweth, C.J.; Bruchez , M.P.; Schultz, P.G. "Organization of 'nanocrystal molecules' using DNA" *Nature,* **1996,** *382*, 609.

[21] Wolf, E. "Nanophysics and nanotechnology" Wiley VCH Weinheim **2004**.

[22] Okumura, M.; Tsubota, S.; Iwamoto, M.; Hauta, M. "Chemical vapor deposition of gold nanoparticles on MCM-41 and their catalytic activities for the low temperature oxidation of CO and H_2" *Chem. Lett.*, **1998**, 315.

[23] Lin, S.T.; Franklin, M.T.; Klabhunde K.J. "Nonaqueous colloidal gold: clustering of metal atoms in organic media" *Langmuir*, **1986**, *2*, 259.

[24] Becker, M.F.; Brock, J. R.; Cai, H.; Henneke, D.E.; Keto, J.W.; Lee, J.; Nichols, W.T.; Glicksman, H.D. "Metal nanoparticles generated by laser ablation*" Nanostruct. Meter*., **1998**, *10*, 853.

[25] Mafune, F.; Kohno, J.; Takeda, Y.; Kondo, T. "Formation of stable platinum nanoparticles by laser ablation in water" *J. phys. Chem. B.*, **2003**, *107*, 4218.

[26] Mafune, F.; Kohno, J.; Takeda, Y.; Kondo, T.; Sawabe, H. "Formation and size control of silver nanoparticles by laser ablation in aqueous solution" *J. Phys. Chem. B,* **2000**, *104*, 9111.

[27] Caruso, R.A.; Ashok kumar, M. "Sonochemical formation of gold sols" *Langmuir*, **2002**, *18*, 7831,

[28] Mizukoshi, Y.; Oshima, R.; Maeda, Y.; Nagata, Y.; "Preparation of platinum nanoparticles by sonochemical reduction of Pt(II) ion" *Langmuir*, **1999**, *15*, 2733.

[29] Gachard, E.; Remita, H.; Khatouri, J.; Keita, B.; Nadjo, L.; Belloni, J. " Radiation induced and chemical formation of gold clusters" *New J. Chem.,* **1998**, 1257.

[30] Turkevich, J.; Stevenson, P.C.; Hillier, J. "Nucleation and growth process in the synthesis of colloidal gold" *Discuss Faraday Soc.,* **1951**, *11*, 55.

[31] Patil, V.; Malvankar, R.B.; Sastry, M. **"**Role of particle size in individual and competitive diffusion of carboxylic acid derivatized colloidal gold particles in thermally evaporated fatty amine films" *Langmuir*, **1999**, *15*, 8197

[32] Lee. P.C.; Meisel, D. "Adsoption and surface enhanced raman dyes on silver and gold sols" *J. Phys. Chem.*, **1982**, *86*, 3391.

[33] Selvakannan, PR.; Mandal, S.; Phadtare, S.; Gole, A.; Pasricha, R.; Adyanthaya S. D.; Sastry, M. "Water-dispersible tryptophan-protected gold nanoparticles prepared by the spontaneous reduction of aqueous chloroaurate ions by the amino acid" *J. Colloid Interface Sci.*, **2004**, *269*, 97.

[34] Mandal, S.; Selvakannan PR.; Phadtare, S.; Pasricha, R.; Sastry, M "Synthesis of a stable gold hydrosol by the reduction of chloroaurate ions by the amino acid, aspartic acid" *Proc. Indian Acad. Sci.* (*Chem. Sci.*), **2002**, *114*, 513.

[35] Milligan; W. O.; Morriss, R. H. **"**Morphology of colloidal gold-a comparative study" *J. Am. Chem. Soc.,* **1964**, *86,* 3461.

[36] Brust, M.; Walker, M.; Bethell, D.; Schiffrin, D.J.; Whyman, R.J.; "Synthesis of thiol derivativetised gold nanoparticles in a two phase liquid liquid system" *Chem Cummun.,* **1994**, 801.

[37] Li, Z.; Liu, Z.; Zhang, J.; Han, B.; Du, J.; Gao, Y.; Jiang, T., "Synthesis of single-crystal gold nanosheets of large size in ionic liquids"**,** *J. Phys. Chem. B.,* **2005**, *109*, 14445.

[38] Ohde, H.; Hunt, F.; Wai C.M. "Synthesis of silver and copper nanoparticles in a water in supercritical carbon dioxide micro emulsions" *Chem. Mater.,* **2001**, *13*, 4130.

[39] Swami, A.; Kumar, A.; Selvakannan, PR.; Mandal, S.; Pasricha, R.; Sastry, M. "Highly oriented gold nanoribbons by the reduction of aqueous chloroaurate ions by hexadecylaniline langmuir monolayers" *Chem. Mater.*, **2003**; *15*; 17.

[40] Kumar, A.; Mandal, S.; Mathew, S. P.; Selvakannan, P. R.; Mandale, A. B.; Chaudhari, R. V.; Sastry, M. "Benzene- and anthracene-mediated assembly of gold nanoparticles at the liquid-liquid Interface" *Langmuir,* **2002,** *18*, 6478.

[41] Mukherjee, P.; Senapati, S.; Mandal, D.; Ahmad, A.; Khan, M.I.; Kumar, R.; Sastry, M. "Extracellular synthesis of gold nanoparticles by the fungus fusarium oxysporum"*, ChemBioChem*, **2002**, *3*, 461.

[42] Klaus-Joerger, T.; Joerger, R.; Olsson, E ; Granqvist, C.G. "Bacteria as workers in the living factory: metal-accumulating bacteria and their potential for materials science", *Trends in Biotechnol.*, **2001**, *19*, 15.

[43] Mukherjee, P.; Ahmad, A.; Mandal, D.; Senapati, S.; Sainkar, S. R.; Khan, M. I.; Ramani, R.; Pasricha, R.; Ajayakumar, P. V.; Alam, M.; Sastry, M.; Kumar, R. "Bioreduction of $AuCl_4^-$ ions by the fungus, Verticillium sp. and surface trapping of the gold nanoparticles formed" *Angew.Chem.Intl.Ed.,* **2001**, *40*, 3585.

[44] Sastry, M.; Ahmad, A.; Khan, M.I.; Kumar, R. "Biosynthesis of metal nanoparticles using fungi and actinomycete" *Curr. Sci.*, **2003**, *85*, 162.

[45] Shiv Shankar, S.; Ahmad, A.; Sastry, M. **"**Geranium leaf assisted biosynthesis of silver nanoparticles" *Biotechnol. Prog.,* **2003,** *19,* 1627.

[46] Shankar, S.; Rai, A.; Ankamwar, A.; Singh, A.; Ahmad, A.; Sastry, M.; "Biological synthesis of triangular gold nanoprisms" *Nat. Mater.*, **2004,** *3***,** 482.

[47] Shiv Shankar, S. ; Ahmad, A.; Pasrichaa, R.; Sastry, M. "Bioreduction of chloroaurate ions by geranium leaves and its endophytic fungus yields gold nanoparticles of different shapes" *J. Mater. Chem.*, **2003**, *13*, 1822.

[48] Selvakannan, PR.; Mandal, S.; Pasricha, R.; Adyanthaya, S. D.; Sastry, M. "One-step synthesis of hydrophobized gold nanoparticles of controllable size by the reduction of aqueous chloroaurate ions by hexadecylaniline at the liquid–liquid interface " *Chem Commun.*, **2002**, 1334

[49] Henglein, A. "Physicochemical properties of small metal particles in solution: "microelectrode" reactions, chemisorption, composite metal particles, and the atom-to-metal transition**"** *J. Phys. Chem.,* **1993**, *97*, 5457

[50] Burda, C.; Chen, X.; Narayanan, R.; El-Sayed, M. A. "Chemistry and properties of nanocrystals of different shapes" *Chem. Rev*., **2005,** *105*, 1025.

[51] Kelly, K.L.; Coronado, E.; Zhao, L.L.; Schatz, G.C. "The optical properties of metal nanoparticles: the influence of size, shape, and dielectric environment" *J. Phys. Chem. B,* **2003**, *107,* 668.

[52] Mie, G. "A contribution to the optics of turbid media, especially colloidal metallic suspensions" *Ann. Phys*., **1908**, *25*, 377

[53] Mulvaney, P. "Surface plasmon spectroscopy of nanosized metal particles" *Langmuir*, **1996**, *12*, 788.

[54] Malinsky, M.D.; Kelly, K.L.; Schatz, G.C.; VanDuyne, R.P. "Chain length dependence and sensing capabilities of the localized surface plasmon resonance

of silver nanoparticles chemically modified with alkanethiol self-assembled monolayers**"** *J. Am. Chem. Soc*., **2001**, *123*, 1471.

[55] Templeton, A.C.; Wvelfing, W.P.; Murray, R.W. "Monolayer-protected cluster molecules" *Acc. Chem. Res*., **2000**, *33*, 27.

[56] Keating, C. D.; Kovaleski, K. M.; Natan, M. J**. "**Protein: colloid conjugates for surface enhanced raman scattering: stability and control of protein orientation" *J. Phys. Chem. B*., **1998**, *102*, 9404.

[57] Xu, H.; Bjerneld, E. J.; Kall, M.; Borjesson, L. "Spectroscopy of single hemoglobin molecules by surface enhanced raman scattering" *Phy. Rev. Lett*., **1999**, *83*, 4357.

[58] Crumbliss, A. L.; Perine, S. C.; Stonehuerner, J.; Tubergen, K. R.; Zhao, J.; O'Daly, J. P. "Colloidal gold as a biocompatible immobilization matrix suitable for the fabrication of enzyme electrodes by electrodeposition" *Biotech. Bioeng.*, **1992**, *40*, 483.

[59] Gole, A.; Dash, C.; Ramakrishnan, V.; Sainkar, S. R.; Mandale, A. B.; Rao, M.; Sastry, M. "Pepsin-gold colloid conjugates: preparation, characterization, and enzymatic activity" *Langmuir*,**2001**, *17*, 1674.

[60] Rosi, N. L.; Mirkin, C. A. **"**Nanostructures in biodiagnostics**"** *Chem. Rev.*, **2005**, *105*, 1547.

[61] Sastry, M.; Lala, N.; Patil, V.; Chavan, S. P.; Chittiboyina, A. G. "Optical absorption study of the biotin-avidin interaction on colloidal silver and gold particles" *Langmuir*, **1998**, *14*, 4138.

[62] Haynes, C. L.; McFarland, A. D.; Van Duyne, R. P. "Surface enahanced raman spectroscopy" *Anal. Chem*., **2005**, 339 A.

[63] Kneipp, K.; Kneipp, H.; Kartha, V. B.; Manoharan, R.; Deinum, G.; Itzkan, I.; Dasari, R. R.; Feld M. S. "Detection and identification of a single DNA base

molecule using surface-enhanced Raman scattering SERS" *Phy. Rev. E*, **1998**, 57, R6281.

[64] Schon, G.; Simon, U. *J. Colloid Polymer Sci.*, **1995**, *273*, 101.

[65] Andres, R. P.; Bein, T.; dorogi, M.; Feng, S.; Jendorson J. I.; Kubiak, C. P.; Mahoney, W. Osifchin, R. G.; Reifenverger, R. "Coulumbic staircase at room temperature in self assembled molecular nanostructure" *Science*, **1996**, *272*, 1323.

[66] Castro, T.; Reifenberger, R.; Choi, E.; Andres, R. P., **"**Size-dependent melting temperature of individual nanometer-sized metallic clusters" *Phys. rev., B, Condens. matter*, **1990**, *13*, 8548.

[67] Volokitin, Y.; Sinzig, J.; Jongh, L. J.; Schmid, G.; Moiseev, I. I. "Quantum-size effects in the thermodynamic properties of metallic nanoparticles" *Nature*, **1996**, *384*, 621.

[68] Weertman, J. R.; Averback, R. S.; "Nanomaterials: synthesis, properties, and applications" eds. Edelstein, A.S. Cammarata , R.C. London institute of Phys. Publ. **1996**, chapter 13, 323.

[69] Atkins, P.W. Physical Chemistry ELBS Oxford 5th edition **1995**

[70] Bonneman, H.; Richards, R. M. "Nanoscopic metal particles: synthetic methods and potential applications" *Eur. J. Inorg. Chem.*, **2001**, 2455

[71] Shon, Y. S. "Metal nanoparticles protected with monolayers: synthetic methods" Dekker encyclopedia of nanoscience and nanotechnology DOI: 10.1081/E-ENN-120034034

[72] Connolly, S.; Fitzmaurice**,** D. **"**Programmed assembly of gold nanocrystals in aqueous solution" *Adv.Mater.*, **1999**, *11*, 1202.

[73] Letsinger, R. L.; Elghanian, R.; Viswanadham, G.; Mirkin, C. A. **"**Use of a steroid cyclic disulfide anchor in constructing gold nanoparticle-oligonucleotide conjugates" *Bioconjugate Chem.***, 2000**, *11*, 289.

[74] Kreuter J. "Microcapsules and nanoparticles in medicine and pharmacy" (Ed.: M. Donbrow), CRC, Boca Raton, **1992**.

[75] Gestwicki, J. E.; Strong, L. E.; Kiessling, L. L. "Visualization of single multivalent receptor-ligand complexes by transmission electron microscopy**"** *Angew. Chem. Int. Ed.*, **2000**, *39*, 4567.

[76] Safer, D. E.; Bolinger, L.; Leigh, J. S. "Undecagold clusters for site-specific labeling of biological macromolecules: simplified preparation and model applications" *J. Inorg. Biochem.*, **1986**, *26*, 77.

[77] Hainfeld, J. F.; Furuya, F. R. "A 1.4-nm gold cluster covalently attached to antibodies improves immunolabeling" *J. Histochem. Cytochem*., **1992**, *40*, 177.

[78] Templeton, A. C.; Hostetler, M. J.; Warmoth, E. K.; Chen, S. W.; Hartshorn, C. M.; Krishnamurthy, V. M.; Forbes, M. D. E.; Murray, R. W. "Gateway reactions to diverse, polyfunctional monolayer- protected gold clusters" *J. Am. Chem. Soc.*,**1998**, *120*, 4845.

[79] Le´ vy, R.; Thanh, N. T. K.; Doty, R. C.; Hussain, I.; Nichols, R. J.; Schiffrin, D. J.; Brust, M.; Fernig, D. G. "Rational and combinatorial design of peptide capping ligands for gold nanoparticles" *J. Am. Chem. Soc.*, **2004**, *126*, 10076.

[80] Shenhar, R.; Rotello, V .M. "Nanoparticles: scaffolds and building blocks" *Acc. Chem. Res.*, **2003**, *36*, 549.

[81] Marinakos, S. M.; Novak, J. P.; Brousseau, L. C.; House, A. B.; Edeki, E. M.; Feldhaus, J. C.; Feldheim, D. L. "Gold particles as templates for the synthesis of hollow polymer capsules. control of capsule dimensions and guest encapsulation" *J. Am. Chem. Soc.*, **1999**, *121*, 8518.

[82] Liz-Marzan, L. M.; Giersig, M.; Mulvaney, P. "Synthesis of nanosized gold-silica core-shell particles" *Langmuir*, **1996**, *12*, 4329.

[83] Evans, C. H.; Gouze, E.; Gouze, J. N.; Robbins, P. D.; Ghivizzani, S. C. "Gene therapeutic approaches transfer in vivo B" *Adv. Drug Deliv. Rev.*, **2006,** *58,* 243.

[84] Budker, V.; Gurevich, V.; Hagstrom, J. E.; Bortzov, F.; Wolff, J.A. "pH-sensitive, cationic liposomes: a new synthetic virus-like vector" *Nat. Biotechnol.*, **1996**, *14*, 760.

[85] Soppimath, K. S.; Aminabhavi, T. M.; Kulkarni, A. R.; Rudzinski, W. E. " Biodegradable polymeric nanoparticles as drug delivery devices" *J. Control. Release*, **2001**, *70*, 1.

[86] Imperiale, M. J.; Kochanek, S. "Adenovirus vectors: biology, design, and production" *Curr. Top. Microbiol. Immunol.*, **2004**, *273*, 335.

[87] Dornburg, R. "The history and principles of retroviral vectors" *Front Biosci.*, **2003**, *8* , d818.

[88] Goncalves, M. A.; "Adeno-associated virus: from defective virus to effective vector" *Virol. J*., **2005**, *2*, 43.

[89] Saraf, A.; Mikos, A. G. "Gene delivery strategies for cartilage tissue engineering" *Adv. Drug Deliv. Rev.*, **2006,** *58*, 592.

[90] Zhang, S. B.; Xu, Y. M.; Wang, B.; Qiao, W. H.; Liu, D. L.; Li, Z. S. "Cationic compounds used in lipoplexes and polyplexes for gene delivery", *J. Control. Release*, **2004,** *100* , 165 .

[91] El-Aneed, A. "An overview of current delivery systems in cancer gene therapy" *J. Control. Release*, **2004**, *94*, 1.

[92] Dass, C. R. "Biochemical and biophysical characteristics of lipoplexes pertinent to solid tumour gene therapy" *Int. J. Pharm.*, **2001**, *241*, 1.

[93] Koping-Hoggard, M.; Mel'nikova, Y.S .; Varum, K. M.; Lindman, B.; Artursson, P. "Relationship between the physical shape and the efficiency of oligomeric

chitosan as a gene delivery system in vitro and in vivo" *J. Gene Med.* **2003**,*5*, 130.

[94] Lee, J. W.; Nah, Y.; Kwon, J. J.; Koh, K. S.; Ko, S. W.; Kim, "Water-soluble and low molecular weight chitosan-based plasmid DNA delivery" *Pharm. Res.*, **2001**, *18*, 427.

[95] Hongtao, L.; Zhang S.; Wang, B.; Cui, S.; Yan, J. "Toxicity of cationic lipids and cationic polymers in gene delivery" *J. Control. Release* (in press).

[96] Sahoo, S. K.; Labhasetwar, V. " Nanotech approaches to drug delivery and imaging" *Drug Discovery Today,* **2003**, *8*, 1112.

[97] Date, A. A.; Patravaleb, V. B. "Current strategies for engineering drug nanoparticles" *Curr. Opin. Colloid Interface Sci.*, **2004**, *9* , 222.

[98] Sandhu, K. K., McIntosh, C. M., Simard, J. M., Smith, S. W., Rotello, V. M.,"Gold nanoparticle-mediated transfection of mammalian cells" *Bioconjugate Chem.,***2002**, *13*, 3.

[99] Paciotti, G. F.; Myer, L.; Weinreich, D.; Goia, D.; Pavel, N.; McLaughlin, R. E.; Tamarkin, L.**"**Colloidal gold: a novel nanoparticle vector for tumor directed drug delivery." *Drug Deli*v. **2004**, *11*, 169.

[100] Daniel, M. C.; Astruc, D. **"**Gold nanoparticles: assembly, supramolecular chemistry, quantum-size-related properties, and applications toward biology, catalysis, and nanotechnology" *Chem. Rev.,* **2004**, *104,* 293.

[101] Graham, F. L.; Van der Eb, A. J., "A new technique for the assay of infectivity of human adenovirus 5 DNA" *Virology*, **1973,** *52*, 456.

[102] Kneuer, C.; Sameti, M.; Haltner, E.G.; Schiestel, T.; Schirra, H.; Schmidt, H.; Lehr, C. S., "Silica nanoparticles modified with aminosilanes as carriers for plasmid DNA" *Inter. J. Pharm.*, **2000**, *196*, 257.

[103] Plank, C.; Schere, F.; Schillinger, U.; Bergemann, C.; Anton, M. "Magnetofection: enhancing and targeting gene delivery with superparamagnetic nanoparticles and magnetic fields" *J. Liposome Res.*, **2003**, *13*, 29.

[104] Tartaj, P.; Morales, M. P.; Veintemillas-Verdaguer, S.; Gonzáles-Carreño, T.; Serna, C. J. "The preparation of magnetic nanoparticles for application in biomedicine" *J.Phy. D: Appl. Phys.,* **2003,** *36,* R182.

[105] Gupta, A. K.; Gupta, M., "Cytotoxicity suppression and cellular uptake enhancement of surface modified magnetic nanoparticles" *Biomaterials*, **2005**, *26*, 1565.

[106] Xua, Z. P.; Zengb, Q. H.; Lua,G. Q.; BingYub, A. "Inorganic nanoparticles as carriers for efficient cellular delivery" *Chem. Eng. Sci.,*, **2006,** *61* 1027.

[107] Hong, R.; Han, G.; Fernández, J. M.; Kim, B. J.; Forbes, N. S.; Rotello, V. M. "Glutathione-mediated delivery and release using monolayer protected nanoparticle carriers " *J. Am. Chem. Soc.*, **2006**, *128*, 1078.

[108] **W**etterauer, B.; Salger, K., Demel, P.; Koop, H.U. "Efficient transformation of Dictyostelium discoideum with a particle inflow gun" *Biochimica et Biophysica Acta,* **2000***, 1499,* 139.

[109] Oyewumi, M. O.; Mumper, R. J. "Engineering tumor-targeted gadolinium hexanedione nanoparticles for potential application in neutron capture therapy". *Bioconjugate Chem.*, **2002**, *13*, 1328.

[110] Oyewumi, M. O.; Liu, S. Q.; Moscow, J. A.; Mumper, R. J. "Specific assocn. of thiamine-coated gadolinium nanoparticles with human breast cancer cells expressing thiamine transporters" *Bioconjugate Chem.*, **2003**, *14*, 404–411.

[111] Oyewumi, M. O.; Yokel, R. A.; Jay, M.; Coakley, T.; Mumper, R. J. "Comparison of cell uptake, biodistribution and tumor retention of folate-coated and PEG-coated gadolinium nanoparticles in tumorbearing mice." *J. Control. Release,* **2004,** *95*, 613.

[112] Salem, A. K.; Searson, P. C.; Leong, K. W. "Multifunctional nanorods for gene delivery" *Nat. Mater.,* **2003**, *2*, 668.

[113] Kneuer, C.; Sameti, M.; Bakowsky, U.; Schiestel, T.; Schirra, H.; Schmidt, H.; Lehr, C. S., "Non-viral DNA delivery systems based on surface modified silica-nanoparticles can efficiently transfect DNA into cells*". Bioconjugate Chem.*, **2000**, *11*, 926

[114] Ito, A.; Shinkai, M.; Honda, H.; Kobayashi, T. "Medical application of functionalized magnetic nanoparticles" *J. Biosci. Bioeng.* **2005,** *100*, 1.

[115] Klabhunde, K. J. "Nanoscale materials in chemistry" chapter 7 Wiley interscience **2001**

[116] Schmid, G. "Clusters and colloids" Schmid, G., Ed.; VCH, Weinheim,**1994**.

[117] Li, Y.; El-Sayed, M. A. **"**The effect of stabilizers on the catalytic activity and stability of Pd colloidal nanoparticles in the Suzuki reactions in aqueous solution" *J. Phys. Chem. B*, **2001**, *105*, 8938.

[118] Li, Y.; Hong, X. M.; Collard, D. M.; El-Sayed, M. A. "Suzuki cross-coupling reactions catalyzed by palladium nanoparticles in aqueous solution" *Org. Lett.*, **2000**, *2*, 2385.

[119] Na, Y.; Park, S.; Han, S. B.; Han, H.; Ko, S.; Chang, S. **"**Ruthenium-catalyzed Heck-type olefination and Suzuki coupling reactions: studies on the nature of catalytic species" *J. Am. Chem. Soc.* **2004**, *126* , 250.

[120] Thathagar, M. B.; Beckers, J.; Rothenberg, G. **"**Copper-catalyzed Suzuki cross-coupling using mixed nanocluster catalysts" *J. Am. Chem. Soc.*, **2002**, *124*, 11858.

[121] Mandal, S.; Das, A.; Srivastava, R.; Sastry, M "Keggin Ion Mediated Synthesis of Hydrophobized Pd Nanoparticles for Multifunctional Catalysis" *Langmuir*, **2005**, *21,* 2408.

[122] Narayanan, R.; El-Sayed, M. A. **"**Shape-dependent catalytic activity of platinum nanoparticles in colloidal solution" *Nano Lett.*, **2004**, *4*, 1343

[123] Narayanan, R.; El-Sayed, M. A. **"**Effect of nanocatalysis in colloidal solution on the tetrahedral and cubic nanoparticle shape: electron-transfer reaction catalyzed by Platinum nanoparticles" *J. Phys. Chem. B*, **2004**, *108*, 5726.

[124] Narayanan, R.; El-Sayed, M. A. **"**Changing catalytic activity during colloidal platinum nanocatalysis due to shape changes: electron-transfer reaction" *J. Am. Chem. Soc.* **2004**, *126*, 7194.

[125] Narayanan, R.; El-Sayed, M. A. "Effect of catalytic activity on the metallic nanoparticle size distribution: electron-transfer reaction between $Fe(CN)_6$ and thiosulfate ions catalyzed by PVP-platinum" *J. Phys. Chem. B*, **2003**, *107,* 12416.

[126] Ohde, H.; Ohde, M.; Wai, C. M. **"**Swelled plastics in supercritical CO_2 as media for stabilization of metal nanoparticles and for catalytic hydrogenation" *Chem. Commun.*, **2004**, *8*, 930.

[127] Fonseca, G. S.; Umpierre, A. P.; Fichtner, P. F. P.; Teixeira, S. R.; Dupont, J. "The use of imidazolium ionic liquids for the formation and stabilization of Ir^0 and Rh^0 nanoparticles: efficient catalysts for the hydrogenation of arenes" *Chem. Eur. J.* , **2003**, *9*, 3263.

[128] Adlim, M.; Abu Bakar, M.; Liew, K. Y.; Ismail, J. "Synthesis of chitosan-stabilized platinum and palladium nanoparticles and their hydrogenation activity" *J. Mol. Catal. A: Chem.*, **2004**, *212*, 141.

[129] Semagina, N. V.; Bykov, A. V.; Sulman, E. M.; Matveeva, V. G.; Sidorov, S. N.; Dubrovina, L. V.; Valetsky, P. M.; Kiselyova, O. I.; Khokhlov, A. R.; Stein, B.; Bronstein, L. M. "Selective dehydrolinalool hydrogenation with poly(ethylene oxide)-*block*-poly-2-vinylpyridine micelles filled with Pd nanoparticles" *J. Mol. Catal. A: Chem.*, **2004**, *208*,273.

[130] Anderson, K.; Cortinas Fernandez, S.; Hardacre, C.; Marr, P. C. "Preparation of nanoparticulate metal catalysts in porous supports using an ionic liquid route; hydrogenation and C–C coupling" *Inorg. Chem. Commun.*, **2003**, *7*, 73.

[131] Shiraishi, Y.; Toshima, N. "Oxidation of ethylene catalyzed by colloidal dispersions of poly(sodium acrylate)-protected silver nanoclusters" *Colloids Surf. A: Physicochem. Eng. Asp.*, **2000**, *169*, 59.

[132] Shiraishi, Y.; Toshima, N. "Colloidal silver catalysts for oxidation of ethylene" *J. Mol. Catal. A. Chem.* ,**1999**, *141*, 187.

[133] Marconi, G.; Pertici, P.; Evangelisti, C.; Caporusso, A. M.; Vitulli,G.; Capannelli, G.; Hoang, M.; Turney, T. W. "Nanostructured ruthenium on γ-Al_2O_3 catalysts for the efficient hydrogenation of aromatic compounds**"** *J. Organomet. Chem.*, **2004**, *689*, 639.

[134] Claus, P.; Hofmeister, H. **"**Electron microscopy and catalytic study of silver catalysts: structure sensitivity of the hydrogenation of crotonaldehyde" *J. Phys. Chem. B,* **1999**, *103*, 2766

[135] Lang, H.; May, R. A.; Iversen, B. L.; Chandler, B. D. "Dendrimer-encapsulated nanoparticle precursors to supported platinum catalysts" *J. Am. Chem. Soc.*, **2003**, *125*, 14832.

[136] Bulushev, D. A.; Yuranov, I.; Suvorova, E. I.; Buffat, P. A.; Kiwi-Minsker, L. "Highly dispersed gold on activated carbon fibers for low-temperature CO oxidation" *J. Catal.,* **2004**, *224*, 8.

[137] Lopez, N.; Janssens, T. V. W.; Clausen, B. S.; Xu, Y.; Mavrikakis, M.; Bligaard, T.; Norskov, J. K. "On the origin of the catalytic activity of gold nanoparticles for low-temperature CO oxidation" *J. Catal.,* **2004**, *223*, 232.

[138] Boudjahem, A. G.; Monteverdi, S.; Mercy, M.; Bettahar, M. M. "Study of nickel catalysts supported on silica of low surface area and prepared by reduction of nickel acetate in aqueous hydrazine" *J. Catal.,* **2004**, *221*, 325.

[139] Bianchini, C.; Dal Santo, V.; Meli, A.; Moneti, S.; Moreno, M.; Oberhauser, W.; Psaro, R.; Sordelli, L.; Vizza, F. "A comparison between silica-immobilized ruthenium(II) single sites and silica-supported ruthenium nanoparticles in the catalytic hydrogenation of model hetero- and polyaromatics contained in raw oil materials" *J. Catal.,* **2003**, *213*, 47.

[140] Liu, Z.; Ling, X. Y.; Su, X.; Lee, J. Y. **"**Carbon-supported Pt and PtRu nanoparticles as catalysts for a direct methanol fuel cell" *J. Phys. Chem. B,* **2004**,*108*, 8234.

[141] Liu, Z.; Ling, X. Y.; Lee, J. Y.; Su, X.; Gan, L. M. **"**Nanosized Pt and PtRu colloids as precursors for direct methanol fuel cell catalysts" *J. Mater. Chem.,* **2003**, *13*, 3049.

[142] Miyazaki, A.; Balint, I.; Nakano, Y. *J.* "Morphology control of platinum nanoparticles and their catalytic properties" *Nano. Res.,* **2003**, *5*, 69

[143] Nakagawa, K.; Yamagishi, M.; Nishimoto, H.; Ikenaga, N.; Suzuki, T.; Kobayashi, T.; Nishitani-Gamo, M.; Ando, T. **"**Oxidized diamond as a simultaneous production medium of carbon nanomaterials and hydrogen for fuel cell" *Chem. Mater.,* **2003**, *15*, 4571.

[144] Bowker, M.; Stone, P.; Bennett, R.; Perkins, N. "Formic acid adsorption and decomposition on TiO_2 (1 1 0) and on Pd/TiO_2 (1 1 0) model catalysts" *Surf. Sci.,* **2002**, *511*, 435.

CHAPTER II

Characterization Techniques

The different experimental techniques used during the course of the present work are discussed in this chapter.

2.1 Introduction

This thesis investigates the binding modes of amino acids with gold nanoparticles and demonstrates these nanoparticles as carrier for drug delivery applications. It also describes phase transfer of metal nanoparticles from aqueous to organic phase and their catalytic applications. Various characterization techniques such as UV-Visible spectroscopy, Fourier Transform Infrared Spectroscopy (FTIR), X-ray Photoelectron Spectroscopy (XPS), Transmission Electron Microscopy (TEM), Gel electrophoresis, Thermo Gravimetric Analysis (TGA) have been used for characterization of nanomaterials. Isothermal Titrations Calorimetry (ITC) has also been used to study binding of amino acids with gold nanoparticles. Inductive Coupled Plasmon (ICP) technique has been used to detect gold concentration in blood serum during the animal studies.

2.2 UV- Visible absorption spectroscopy

UV-visible range is a small window of total electromagnetic spectrum, which ranges from 190 nm to 800 nm. Electromagnetic radiations in microwave and infra red regions cause rotational and vibrational transitions of electrons respectively. The absorption in visible and ultraviolet regions leads to transition between electronic energy levels of the molecule as well as transition between vibrational and rotational levels simultaneously. Since electronic levels in the atoms and molecules are quantized, The frequency of the radiation absorbed is given by

$$E = E_2 - E_1 = h\nu \quad \text{.....(2.1)}$$

Where, E_2, E_1, h and ν and are energies of upper energy state, lower energy state, planck's constant and frequency respectively [1].

The absorption of UV-Vis radiations causes excitation of valence electrons. Optical properties of organic and inorganic materials are dependent on transitions involving nonbonding, sigma, pi orbitals and transition involving d and f electrons. Noble metal nanoparticles absorb strongly in visible region due to surface plasmon

resonance phenomenon as described in Chapter 1. UV-Visible absorption spectroscopy is a primary characterization tool to study environment around nanoparticles, size and shape of the nanoparticles [2, 3].

Dual beam spectrophotometer consists of source, monochromator, chopper, mirrors and detectors. In a dual beam spectrophotometer, light radiation from source enters the grating monochromator before it reaches the filter. Monochromator provides continuous variation of wavelength during the measurement. Radiation emitted from the source enters monochromator through first slit. It falls on a collimating mirror and get reflected to diffraction grating. Diffraction grating is made up of optically reflecting surface with large number of parallel grooves on it. These parallel grooves allow diffraction of incident radiation and disperse it in space, while second mirror focuses these radiations onto exit slit. Monochromator converts polychromatic light into monochromatic light with finite effective band width. The radiations from the monochromator are alternatively split into one of two beams by a rotating mirror called a chopper. It controls radiation path by alternating sample and blank. Known speed of rotation of chopper resolves signal reaching to detector. The detector alternately sees the beam from the sample and then the reference. Output of oscillating square-wave gives the ratio of I to I_0 directly i.e. the reference correction is made automatically. [4] Detectors are essentially made up of photomultipliers where the radiation is absorbed. When it absorbs radiation, valence electrons jump in to conduction band which result in the production of current.

In this thesis, all UV-visible absorption spectra were carried out on Jasco V-570 dual beam spectrophotometer operated at resolution at 2 nm. UV-Visible spectroscopy is used for monitoring of surface plasmon resonance of gold nanoparticles before and after binding of amino acid or insulin.

2.3 Fourier transform infrared spectroscopy (FTIR)

The electromagnetic radiation range between 400 to 4000 cm^{-1} falls under infra red region. This range of electromagnetic radiations causes vibrational transitions in the

bond. This happens when the frequency of incident IR radiation matches with the difference between vibrational levels belonging to the bonds. Optical systems in an FTIR spectrophotometer consists of interferometer, infrared light source, an infrared detector, and beam splitter [5]. Michelson interferometer is used in FTIR instruments.

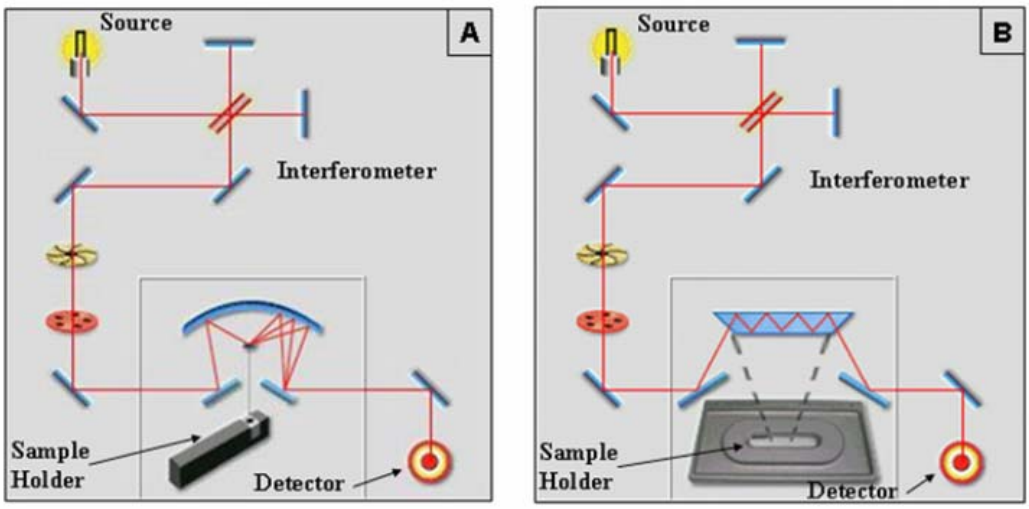

Figure 2.1: *Schematic shows the diagram of FTIR A) Diffuse reflectance mode B) Horizontally attenuated total reflectance mode (picture taken from FTIR spectrum one instrument's software provided by Perkin Elmer company, not to scale).*

It consists of a moving mirror, a fixed mirror perpendicular to each other and a beam splitter. The beam splitter is semi reflecting device which is made up of thin film germanium on flat KBr substrate. At beam splitter, half of the radiations incoming from IR source, are transmitted to a fixed mirror while remaining half are reflected to moving mirror. Divided beam recombines at the end of beam splitter. Change in the relative position of the moving mirror constructs interference pattern which eventually passes through sample and get focused on detector. If two beam path lengths are equal, splitted beam travels same distance and forms constructive interference leading to maximum detector response. Due to movement of mirror with constant velocity, intensity reaching at the detector is in sinusoidal manner to produce interferogram. It is a time domain spectrum which records the response changes versus time within mirror scan. When IR radiation is directed through sample, some of it gets absorbed where the frequencies of radiation match with characteristic frequencies of the sample. Under the

limits of detector response, interferogram contain all the information over the entire IR region (information in time domain), which is transformed into frequency domain with mathematical operation known as Fourier transformation.

2.3.1 Diffuse reflectance mode (DRS)

As shown in the Fig. 2.1 A, in this mode, IR radiation is reflected from rough surface such as powders. Powdered sample is mixed with powdered KBr. Reflected light is collected and analyzed.

2.3.2 Horizontally attenuated total reflectance mode (HATR)

IR spectra of aqueous samples can be obtained with help of this mode. As seen in Fig. 2.1 B, it consists of IR transparent crystal of high refractive index such as ZnSe. Radiation from source enters the crystal where it undergoes series of total internal reflections before exiting crystal. The evanescent radiation penetrates into a sample to a depth of a few microns. The result is a selective attenuation of the radiation at those wavelengths at which the sample absorbs. Apart from aqueous samples, solid samples such as polymers, fibers, fabrics, powders, and biological tissue samples can be analyzed [4].

FTIR data presented in the thesis were taken from Perkin-Elmer FTIR Spectrum one spectrophotometer operated at a resolution of 4 cm^{-1}. Diffuse Reflectance Infrared Fourier Transform (DRIFT) and horizontally attenuated total reflectance mode (HATR) methods were used for recording the IR spectra of Pt-ODA and insulin loaded gold nanoparticles bioconjugates respectively.

2.3.3 Peak assignments for lipid and proteins

As we have seen in first chapter, generally nanoparticles are synthesized in the presence of capping agents, are added to solution after synthesis of nanoparticles. Binding modes of these capping agents to nanoparticles are monitored by infrared spectroscopy since it can give information about vibrational transitions of the bonds. Functional groups have their own characteristic vibrational frequencies depending on

the bond strength of the atoms and their reduced mass. When capping agents adsorb on nanoparticles surface, functional groups which are taking part in the bonding either shifts fully or partially depending on the strength and nature of newly form bonds. The fatty lipid and protein used in this thesis is octadecylamine (ODA) and insulin respectively. The peak assignments have been discussed in general.

2.3.3 A) C-H stretch

The two bands at 2920 and 2850 cm^{-1} have been assigned to the antisymmetric and symmetric methylene (CH_2) stretching vibrations respectively and two weak bands at about 2960 and 2875 cm^{-1} to the asymmetric/degenerate and symmetric methyl (CH_3) stretching vibrations respectively.

2.3.3 B) N-H vibrations

N-H peaks for the free amine are seen at 3333 cm^{-1}. This band shifts to 3198 cm^{-1} on salt formation of primary amine [6]. NH_3 symmetric deformation band is observed at 1487 cm^{-1} in case of pure amine and is absent in case of amine salts as observed in the case of chloroplatinic acid complexed with octadecylamine [7]. The NH_3 antisymmetric deformation appears in the region of 1587 cm^{-1} [8].

2.3.3 C) Peak assignments for proteins

FTIR is a powerful tool to study protein-nanoparticles bioconjugates. The amide linkages between amino acid residues in polypeptides and proteins give rise to well known signatures in the infrared region of the electromagnetic spectrum. The position of the amide I (C=O band in amide linkage at ca. 1650 cm^{-1}), and amide II band (N-H stretch mode of vibration in the polypeptide linkage at ca. 1546 cm^{-1}) bands in the FTIR spectra of proteins is a sensitive indicator of conformational changes in the protein secondary structure[9-13].

2.4 X-ray photoelectron spectroscopy (XPS)

X-ray photoemission spectroscopy is well known characterization technique which is basically used for obtaining chemical information of various material surfaces. It is also known as electron spectroscopy for chemical analysis (ESCA). It is based on the photoelectric effect discovered by Heinrich Hertz and explained later by Albert Einstein. Measurement in ESCA are generally performed by irradiating a sample with monoenergetic soft x-rays and analyzing the emitted electrons of different energies. Generally Mg Kα x-rays (1253.6 eV) or Al Kα (1484.6 eV) x-rays are used for measurements. These low energy photons have limited penetration power of the order of 1-10 micrometers [14].

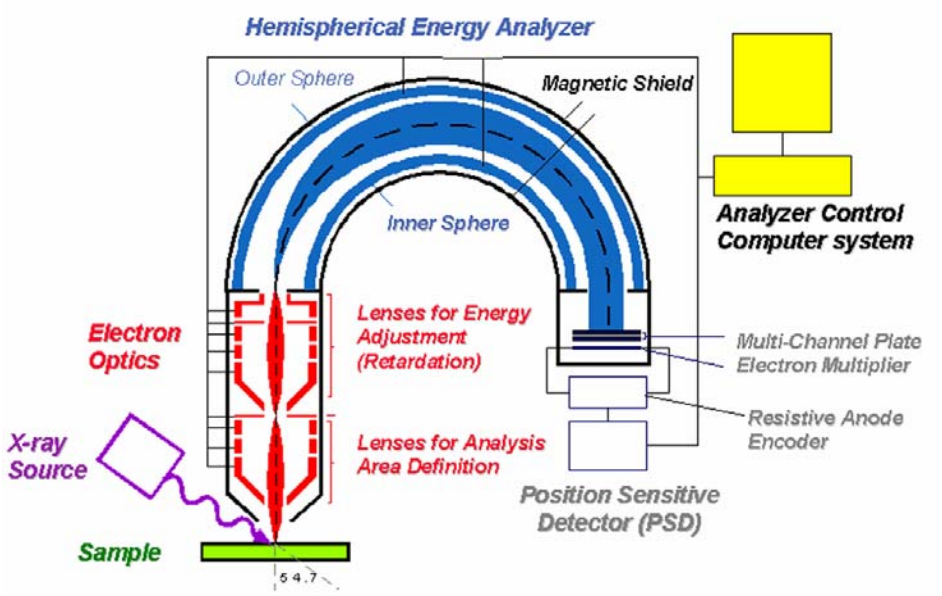

Figure 2.2: *Schematic shows the diagram of X-ray photoelectron spectrophotometer (not to scale) [15].*

These photons interact with atoms in above mentioned surface region by photoelectric effect causing electrons to be emitted. XPS is a very surface-sensitive technique and it is used to analyze the sample surface within in the range of few nanometers. Photoelectrons are collected and analyzed by the instrument to produce a spectrum of emission intensity versus electron binding energy. In general, the binding energies of the photoelectrons are characteristic of the element from which they are

originated therefore the spectra can be used for surface elemental analysis. Small shifts in the elemental binding energies provide information about the chemical state of the elements on the surface [16].Therefore, the high-resolution XPS studies can provide the chemical state information of the surface.

An atom absorbs a photon of energy hν from an X-Ray source; next a core or valence electron with binding energy E_b is ejected with kinetic energy

$$E_k = h\nu - E_b - \phi \ldots\ldots\ldots\ldots\ldots\ldots\ldots\ldots\ldots\ldots(2.2)$$

Where, E_k is the kinetic energy of the photoelectron, h is Planck's constant, ν is the frequency of the exciting radiation, E_b is the binding energy of the photoelectron with respect to the fermi level of the sample and ϕ is the work function. Photoelectron peaks are labeled according to quantum numbers of the level from which the electron originates. An electron coming from an orbital with principle quantum numbers n, orbital momentum quantum number l, and spin momentum quantum number is indicated as nl_{l+s}. For a non-zero orbital quantum number ($l > 0$), spin moment is coupled with orbital moment (called L-S coupling) and it has the total momentum j = l+1/2 and j = l-1/2 (generally, j = l±s), each state being filled with 2j+1 electrons. Hence most XPS peaks come in doublets and the intensity ratio of the components is (l+1)/l.

In contrast with valance electron, which is delocalized in molecules and condensed matter, the core electrons are localized, that is, they are atomic like in all matter. Therefore, the electron binding energy associated with a given orbital is essentially the same; independent of which system the atom happens to be a part of. X-rays illuminate an area of a sample causing electrons to be ejected with range of energies and directions [17]. As shown in Fig. 2.2, the electron optics, which may be a set of electrostatic and/or magnetic lens units, collect a proportion of these emitted electrons defined by those rays that can be transferred through the apertures and focused onto the analyzer entrance slit. Electrostatic fields within the hemispherical

analyzer (HSA) are established to only allow electrons of a given energy (Pass Energy) to arrive at the detector slits and onto the detectors themselves.

A hemispherical analyzer and transfer lenses can be operated commonly in the mode called Fixed Analyzer Transmission (FAT), also known as Constant Analyzer Energy (CAE), or Fix Retard Ratio (FRR) or Constant Retard Ratio (CRR). In FAT mode, the pass energy of the analyzer is held at a constant value and it is entirely the job of the transfer lens system to retard the given kinetic energy channel to the range accepted by the analyzer. Most XPS spectra are acquired using FAT.

A way of measuring the kinetic energy of the photoelectrons is to let them pass through a spherically symmetric field that is created between two hemispherical electrodes. In this field, electrons with different energies will follow paths with different radii, that is, the electrons are energy dispersed and an energy spectrum can be recorded.

All the XPS data presented in the thesis were carried out on a VG microtech ESCA 3000 instrument at a pressure greater than 10^{-9} torr with un-monochromatized Mg K_α radiation (photon energy = 1253.6 eV) at a pass energy of 50 eV and electron takeoff angle (angle between electron emission direction and surface plane) of 60^o. The overall resolution was ~ 1 eV for the XPS measurements.

2.5 Isothermal titrations calorimetry (ITC)

Isothermal titration calorimetry is a very powerful and highly sensitive technique commonly used to study interactions between biomolecules in dilute aqueous solutions from thermodynamic points of view [18]. During molecular interactions, heat is either generated or absorbed. However, the heat changes associated with these binding are too small to detect. ITC enables to measure these heat changes even of micro calories scale range. It is the only technique which provides a complete thermodynamic profile of the interaction including the binding constant (Ka), the number of binding sites (n), enthalpy (H), entropy (S), and free energy (G) in single experiment. As shown in the Fig. 2.3, it consists of two identical cells i.e. sample cell

and reference cell. These cells are surrounded by an inner shield to maintain the same temperature in order to minimize any heat flow to or from the cell. The outer shield is maintained at the same temperature, to compensate for changes in room temperature. It also consists of injection syringe with motor. Injection syringe is used to inject titrant in sample cell. Various parameters such amount of titrant be added, time interval between two injections, rotating speed of motor is controlled by a computer programme. During the titration, very small constant power is supplied to a heater on the reference cell. Simultaneously, power is supplied to sample cell in such a way that its temperature will be always identical to the reference cell [19].

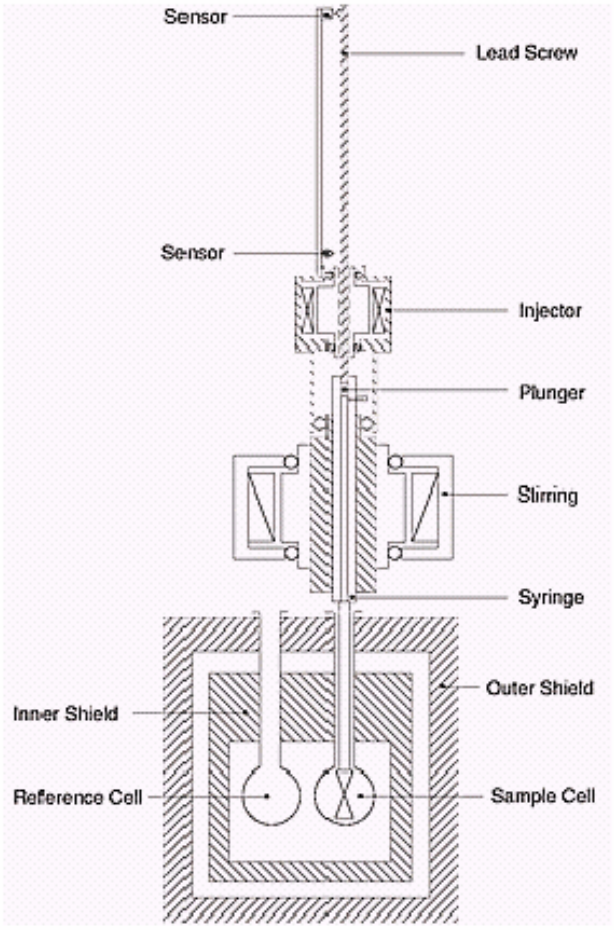

Figure 2.3: *Schematic shows the diagram of an isothermal titration calorimeter (not to scale).*

The precise amount of heat released or absorbed can then be determined since it is exactly equal to the amount of feedback power necessary to re-establish the temperature null between the cells. The heat change is expressed as the electrical power (Js^{-1}) required for maintaining a constant small temperature difference between the sample cell and the reference cell, which are placed in an adiabatic jacket. During the experiments, macro molecules or ligands solution are loaded in to syringe and buffer with other biomolecules, whose interactions with ligand is to be studied, is loaded in sample cell.

Long-needle syringe, depicted in Fig. 2.3, with a paddle fastened to its end, is filled with the appropriate ligand solution. After filling, the syringe is seated into a holder, which is coupled to a linear-motion injector system under software control. The syringe paddle is located inside the sample cell and the entire syringe assembly rotates at a preselected speed to continuously provide proper mixing to the contents of the sample cell. Each experiment consists of a number of equal-volume injections of a ligand solution from the syringe into the macromolecule solution contained in the sample cell. Typical results are obtained for exothermic or endothermic binding process, where each peak is the result of a single injection. It can be seen that with the early injections, the peaks are of almost equal size, which indicates that nearly all of the injected ligand is bound to the macromolecule. As the injections progress, the injection peaks decreases in size as the binding sites become saturated and less of the injected ligand is bound. The last several injections, of very small size, show that saturation is virtually complete by the end of the experiment. When the experimental results are analyzed using Origin data analysis software, the area of each injection peak is automatically determined and results are plotted, and this plot is referred to as a binding isotherm, where the total heat per injection (kcal per mole of ligand injected) is plotted against the molar ratio of ligand and macromolecule. The precise shape of the binding isotherm contains all of the information necessary to complete the characterization binding reaction. The ITC data presented here was carried out in a Micro Cal VP-ITC instrument. In this thesis, study of interaction of amino acid with gold nanoparticles has

been done in which, attempt has been made to design as adsorption model and calculate the interaction of aspartic acid to gold nanoparticles with the help of this model.

2.6 Inductive coupled plasmon spectrometry (ICP)

Inductive coupled plasmon spectrometry works on similar principles as that of atomic emission spectrometry. In ICP spectrometry, high-temperature atomization sources, such as flames, discharges, or plasmas, provide sufficient energy to excite atoms into high energy levels. When as excited atom or ion returns to ground state, it releases its absorbed energy in the form of light (photon) at particular unique wavelength. Decay of electrons to the ground state and its subsequent energy transfer is dependant upon the electronic configuration of the orbital of a specific element. This energy transfer is inversely proportional to the wavelength of electromagnetic radiation,

$$E = \frac{hc}{\lambda} \quad \text{.....(2.3)}$$

Where h is Planck's constant, c is the velocity of light and λ is wavelength Thus, wave-length of emitted light is also unique.

Since all atoms in a sample are excited simultaneously, they can be detected simultaneously using a polychromator with multiple detectors. It allows us to detect and analyze individual elements without separating them chemically. This is the major advantage of ICP over Atomic absorption spectroscopy.

2.6.1 Excitation of atoms in ICP

Initially, argon gas is passed through the quartz tube and exit from the tip. The top of the quartz tube is surrounded by induction coils that create a magnetic field. An AC current flows through the coils at a frequency of about 30 MHz and a power level of approximately 2 kW. A Tesla discharge coil charges the stream of argon gas with electrons. The induced magnetic field excites these electrons. These electrons then collide and ionize the argon atoms. The cations and anions present from the initial Tesla spark accelerate due to the magnetic field in a circular pattern that is

perpendicular to the stream exiting from the top of the quartz tube. By reversing the direction of the current in the induction coils, the magnetic field is also reversed. This changes the direction of the excited cations and anions, which causes more collisions with argon atoms. This results in further ionization of the argon atoms and intense thermal energy. As a result, a flame shaped plasma forms on top of the torch. The sample is introduced into the plasma stream, as an aerosol by use of a nebulizer or atomizer.

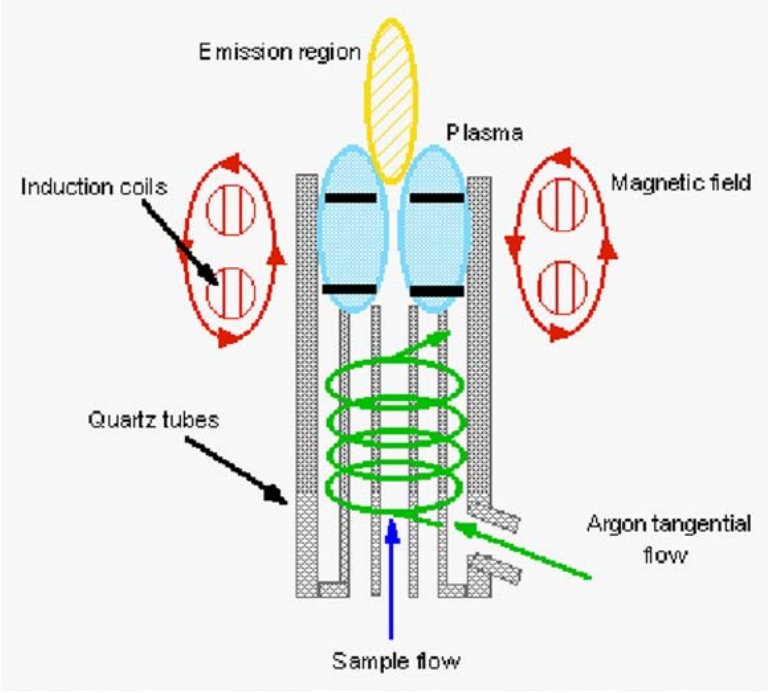

Figure 2.4: *Schematic of an ICP Plasma source (not to scale).*

Pneumatic nebulation is typically used. Blockage is usually overcome by using either cross-flow nubulizers or Babington-type nubulizers. Other nebulization methods include high solid nebulizers and electrothermal vaporizers. When the sample flows into the plasma, the atoms are excited by the high temperatures (6,000 - 10,000 ^{o}C). A longer resident time within the plasma is necessary for the detection limits for several elements. The resulting detection limits usually range from 1-10 ppb. The tip of the torch has a well defined tail, which contains all the excited analyte atoms. The ideal analysis region is just above the apex of the primary plasma cone and under the

base of the flame-like glow. This region is optimal for analysis, because the high background from the current-carrying part of the plasma is effectively excluded. Since there is no electrode contact in the plasma source, a simple background spectra with a high signal to noise ratio is created [20]. In this thesis, ICP spectrometry is used to detect the gold concentration in the blood serum.

2.7 Transmission electron microscopy (TEM)

Transmission electron microscopy is a very powerful technique to study size, shape, and morphology of the nanoparticles. It gives a real space image of atomic distribution in nanocrystals. It can provide atomic resolution lattice images and chemical information at spatial resolution of 1 nm or less than that [21]. Imaging system of TEM consists of objective lens and one or more projector lenses. Objective lens is heart of the transmission microscopes. It determines the degree of resolution in the image. It forms the initial enlarged image of the illuminated portion of the specimen in a plane that is suitable for further enlargement by the projector lens. The projector lens, as it implies, serves to project the final magnified image on the screen or photographic emulsion. The depth of focus provides the high magnification of the sample.

In TEM, a beam of accelerated electron interacts with an object in one of the two ways i.e. elastic scattering and inelastic scattering [22]. In elastic scattering, electron changes their path without loss of energy while loss of energy occur in the case of inelastic scattering due to an interaction of the incident electrons with the orbital electrons surrounding the nucleus of each atom in the object. Electrons which are not scattered by the object contribute positively to image while electrons which are deflected are unable to do so. As a result of this, differences in light intensity (contrast) occurs in the final image, which relate to areas in the object with different scattering potentials. This can be deduced by Rutherford's formula which describes the deflection potential of an atom is,

$$K = \frac{-e.eZ}{r^2} \text{ ……..……..(2.4)}$$

Where, K is deflection potential, e = electron charge, Z = positive charge and r = distance from electron to nucleus. Increase in atomic number leads to increase in scattering efficiency. Therefore heavy metal can form images with good contrast. All the TEM images presented in the thesis were recorded on a JEOL model 1200 EX instrument at an accelerating voltage of 120 kV. Samples for TEM have been made by drop coating the sample on the carbon coated copper grids and allowing the solvent to evaporate.

2.8 Thermo gravimetric analysis (TGA)

Thermal gravimetric technique is used to determine the thermal stability of given compound. It provides a quantitative measurement of weight loss associated with a temperature. In TGA, the sample is continuously weighed as it is heated to elevated temperatures. Samples are placed in a crucible or shallow dish that is attached to an automatic recording balance. The automatic null-type balance incorporates a sensing element, which detects a deviation of the balance beam from its null position. One transducer is a pair of photocells, a slotted flag connected to the balance arm, and a lamp. Once an initial balance has been established, any changes in sample weight cause the balance to rotate. This moves the flag so that the light falling on each photocell is no longer equal. The resulting nonzero signal is amplified and fed back as a current to a taut-band torque motor to restore the balance to equilibrium. This current is proportional to the weight change and is recorded on the y-axis of the recorder. The sample container is mounted inside quartz or pyrex housing, which is located inside the furnace. Furnace temperature is continuously monitored by a thermocouple whose signal is applied to the x-axis of the recorder. Linear heating rates from 50 °C to 100 °C are generally employed. All TGA measurements of the nanoparticle samples in the form of purified powders were recorded on a Seiko instruments model TG / DTA 32 instrument at a heating rate of 10 °C per minute.

2.9 Electrophoresis

Gel electrophoresis is the technique used to separate bio macromolecules such as nucleic acid or proteins on the basis of size, electric charge and other physical properties. In gel electrophoresis molecules are forced across span of a gel, motivated by an electrical current. Activated electrodes at either end of the gel provide the driving force. Mass, charge, size and electric field applied across electrodes determines the movement of molecules through a gelatinous medium. The gel is cast in the shape of thin slab with wells for loading of samples. The gel is immersed within an electrophoresis buffer that provides ions to carry a current and to maintain the pH at constant value [23].

Gel is composed of agarose or polyacrylamide. Agarose is a linear polysaccharide (average molecular mass about 12,000) made up of the basic repeat unit agarobiose, which comprises alternating units of galactose and 3,6-anhydrogalactose. Agarose is generally used at concentrations between 1% and 3%. Agarose gels are formed by suspending dry agarose in aqueous buffer, then boiling the mixture until a clear solution forms. This is poured and allowed to cool to room temperature to form a gel. Higher concentration of agarose makes the gel stiff. It is very easy to prepare and is non-toxic in nature. It is very fragile and can be easily destroyed by handling. Agarose gels have very large pore size and are used primarily to separate very large molecules with a molecular mass greater than 200 kDa. It has a large range of separation, but relatively low resolving power.

Polyacryamide is a cross linked polymer of acrylamide. The length of the polymer chain depends on concentration of acrylamide used which is generally between 3 to 30 %. The percentage of polyacrylmide can be controlled in a given gel to control the pore size between 5 to 2000 kDa. Polyacrylamide gels can be cast in a single percentage or with varying gradients. Gradient gels provide continuous decrease in pore size from the top to the bottom of the gel, resulting in thin bands. Because of this banding effect, detailed genetic and molecular analysis can be performed on

gradient polyacrylamide gels. Acrylamide is a potent neurotoxin and should be handled with care. Polyacrylamide has small range of separation with high resolution power [23]. In this thesis, agarose gel electrophoresis is used to determine the charge on the amino acid modified nanoparticles.

References:

[1] Atkins, P.W., physical chemistry ELBS Oxford 5th edition 1995

[2] Kelly, K.L.; Coronado, E.; Zhao, L.L.; Schatz, G.C. "The Optical properties of metal nanoparticles: the influence of size, shape, and sielectric sevironment" *J. Phys. Chem. B,* **2003**, *107,* 668.

[3] Ghosh, S. K.; Nath, S.; Kundu, S.; Esumi, K.; Pal, T. "Solvent and ligand effects on the localized surface plasmon resonance (LSPR) of gold colloids" *J. Phys. Chem. B*., **2004**, *108*, 13963.

[4] Harvey, D., Modern analytical chemistry chapter 10 Mc-Graw Hill higher education, **2000.**

[5] Hsu, C.P.S., "Handbook of instrumental techniques for analytical chemistry, infrared spectroscopy" chapter 15 Ed. Settle F.A. prentice hall New jersey

[6] Bardosova, M.; Tredgold, R. H.; Ali-Adib, Z. "Langmuir-blodgett films of docosylamine" *Langmuir*, **1995**, *11*, 1273.

[7] Ganguly, P.; Paranjape, D. V.; Sastry, M. "Novel structure of langmuir-blodgett films of chloroplatinic acid using n-octadecylamine: evidence for interdigitation of hydrocarbon chains" *J. Am. Chem. Soc.* **1993**, *115*, 793.

[8] Ning, G.; Guangfu, Z.; Shiquan, X. "An infrared spectroscopic study of the structural phase transition in the perovskite-type layer compound [*n*-$C_{16}H_{33}NH_3]_2CoCl_4$" *J. Mol. Struct*. **1992**, *275*, 85.

[9] Timasheff, S. N.; Fasman, G. D. Structure and stability of biological macromolecules, Marcel Dekker Inc; New York, **1969**

[10] Dong, A.; Huang, P.; Caughey, W. S. "Redox-dependent changes in .beta.-extended chain and turn structures of cytochrome c in water solution determined by second derivative amide I infrared spectra" *Biochemistry* **1992**, *31*, 182.

[11] Kumar, C. V.; McLendon, G. L. "Nanoencapsulation of cytochrome *c* and horseradish peroxidase at the galleries of α-zirconium phosphate" *Chem. Mater.* **1997**, *9*, 863.

[12] Templeton, A. C.; Chen, S.; Gross, S. M.; Murray, R. W. "Water-soluble, isolable gold clusters protected by tiopronin and coenzyme a monolayers" *Langmuir* **1999**, *15*, 66.

[13] Caruso, F.; Furlong, D. N.; Ariga, K.; Ichinose, I.; Kunitake, T. "Characterization of polyelectrolyte-protein multilayer films by atomic force microscopy, scanning electron microscopy, and fourier transform infrared reflection-absorption spectroscopy" *Langmuir* **1998**, *14*, 4559.

[14] Wanger, C.D.; Riggs, W. M.; Davis, L. E.; Moulder, J. F. ; Muilenberg, G. E. Handbook of X-ray photoelectron spectroscopy, Perkin Elmer Corp. Publishers, Eden.

[15] Carlson, T.A. "X-ray photoelectron spectroscopy" plenum publishing corporation New York **1975.**

[16] XPS instrumentation diagram is available online at http://augustus.scs.uiuc.edu/nuzzogroup/PPT/XPS%20Class%2099.PPT.

[17] XPS instrumentation is available online at http://www.iop.res.in/~dipakpk/IOP_XPS.html.

[18] Dam, T.K.; Brewer C.F. "Thermodynamic studies of lectin-carbohydrate interaction by isothermal titration calorimetry" *Chem. Rev.* **2002**, *102*, 387

[19] Chellani, M. Application Notes (ITC manual) 1999, 14.

[20] ICP instrumentation is available online at http://msewww.engin.umich.edu:81/people/smy/mse465_02/Haug%20HTML/How%20does%20it%20work.htm.

[21] Wang, Z.L. characterization of nanophase materials, Wiley-VCH weinheim,**2000**.

[22] Williams, D.B. "Transmission electron microscopy a textbook of material science" plenum press new york and London, **1996**.

[23] Gel elctrophoresis information is available on

http:// www. Bergen.org/AAST/projects/Gel/index

CHAPTER III

The Energetics of the Binding of Amino Acids to Gold Nanoparticles

In this chapter, binding of one basic amino acid i.e. lysine mono hydrochloride (lysine), and an acidic amino acid i.e. aspartic acid, with aqueous gold nanoparticles has been studied at physiological pH. Strong binding of aspartic acid with the gold nanoparticles under these conditions is indicated by ITC, while weak binding was observed in the case of lysine. The differences in binding are attributed to protonation of amine groups in lysine at physiological pH (pI ≈ 9.4) while they are not protonated for aspartic acid (pI ≈ 2.77). The binding of the amino acids with gold nanoparticles has been validated with other techniques such as gel electrophoresis, XPS, and TGA. An attempt has been made to design a model of adsorption of aspartic acid with gold nanoparticles and quantification of various thermodynamic parameters of aspartic acid-gold nanoparticles interaction.

Part of the work presented in this chapter has been published in the following article:

Joshi, H.; Shirude, P.; Bansal, V.; Ganesh, K. N.; Sastry, M. "Isothermal titration calorimetry studies on the binding of amino acids to gold nanoparticles" *J. Phys.Chem. B,* **2004**, *108,* 11535.

3.1 Introduction

Nanoparticles are potential candidates for numerous biological as well as chemical applications due to their exotic properties [1]. Gold nanoparticles are among the most studied nanoparticle systems and have a history dating back to at least around 150 years [2]. It is one of the most stable nanoparticles system. It has attracted considerable interest for the last few decades mainly due to size [3] and shape [4] dependent optical and electrical properties. They have been used in ceramics and glasses as a colorant [5]. The utility of the gold nanoparticles has also been shown in various applications such as catalysis [6], drug delivery [7], sensors [8], enzyme immobilization [9], and gold nanoparticles DNA assemblies [10] etc. However, gold nanoparticles cannot be used directly after synthesis for most of the applications due to incompatible surface characteristics of the nanoparticles. Therefore it becomes necessary to modify the surface of the nanoparticles with suitable ligands to make them application compatible [11]. Various protocols have been established to modify the surface of nanoparticles; for example, xanthates [12], disulfides [13], di-tri thiols [14], alkane thiols [15], amines [16, 17], isocyanides [18], acetone [19], iodine [20] etc.

Among the various ligands, thiols are well known to bind strongly to noble metals [15]. This might be because of multiple bond formation of sulfur with the surface of metal and soft character of Au and S [21]. Thiols chemisorb on noble metal surface in thiolate form. Chemisorption of alkanethiols may be via formation of Au (I) thiolate (RS^-) linkage. The reaction may be considered as oxidative addition of the S-H bond, followed by reductive elimination of hydrogen [22]. While thiol-mediated binding of ligands continue to be the chemistry of choice for gold nanoparticle surface modification, amine group containing ligands are attracting considerable interest. This is because amine groups can also bind to gold nanoparticles strongly [16, 17] and amine groups are present in most of the naturally occurring biomolecules.

Amphoteric nature of amino acid which can be used to alter the sign of charge on the nanoparticle surface [23], biocompatibility and ability to form peptide linkage

with other molecules of same class make them potential candidate for surface modification of nanoparticles. Amino acids like tryptophan [24], tyrosine [25], lysine [23] and aspartic acid [26] have been used to synthesize and modify the surface of nanoparticles. In these reports, it has been shown that amino acids interact with gold nanoparticles through amine group. In spite of this there is little information available about the interaction of gold nanoparticles with amino acids on fundamental level. In this chapter, the interaction between gold nanoparticles with amino acids has been investigated. More specifically, the binding of aspartic acid (pI ≈ 2.7) and lysine (pI ≈ 9.2) with aqueous gold nanoparticles as a function of pH has been studied. The complexation of these amino acids with gold nanoparticles has independently been characterized by X-ray photoemission spectroscopy, agarose gel electrophoresis, isothermal titration calorimetry and thermo gravimetric analysis. An attempt has been made to quantify these interactions with the help of ITC. The main aim of this work is to investigate the interaction of amino acids with gold nanoparticles. It has important implications for biomedical applications such as drug delivery, biological markers, cell imaging etc.

3.2 Synthesis of amino acid-capped gold nanoparticles

In a typical experiment, aqueous gold nanoparticles were synthesized by sodium borohydride reduction of chloroauric acid (10^{-4} M aqueous solution of $HAuCl_4$). 100 mL of 1 x 10^{-4} M concentrated aqueous solution of chloroauric acid ($HAuCl_4$) was reduced by 0.01 g of sodium borohydride ($NaBH_4$) at room temperature to yield a ruby-red solution of gold nanoparticles [27]. The ruby-red solution yielded an absorbance maximum at 518 nm. The gold nanoparticles solution was dialyzed in deionized water using a dialysis membrane (12 kDa cut off membrane) to remove the free borohydride ions and unreduced chloroaurate ions present in the solution. Gold nanoparticles solution was dialyzed until pH of the gold nanoparticles solution become 7. The dialyzed gold nanoparticles were capped by addition of 5 mL of an aqueous solution of 10^{-3} M lysine to 20 mL of the dialyzed gold nanoparticles solution. After the addition of lysine and ageing the gold nanoparticles solution for 12 h, this lysine-capped gold

nanoparticles solution (Au-lys) was again subjected to dialysis to remove uncoordinated lysine molecules. In a similar way, Au-lys at pH 11 (pH adjusted using 0.1 N KOH) and aspartic acid-capped gold nanoparticles solutions (Au-asp) were also prepared. To understand the effect of ligand concentration on charge of the nanoparticles, 1.5 mL of 10^{-3} M aqueous aspartic acid was added to 20 mL of the dialyzed gold hydrosol and the volume was made up to 25 mL with deionized water (partially aspartic acid capped gold nanoparticles with respect to aspartic acid capped gold nanoparticles mentioned in the first case). The volume of sodium borohydride reduced gold nanoparticle solution and amino acid-capped gold nanoparticle solutions were reduced by rotavapping at 72 mm pressure and at 60 ºC temperature prior to further analysis in gel electrophoresis experiments. Amino acid capped gold nanoparticles in powder form were prepared for thermo gravimetric analysis in similar manner as procedure mentioned for gel electrophoresis experiments.

3.3 UV-Visible spectroscopic analysis

Fig. 3.1 shows the UV-visible spectra recorded from the partially and fully aspartic acid-capped gold nanoparticles and lysine-capped gold nanoparticles at various pH values. Curve a in the Fig. 3.1 corresponds to the spectrum of the dialyzed gold nanoparticles solution obtained by sodium borohydride reduction of aqueous chloroauric acid; curves b and c are the spectra of gold nanoparticles solutions after partially and fully capping with aspartic acid, while curves d and e represent the spectra of lysine-capped gold nanoparticles in water at pH 7 and 11, respectively. A strong absorption in curve a at ca. 527 nm is observed that corresponds to excitation of surface plasmon vibrations in the gold nanoparticles. When the gold nanoparticles are capped with aspartic acid or lysine, a broadening and red shift of the surface plasmon band is observed (curves b-e), which indicates surface complexation of the amino acids and possibly some aggregation of the gold nanoparticles consequent to surface modification. Interestingly, the spectrum recorded from Au-lys nanoparticles at pH 11 shows greater broadening and red shift when compared with that of Au-lys

nanoparticles at pH 7. The interaction between aqueous gold nanoparticles and the various amino acids thus appears to be quite complex.

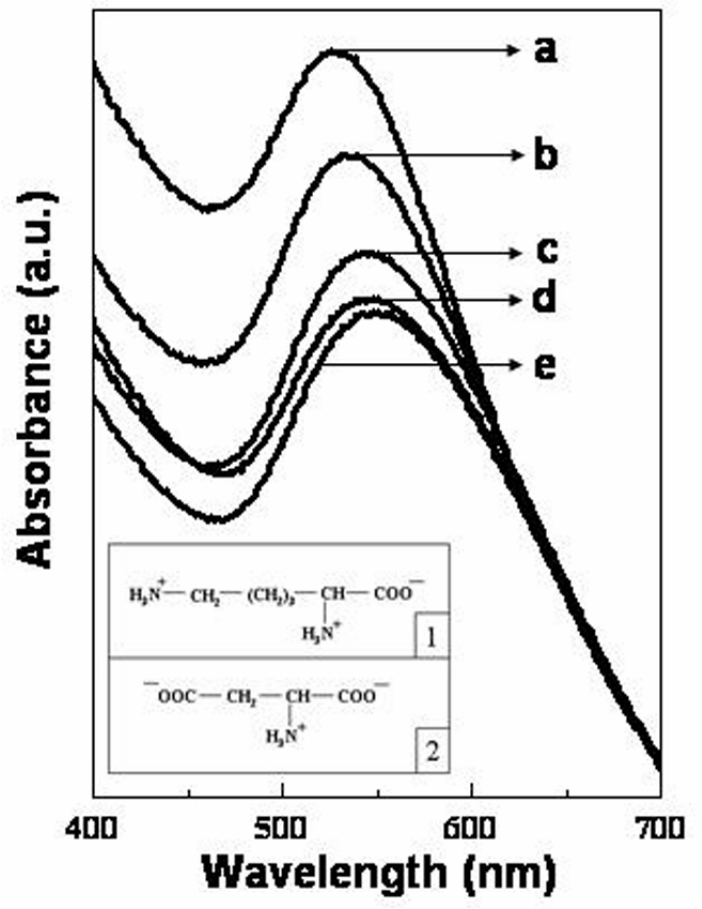

Figure 3.1: *UV-visible spectra recorded from dialyzed sodium borohydride-reduced gold (curve a), partially capped Au-asp (curve b), fully capped Au-asp (curve c), Au-lys pH 7 (curve d), and Au-lys pH 11 (curve e). Inset picture shows structure of 1. lysine 2. aspartic acid in zwitterionic form.*

3.4 Transmission electron microscopic analysis

The TEM images recorded from the as-prepared dialyzed sodium borohydride reduced gold nanoparticles, Au-asp (pH 7), Au-lys nanoparticles (at pH 7 and 11) are shown in Fig. 3.2 A-D, respectively. A comparison of the images shows that while the average shape of the particles is spherical and the overall size distribution is uniform in all the cases, the degree of aggregation of the particles is different in each of these experiments. The as-prepared sodium borohydride reduced gold particles are in close

contact after water evaporation (Fig. 3.2 A), as is to be expected from the fact that they are not stabilized with an amino acid.

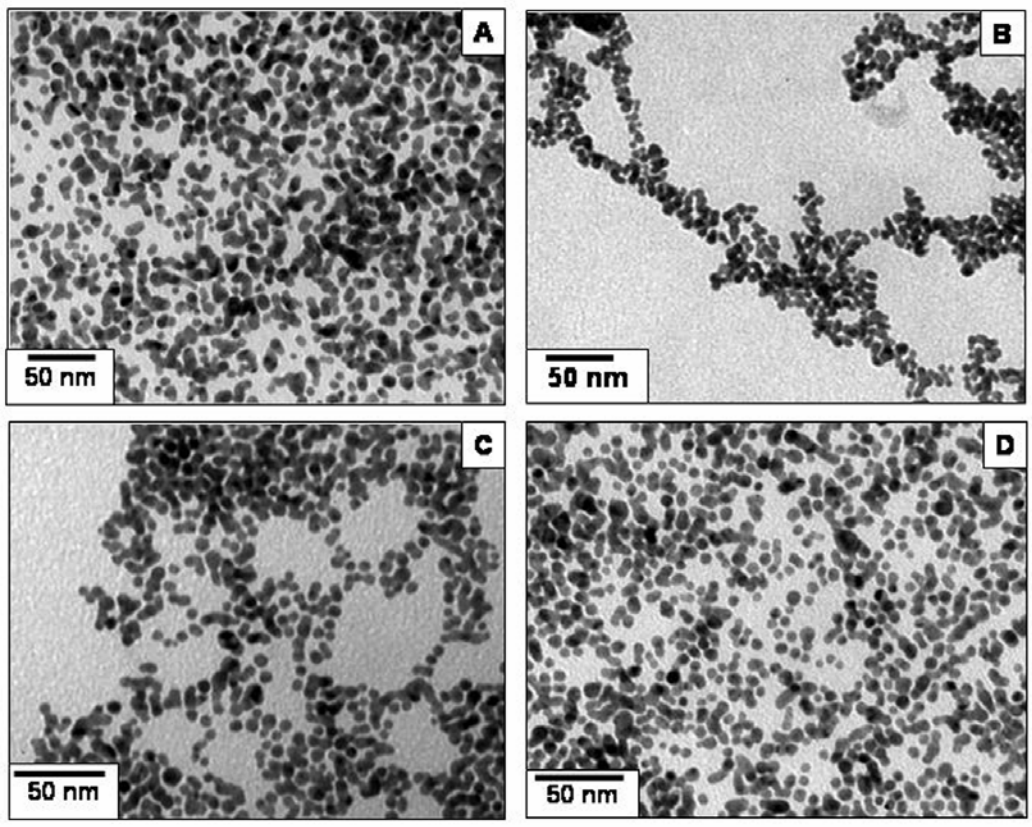

Figure 3.2: *Representative TEM images recorded from the as-prepared A) sodium borohydride-reduced gold nanoparticles; B) aspartic acid-capped gold nanoparticles; c) lysine-capped gold nanoparticles at pH 7 and D) lysine-capped gold nanoparticles at pH 11.*

The Au-asp and Au-lys (pH 7) nanoparticles appear to be assembled into open, string like structures (Fig. 3.2 B, 3.2 C) and would explain the broadening and shift in the surface plasmon band observed in the UV-vis measurements from these samples (Fig. 3.1). The extent of aggregation is maximum for Au-lys at pH 11 (Fig. 3.2 D), suggesting inter particle hydrogen bonding in this case.

3.5 Isothermal titration calorimetric analysis

ITC experiments were performed using a Micro-Cal VP-ITC instrument at 4°C. In different experiments, 300 µl of 0.25 x 10^{-3}, 0.5 x 10^{-3}, 1 x 10^{-3} M aqueous solutions of aspartic acid were injected in equal steps of 10 µl into 1.47 mL of dialyzed sodium

borohydride-reduced gold nanoparticle solution (pH 7) at time intervals of 3 min. Under similar conditions, 1 x 10^{-3} M aqueous solution of lysine was titrated against dialyzed gold nanoparticles (pH 7) with a time interval of 2 min between two consecutive injections. Since gold nanoparticles are not stable in buffer solution, buffer solutions were not used during this titration as demonstrated for metal ion-amino acid ITC experiments of an earlier study [28]. A background titration involving the identical titrant solution i.e. aspartic acid or lysine with only milli Q treated water in the sample cell, was subtracted from each experimental titration to account for the heat of dilution of these amino acids.

Fig. 3.3.1 to 3.3.4 show the calorimetric titration response of 0.25 x 10^{-3}, 0.5 x 10^{-3}, 1 x 10^{-3} M aqueous solutions of aspartic acid, and 1x10^{-3} M aqueous solution of lysine (in all cases pH of solution is 7) against dialyzed sodium borohydride-reduced gold nanoparticles respectively. Fig. 3.3.1 to 3.3.4 part A, correspond to the raw calorimetric data obtained during titration while part B corresponds to the integrated heat response obtained from the raw data plotted against the total volume of amino acid solution added to the reaction vessel containing the aqueous gold nanoparticles. Each negative peak shown in the heat signal curves from Au-asp (Fig. 3.3.1 A to 3.3.3 A) and Au-lys (Fig. 3.3.4 A) represents an exothermic process, which denotes the heat released in one injection of the aqueous amino acid into the gold nanoparticles solution as a function of time.

The integrated heat response in Fig 3.3.1 to 3.3.4 part B corresponds to binding isotherms of the amino acid on the gold nanoparticle surface. Unlike in other studies on the binding of two reacting species in solution (e.g. protein-metal ion reaction) where the binding isotherm can be directly plotted against the molar ratio of reactants in solution, the lack of accurate information on the exact surface area of the nanoparticles (i.e., number of moles of surface gold atoms) precludes plotting the binding isotherms against a molar ratio involving the amino acid and gold nanoparticles. Consequently, plots of binding isotherms against the total volume of amino acid added to the reaction cell have been chosen for analysis of energetic response.

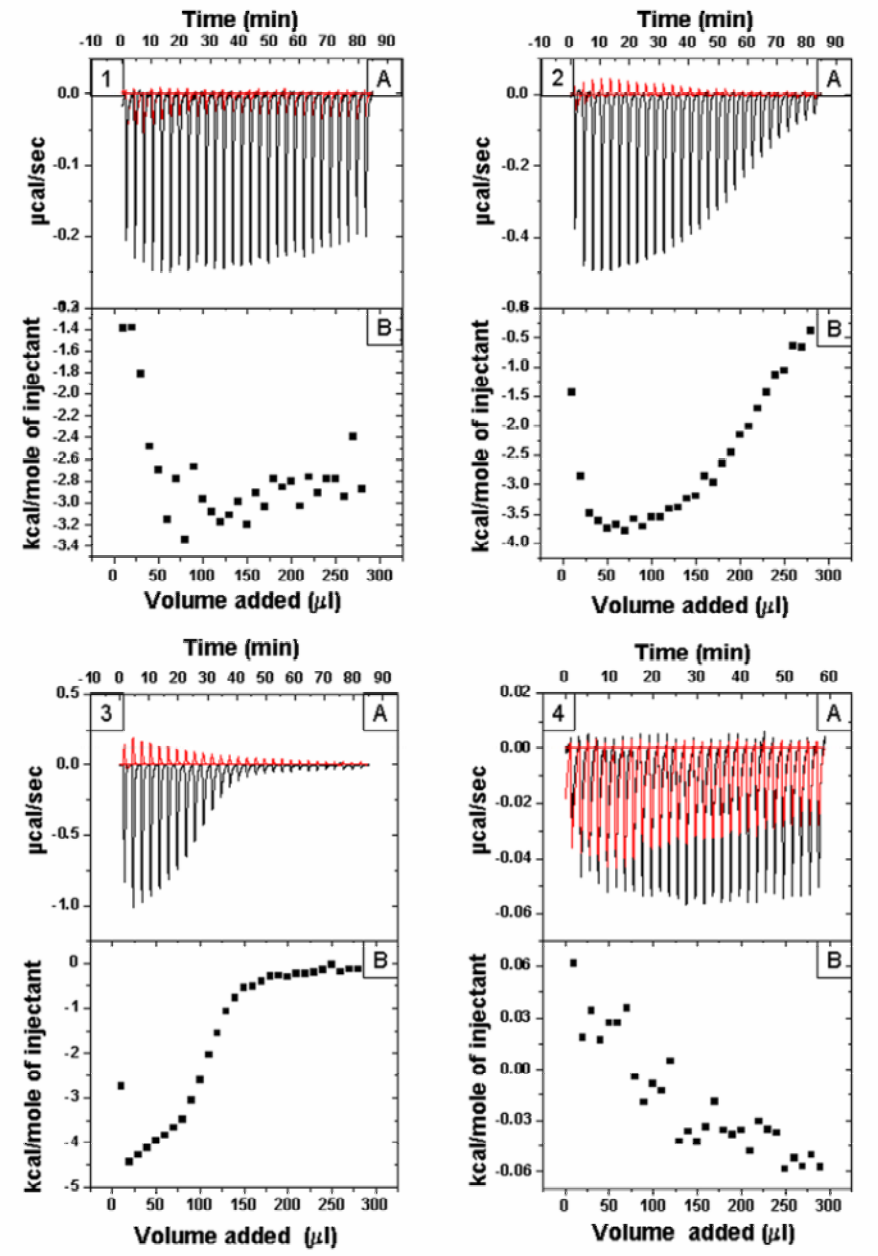

Figure 3.3: *ITC titration data describing the interaction of aspartic acid with gold nanoparticles at physiological pH. Panels 3.3.1 A, 3.3.2 A, 3.3.3 A, 3.3.4 A show the raw calorimetric data obtained during injection of 0.25 x 10 $^{-3}$, 0.5x10^{-3}, 1 x 10^{-3} aqueous aspartic acid solutions and 1 x 10^{-4}aqueous lysine solutions into the calorimetric cell containing 1.47 mL of aqueous gold nanoparticles solution, respectively. 3.3.1 B, 3.3.2 B, 3.3.3 B and 3.3.4 B show the integrated data of the curves in panels 3.3.1 A, 3.3.2 A ,3.3.3 A and 3.3.4 A respectively plotted as a function of total volume of the amino acid solution added to the reaction cell. Red curves corresponds to control experiment i.e. titration of aspartic acid with water.*

The exothermicity of the calorimetric peaks in Fig. 3.3.1 to 3.3.3 is believed to be due to the strong interaction between the gold nanoparticles and the amino acids. As the sites available on the surface of the gold nanoparticles become progressively occupied during titration, the exothermicity of the peaks decreases and eventually saturates. In all cases, strong binding of aspartic acid with the gold nanoparticles is indicated by the intense exothermic peaks during injection of the amino acid.

It is interesting to note that the number of injections required for achieving saturation of the gold nanoparticles surface by aspartic acid in the 0.5 x 10^{-3} M experiment is almost double that in the 1 x 10^{-3} M experiment, as would be expected on the basis of the number of available sites for binding and the number of binding molecules. These results clearly show that, while accurate quantitative information of the molar ratios of the reacting species is not known in these nanoparticles binding experiments, the trends are quite accurate and quantitative. Fig. 3.3.4 shows the calorimetric response of gold nanoparticles during reaction with 1 x 10^{-3} M lysine at pH 7. The data obtained shows a great deal of scatter with no discernible trend, this being more evident in the corresponding binding isotherm plot (Fig. 3.3.4 B). A comparison of the heats evolved during injection of lysine (Fig. 3.3.4) versus that obtained during reaction of gold with aspartic acid (Fig. 3.3.3) shows that the binding of lysine with gold nanoparticles at pH 7 is weak. It is well-known that amine functional groups bind strongly to gold nanoparticles; previous studies indicate that the strength of interaction is comparable to thiol binding with gold nanoparticles [29]. In the comparison between aspartic acid and lysine binding at pH 7 with gold nanoparticles, the only difference that could be identified as being responsible for the variation in the strength of binding of the amino acid with gold nanoparticles is the fact that the amine groups would be protonated in lysine at pH 7 (lysine pI ≈ 9.2) while aspartic acid exist in $-NH_2$ form (aspartic acid pI ≈ 2.77). Apparently, the amine groups bind strongly with gold nanoparticles only in the unprotonated state.

These measurements thus highlight an important criterion for binding of amine-functionalized ligands with gold nanoparticles and establish firmly that the nature of interaction with gold nanoparticles is quite strong. At this stage, it is not clear just what kind of bond is formed between the amine groups and the gold nanoparticles, but the nitrogen lone pair of electrons is clearly involved.The ITC measurements indicate strong binding of aspartic acid with gold nanoparticles at pH 7, while the interaction is considerably weaker for lysine under identical conditions. This does not, however, rule out the presence of lysine on the surface of the gold nanoparticles at pH 7 and it was therefore decided to estimate spectroscopically the relative amounts of aspartic acid at pH 7 and lysine on the gold nanoparticles at pH 7 and pH 11. Since at pH 11 lysine is non-protonated and is likely to bind with gold nanoparticles.

3.6 X-ray photoelectron spectroscopy measurements and analysis

Samples for XPS were prepared by drop-coating films of Au-asp (pH 7) and Au-lys (pH 7 and 11) solutions on Si (111) wafers and analyzing these films in a VG MicroTech ESCA 3000 instrument at a pressure of better than 1 x 10^{-9} Torr. Prior to XPS measurements of the Au-lys and Au-asp films, the solutions were dialyzed to remove uncoordinated amino acid molecules that could interfere with the measurements. The general scan, C 1s, Au 4f and N 1s core level spectra were recorded. The core level spectra were background corrected using the Shirley algorithm [30] and the chemically distinct species resolved using a non-linear least squares fitting procedure. For XPS analysis, the different core level binding energies (BEs) were referenced with respect to the Au $4f_{7/2}$ core binding energy of 84 eV. The films were sufficiently thick, and therefore, no signal was measured from the substrate (Si 2p core level). Fig. 3.4 A, C, E shows the Au 4f core level spectra recorded from Au-asp, Au-lys at pH 7 and Au-lys at pH 11 respectively. The Au 4f spectrum could be resolved into two spin-orbit pairs (spin-orbit splitting 3.68 eV for Au-asp, 3.708 eV for Au-lys at pH 7, and 3.670 eV for Au-lys at pH 11) with the two chemically shifted components having Au $4f_{7/2}$ BEs of 84 and 85.73 eV for Au-asp, 84 and 85.78 eV for Au-lys at pH 7, and 84 and 85.70 eV for Au-lys at pH 11.

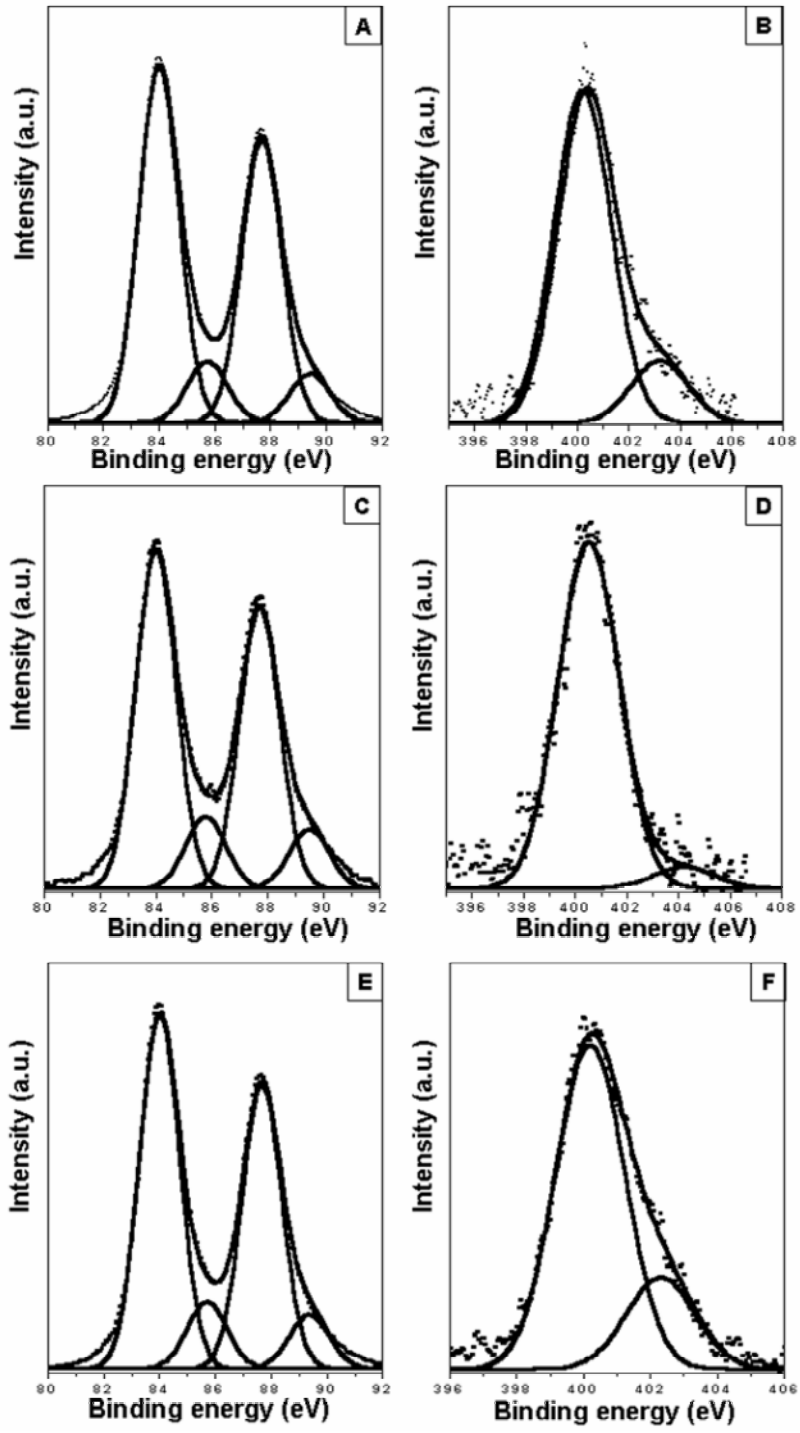

Figure 3.4: *Au 4f (panel A, C, E), N 1s (panel B, D, F) core level recorded from Au-asp pH 7 Au-lys pH 7 and Au-lys pH 11 respectively. The resolved components are shown as solid lines in the figure and are discussed in the text.*

The low BE component may be assigned to electron emission from Au^0, while the high BE component is attributed to $Au(III)Cl_4^-/Au(I)Cl_2^-$ ions bound to the surface of the gold nanoparticles [29]. The N 1s spectra recorded from, Au-asp, Au-lys at pH 7 and Au-lys at pH 11 are shown as in Fig 3.4 B, D, F respectively. The N 1s signal could be fitted to two components, a strong signal centered at 400.4 eV, 400.5 eV, 400.2eV BE and a much weaker peak at ca. 403.2 eV, 404.2 eV, 402.3 eV for Au-asp, Au-lys at pH 7 and Au-lys at pH 11 respectively . The low BE peak can be assigned to $-NH_2$ and $-NH_3^+$ groups in the two amino acids.

An interesting observation is that the intensities of the N 1s signal in the Au-lys samples at both pH i.e. pH 11 (Fig. 3.4 F) and pH 7 (Fig. 3.4 D) are quite similar and indeed quite comparable to the N 1s signal recorded from the Au-asp film (Fig. 3.4 B). Even though the ITC data indicated weak binding of lysine with gold nanoparticles at pH 7, XPS measurements clearly show the presence of lysine on the gold nanoparticles at concentrations comparable to lysine binding at pH 11. Another important observation is that high binding energy peak of N 1s in Au-asp at pH 7 and Au-lys at pH 11 is appreciably high as that of Au-lys at pH 7. This shift in the N 1s core binding energy level may be due to redistribution of charge on the 1s orbital electrons of nitrogen because of electron lone pair sharing of $-NH_2$ with Au I/III ions [29]. The combined ITC and XPS study clearly indicates that the interaction of lysine at pH 7 is weak, but still considerable immobilization of lysine occurs. These results indicate that there are two modes of binding of amine groups with gold nanoparticles and pH is the deciding factor for such differential binding. Such differential binding arises because the amine group present in the amino acid switches between the protonated and non-protonated form. Amine groups present in lysine at pH 11 exists in non protonated form, while at pH 7, lysine exists in the protonated form where no lone pair of electrons is available for bonding. Hence, when amine group is in the non protonated form (where lone pair of electrons are available), it binds to the gold nanoparticles through its lone pair of electrons, like co-ordinate bond. At pH 7 the amine group in lysine exists in the protonated form and thus has a positive charge.

In these conditions it binds electrostatically with the nanoparticles. Thus we believe that lysine is bound to the gold nanoparticles electrostatically at pH 7.It is known that sodium borohydride reduced gold nanoparticles are negatively charged at physiological pH due to surface bound $AuCl_4^-$/ $AuCl_2^-$ ions and lysine, which would be charged positively at pH 7, could complex electrostatically with the gold surface under these conditions. Weak electrostatic interactions would not be detected by ITC, and hence, as shown in the case of lysine binding at pH 7, caution must be exercised under conditions, where interactions are not detected by ITC.

Quantitative estimates of the N/Au ratios were made from the XPS measurements. The values obtained for the Au-asp (pH 7), Au-lys (pH 7), and Au-lys (pH 11) films are 0.0544, 0.0726, and 0.0486, respectively. Please note that the last two ratios have been divided by two to account for the two amine groups present in lysine as opposed to the one amine group in aspartic acid. As mentioned earlier, lysine is expected to electrostatically complex with the surface of gold nanoparticles. In the case of lysine binding at pH 11, the strength of the interaction indicates that it is like a covalent co-ordination bond, and therefore, it may be expected to be directional. This would impose steric constraints on lysine binding to the gold surface and therefore limit the coverage of lysine to less than optimum packing values. On the other hand, electrostatic interactions being non directional would not suffer from such limitations and could thus lead to higher coverage of lysine. This is at best a tentative explanation. The N/Au ratio in the Au-lys (pH 11) and Au-asp nanoparticle films are quite similar to each other, indicating roughly the same number of amino acid molecules bound to the surface in each case.

3.7 Electrophoresis measurements

If lysine is bound to the surface of the gold nanoparticles through electrostatic interactions at pH 7, then charge neutralization should occur. In a similar manner, controlling the coverage of aspartic acid on the gold surface would result in an effective variation in the surface charge. These hypotheses were tested by carrying out horizontal

gel electrophoretic measurements of the different amino acid-capped gold nanoparticles at physiological pH. The use of gel electrophoresis in nanoscience is relatively recent and has been applied to separate DNA-capped gold nanoparticles [31], and protein-capped gold nanoparticles [32]. Gel electrophoresis experiments were conducted in which 1% agarose gel was prepared in Tris Borate EDTA (TBE) buffer at pH 7.2 (Tris-0.02 M, Borate-0.1 M, EDTA-0.001 M). The concentrated solutions of dialyzed sodium borohydride-reduced gold nanoparticles, Au-lys at pH 7 and 11 and partially and fully capped Au-asp after rotavapping was loaded in the gel-wells. The samples were run under the effect of an electric field of 60 V in TBE buffer for 1 h and the gel image was recorded. During gel electrophoresis, charged nanoparticles may be separated on the basis of magnitude of the charge on their surface.

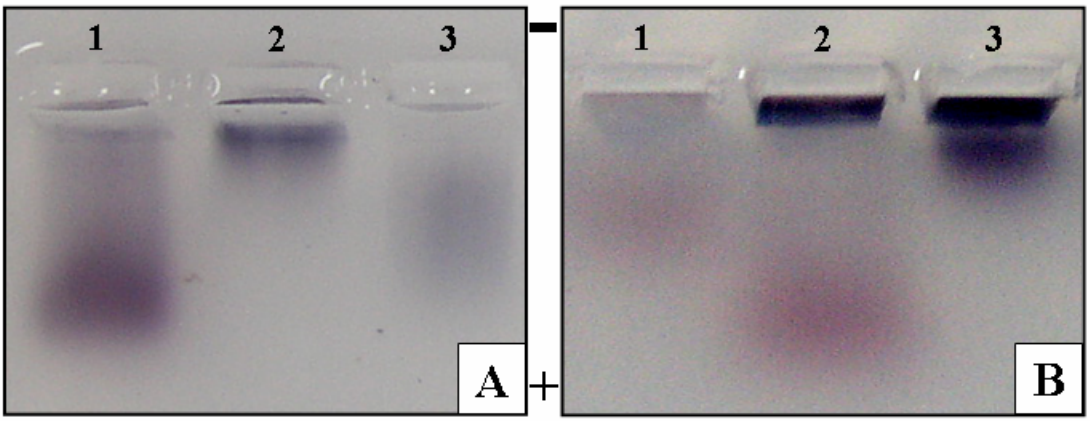

Figure 3.5: *Gel electrophoresis experiment showing the behavior of different charged gold nanoparticles under the effect of an electric field. Panel A shows Au-lys prepared at pH 11 (lane 1), Au-lys prepared at pH 7 (lane 2), and sodium borohydride-reduced gold nanoparticles (lane 3) run through the gel. Panel B shows partially capped Au-asp (lane 1), fully capped Au-asp (lane 2), and sodium borohydride-reduced gold nanoparticles (lane 3) run through the gel.*

When lysine-capped gold nanoparticles prepared at pH 7 and 11 were run through the gel along with sodium borohydride-reduced gold nanoparticles (after dialysis, Fig. 3.5 A), the Au-lys nanoparticles prepared at pH 11 (lane 1) showed significantly more mobility toward the anode than both the sodium borohydride-reduced gold nanoparticles (lane 3) and Au-lys prepared at pH 7 (lane 2).Indeed, there was little movement of the Au-lys at pH 7 sample, indicating almost complete

neutralization of the negative surface charge by the electrostatically bound lysine molecules. The larger electrophoretic mobility of Au-lys at pH 11 sample (lane 1) than sodium borohydride-reduced gold nanoparticles (lane 3) clearly indicates that the negative surface charge in the former case is much higher and arises from the carboxylate ions of lysine, while the smaller negative charge on the sodium borohydride reduced gold nanoparticles is due to surface bound $AuCl_4^-$ and $AuCl_2^-$ ions. Fig. 3.5 B shows the gel tracks obtained during electrophoresis of partially capped Au-asp (lane 1), fully capped Au-asp (lane 2), and as-prepared sodium borohydride reduced gold nanoparticles (lane 3). The Au-asp and sodium borohydride reduced gold nanoparticles move toward the anode, indicating that they are negatively charged. Furthermore, the fully capped Au-asp nanoparticles have a larger electrophoretic mobility (lane 2) than the partially capped sample (lane 1), as would be expected from the number of carboxylate ions in the amino acid bound through the amine groups to the surface. Thus, differences in surface charge due to variation in the coverage of ionized species on nanoparticle surfaces may be monitored quite easily in a standard gel electrophoresis setup.

3.8 Thermo gravimetric analysis

Thermo gravimetric analysis of aspartic acid, lysine, Au-lys at pH 7 and pH 11, Au-asp at pH 7 were carried out to study the binding strength of given amino acids with nanoparticles by measuring their desorption and decomposition temperature.Fig. 3.6 shows plot of TGA profiles recorded from weighed powders of aspartic acid, Au-asp at pH 7, lysine, Au-lys at pH 7 and at pH 11. In the TGA study of aspartic acid (Fig. 3.6 A), two sharp weight losses were observed between 235 to 288 °C temperature interval, 30 % weight loss occurred which was followed by the 44 % weight loss between 330 to 540 °C. TGA profiles of lysine shows similar trend, where again two weight loses were observed. Nearly 70 % weight loss was observed between the temperature range between 225-365 °C which was followed by 25 % weight loss between 470 to 590 °C. In both the cases the initial weight loss was attributed to the decarboxylation and was followed by complete decomposition of the amino acid.

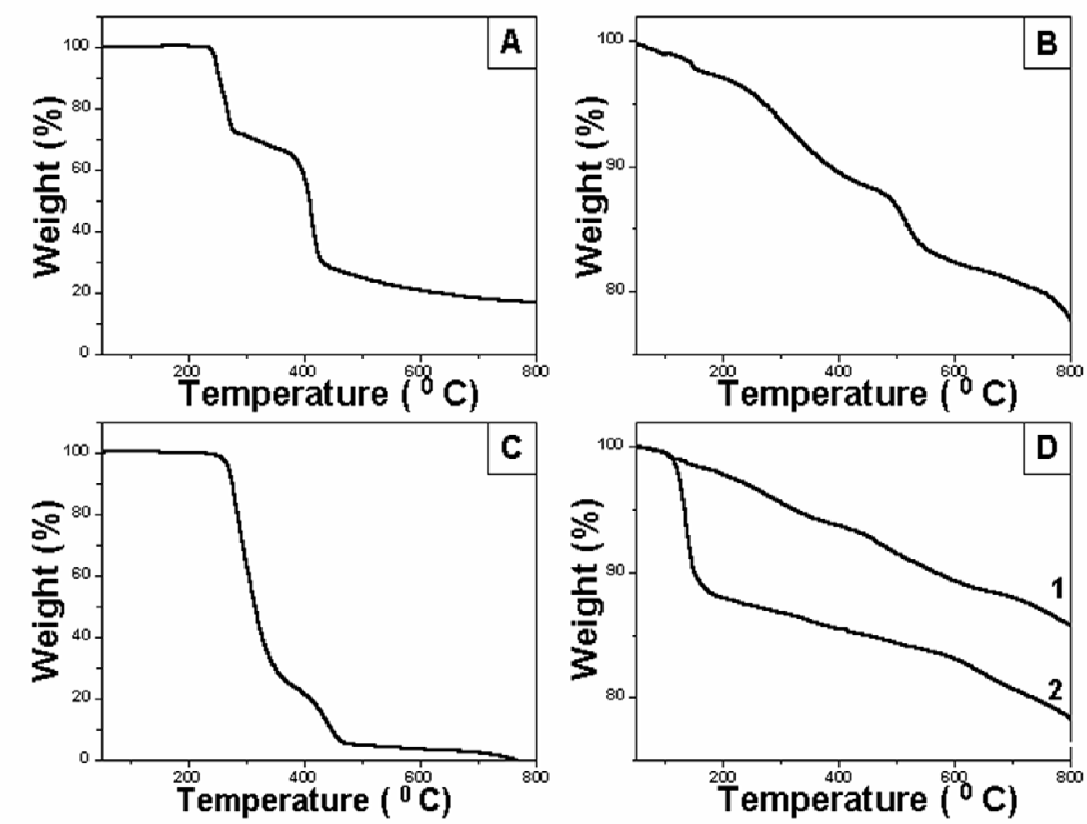

Figure 3.6: *TGA data recorded from carefully weighed powders of A) aspartic acid B) aspartic acid capped gold nanoparticles C) lysine D) lysine-capped gold nanoparticles at pH 11(curve 1) and at pH 7 (curve 2).*

Aspartic acid capped gold nanoparticles (Fig. 3.6) showed three weight losses at the temperature intervals between 150 - 350 °C (7%), 350-550 °C (8%) and 650-800 °C (5%). Lysine capped gold nanoparticles at pH 7 (Fig. 3.6 D, curve 2) showed two weight losses at the temperature intervals between 50-200 °C (12 %) and 500-700 °C (10%). Lysine capped gold nanoparticles at pH 11 (Fig. 3.6 D, curve 1) showed three weight losses at the temperature intervals between 50-350 °C (5%), 355-575 °C (6%) and 600-800 °C (5%). Initial two weight losses in all three cases are due to evaporation of water molecules trapped in the sample and decomposition of amino acid respectively. It is interesting to note that TGA profile of Au-asp at pH 7 and Au-lys at pH 11 are similar. The third weight loss in the case Au-asp and Au-lys at pH 11 is due to decomposition of aspartic acid or lysine bound to gold nanoparticles. Thus, the only

possible reason for this weight loss is strong co-ordinate bond between gold nanoparticles and amino acids.

3.9 The integral heat mode of isothermal titration calorimetry

Isothermal Titration Calorimetry (ITC) has emerged as a powerful diagnostic technique for mapping inhibitor-substrate [33], protein-protein [34], protein-ligand [35], drug receptor [36] interactions etc. The main feature of this method is that it concerns only with isothermal measurements of the said interactions by directly estimating the change in the heat content. Once this is done, by adoption of a simple physical picture, one can compute the equilibrium constant of the binding and the free energy change (ΔG) associated with the process [37]. It is then relatively straight forward procedure to estimate the entropy and enthalpy changes. This method can be also used to analyze conformational changes involved in the binding and changes in the profile of the hydrogen bonds *viz*. acceptor or donor types of interactions. In this part of the chapter, we have made an attempt to model the adsorption isotherm and also to measure the interaction between aspartic acid and gold nanoparticles.

3.9.1 Theory of isothermal titration calorimetry

We assume that heat response during the isothermal titrations is only due to binding of aspartic acid with gold nanoparticles. We adopt the following physical picture for the binding process (assumed to be reversible),

$$L + M \overset{K_A}{\rightleftharpoons} LM$$

Where, L, M represent the ligand (aspartic acid) and the gold nanoparticle respectively. If $[M]$represents the total number of sites (in molar units) and $[LM]$represents the bound moles, then we have, as per the well-known, langmuir-michaelis menton model (LMM) [38],

$$\frac{[LM]}{[M]_0} = \theta = \frac{K_A[L]}{1 + K_A[L]} \quad \text{.....(3.1)}$$

We adopt the symbols $\overline{H}$, $\bar{h}$, K_A for the molar integral heat and differential heat of binding and binding constant respectively. Since by definition, the molar integral heat is the added up heat from zero surface coverage up to the mean surface coverage θ (in other words fractional loading), we have,

$$\overline{H} = \frac{\int_0^{\theta} \bar{h} d\theta}{\int_0^{\theta} d\theta} = \frac{\int_0^{\theta} \bar{h} d\theta}{\theta} \quad \text{.....(3.2)}$$

If $\overline{H}^{obs}$ is the summed up integral heat observed after attaining a surface coverage (binding fraction) of θ, then we have,

$$\int \bar{h} d\theta = \frac{\overline{H}^{obs}}{\overline{H}} = \theta \text{ .....(3.3)}$$

Thus by noting $\overline{H}^{obs}$ equation 3.3 provides us a direct means of measuring the fractional loading of the receptor site θ.

In terms of the total surface atoms concentration (mmoles of nano particles/ litre), the above equation can be rewritten [39],

$$\overline{H}^{obs} = nC_R^0 \overline{H}\theta \text{ .....(3.4)}$$

Where n is the stoichiometric number associated with the binding process. As the definition implies, n can be only an integer viz. 1, 2, 3 etc and C_R^0 is the concentration of the receptors, i.e. gold nanoparticles in the present case. In actual practice, what is measured is the incremental heat h_i associated with the addition of the ligands at the i^{th} step through a micro syringe. Then all the $\bar{h}_i$ are summed up to the give the integral heat $\overline{H}^{obs}$ upto and after the i^{th} addition.

The most important experimental aspect of the ITC study is the variation of the $\bar{h}_i$ with molar ratio. The molar ratio represents the ratio of molar concentration of the ligands added to the titration cell to the moles of the receptor (gold nanoparticles) at any given instant. Mention may be made of the appropriate volume change corrections to be made, before any quantitative analysis is attempted.

The number of moles of ligands added up to i^{th} step (N_L^i) will be present in two forms, the bound and free forms, denoted respectively by the suffixes b, f respectively.

$$N_L^i = N_b^i + N_f^i \qquad (3.5)$$

The bound fraction to the receptor will be expressed in terms of the binding isotherm and the total number of receptor molecules (which undergoes only marginal change with dilution) remaining in the cell volume V_0, which is only calorimetrically sensed.

$$\theta = \frac{N_b^i}{N_R^i} = \frac{K_A C_L}{1 + K_A C_L^i} \qquad (3.6\ a)$$

$$C_L^i = \left(\frac{1}{K_A}\right)\left[\frac{\theta}{(1-\theta)}\right] \qquad (3.6\ b)$$

where, C_L^i, C_L denote the concentrations of the unbound aspartic acid and ligand molecules after ith addition respectively.

From simple mass balance, it also follows that,

$$N_L^i = V_0 C_L^i + N_R^i \theta \qquad (3.7)$$

Where, N_R^i total number of moles of the receptor i.e. gold nanoparticles.

Eliminating C_L^i, using equation 3.6 b, We finally have an expression for θ, which is directly related to the integral heat expression given by equation 3.4,

We also rearrange the equation 3.7 as

$$\frac{\theta}{(1-\theta)} + E_R\theta = E_L \qquad (3.8)$$

With the substitutions,

$$\frac{K_A N_R^i}{V_0} = E_R, \; \frac{K_A N_L^i}{V_0} = E_L, \; C_L^i = \frac{N_L^i}{V_0}, \; C_R^i = \frac{N_R^i}{V_0}$$

Finally we get a quadratic equation for the θ,

$$(1 + E_L + E_R)\theta - E_R\theta^2 - E_L = 0 \qquad (3.9)$$

Only one root of the above equation is meaningful, i.e. which corresponds to θ, and finally we get the simple expression for θ:

$$\theta = \frac{\left\{(1 + E_L + E_R) - \left[(1 + E_L + E_R)^2 - 4E_L E_R\right]^{0.5}\right\}}{2E_R} \qquad (3.10)$$

This result is analogous to the expression given in ref [40] even though the functional form is slightly different. The integral heat $\overline{H}^{obs}$ is directly proportional to the mean surface coverage θ , after assuming that all the receptor sites have the same binding energy (there are many experimental systems where this may be invalid).

Fig. 3.7 gives S type ITC curves for the addition of the 0.25 x 10^{-3}, 0.5 x 10^{-3}, 10^{-3} M of the ligand to a cell containing the gold nanoparticles solution. Since the surface area of gold nanoparticles is unknown, the surface coverage θ (or in other words the fractional loading)[c.f. equations 3.6 a, 3.6 b] is expressed in terms of the moles of gold nanoparticles in the volume V_0. V_0 is fixed at 1.47 mL in all our studies.

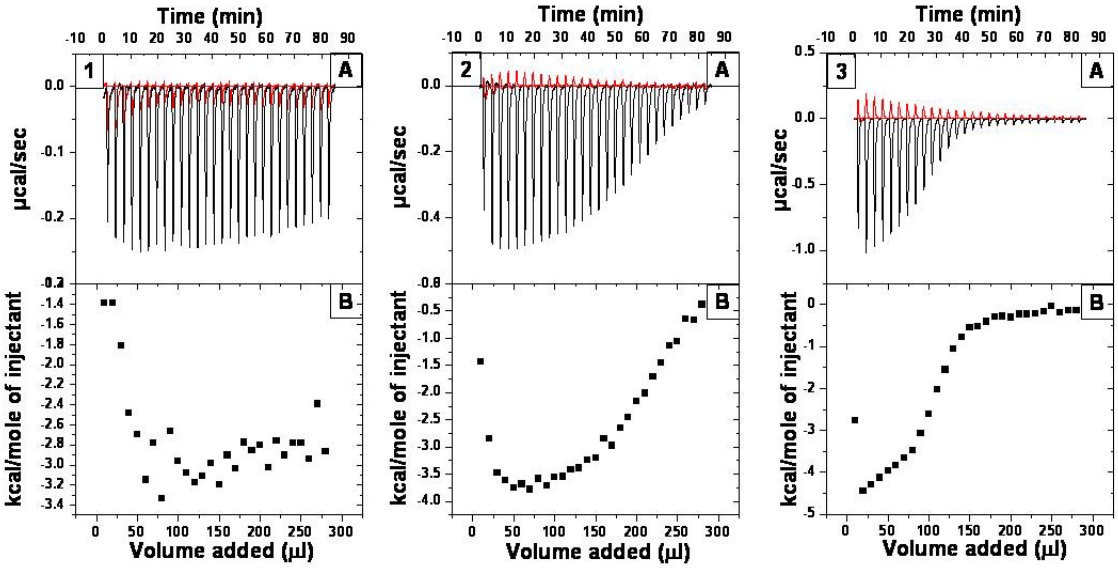

Figure 3.7: *ITC titration data describing the interaction of aspartic acid with gold nanoparticles at physiological pH. Panels 7.1A, 7.2 A, 7.3 A show the raw calorimetric data obtained during injection of 0.25 x 10 $^{-3}$M, 0.5x10^{-3}M, 1 x 10^{-3} M aqueous aspartic acid solutions into the calorimetric cell containing 1.47 mL of water (red) as control experiment and gold nanoparticle solution (black), respectively. 7.1B, 7.2 B, 7.3 B show the integrated data of the curves in panels 7.1A, 7.2 A and 7.3 A respectively plotted as a function of total volume of the amino acid solution added to the reaction cell. Integrated data in panel B is subtracted from aspartic acid solvation energy (All plots in this figure are identical to those shown in Fig. 3.3).*

What we need to do is to compute the H^{obs}, by integrating the area under the curve. Notice the sigmoid nature of the binding curve, which implies a fairly large product of the binding constant (panel 3.7.2 B and 3.7.3 B)with the total receptor molecules i.e.

$$K_A N_0^R >> 1$$

Fig. 3.7 B gives typical integral heat $\overline{H}^{obs}$ curve as a function of the injection number. Notice the characteristic dip in the $\overline{H}^{obs}$ Vs volume of the ligand added. To compute the total integral heat evolved up to a given i^{th} injection a simple interpolation between successive points was done so as to give accurate estimates of $\overline{H}^{obs}$. The surface coverage calculated by taking ratios (c.f. equations 3.2, 3.3) were reproducible,

and a detailed interpolation between successive points was unnecessary. Thus we have $\overline{H_i}^{obs}, \theta_i$ profile for further analysis.

At this juncture a detailed non-linear estimation may be employed for determining K_A, n, $\overline{H}$ etc. A down-hill Simplex method may be advantageous and employed for parameter estimation. Marquardt's method works and also sometimes fails for many data sets. It was also found that in many cases, the confidence interval of the estimates were poor to make the numerical values of the binding parameter K_A, n etc meaningful.

3.9.2 Ionic equilibrium among the various species of aspartic acid

It is observed that even though aspartic acid is a weak dibasic acid, it can ionize to a significant extent. Besides, it has also an amine group, which can be protonated. There is some evidence that the unprotonated $\sim NH_2$ group contributes to a significant extent in the enthalpy of binding. Therefore it is very important to calculate to analyze the detailed ionization equilibrium and quantitatively estimate the mole fraction of the various ionic forms of aspartic acid.

We consider the ionization of the carbonyl groups first. Each of these species (see top layer) can in turn be protonated to the corresponding $\sim NH_3^+$ form. Ideally speaking, we have to consider 8 molecular species in all, with one type corresponding to the completely uncharged molecule. However in the present study, we are considering only the 5 most predominant species (Fig. 3.8).

A simplification is further made that the state of ionization of the carboxyl groups (α, β) does not depend on the state of protonation of the amine group. Likewise, it is presupposed that the equilibrium of the protonation step of the amine group is unaffected by the state of ionization of the carboxyl groups. Let $[H_2A]$, $[HA^-]$, $[A^{2-}]$ denote the concentrations of the unionized, singly and doubly ionized aspartic acid molecules respectively. $[RH^+]$ Symbolizes the total concentration of the protonated

form of each of these species summed up together, i.e. protonation of $[H_2A]$, $[HA^-]$, $[A^{2-}]$ at the amine group .

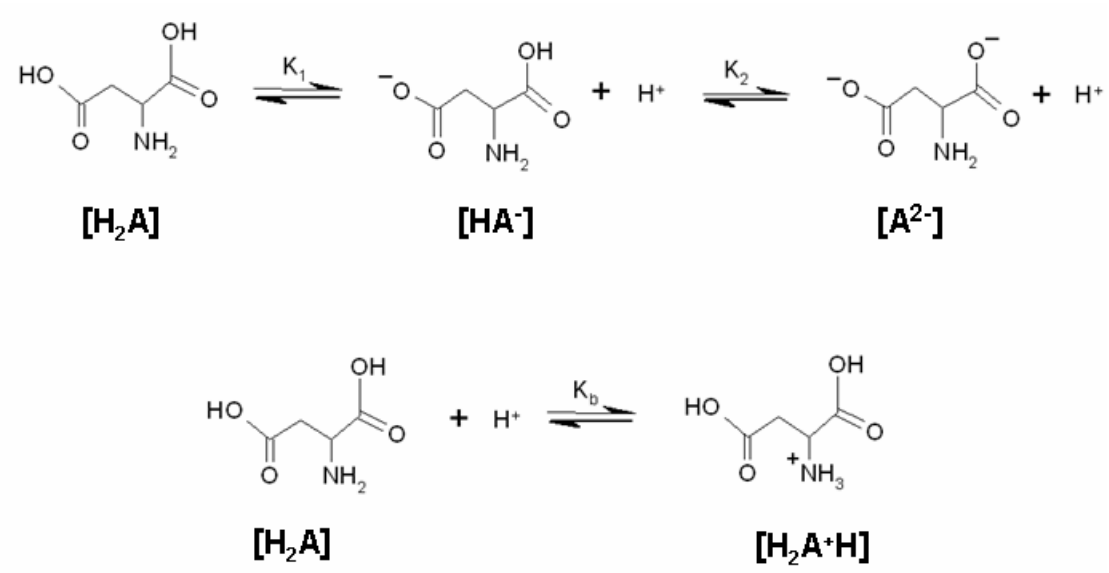

Figure 3.8: *Scheme shows various ionized forms of aspartic acid at a given pH.*

This finally enables us to write all the ionization steps (carboxyl groups releasing protons) as two equilibria and the amine protonation step as one equilibrium step (see Fig. 3.8, lower layer)

Based on the above discussion, we have,

$$H_2A \xleftrightarrow{K_1} [HA^-] + [H^+]$$

$$K_1 = \frac{[HA^-][H^+]}{[H_2A]} \quad \ldots\ldots\ldots\ldots\ldots\ldots\ldots\ldots\ldots\ldots\ldots\ldots .(3.11)$$

$$[HA^-] = \frac{K_1[H_2A]}{[H^+]} \quad \ldots\ldots\ldots\ldots\ldots\ldots\ldots\ldots\ldots\ldots\ldots\ldots\ldots\ldots\ldots\ldots\ldots\ldots(3.12)$$

$$[HA^-] \xleftrightarrow{K_2} [A^{2-}] + [H^+] \ldots\ldots\ldots\ldots\ldots\ldots\ldots\ldots\ldots\ldots\ldots\ldots\ldots\ldots\ldots\ldots\ldots\ldots(3.13)$$

$$K_2 = \frac{[A^{2-}][H^+]}{[HA^-]} \quad \ldots\ldots\ldots\ldots\ldots\ldots\ldots\ldots\ldots\ldots\ldots\ldots\ldots\ldots\ldots\ldots\ldots\ldots .(3.14)$$

Considering the above equilibria together, we have,

$$\left[A^{2-}\right]=\frac{K_1K_2\left[H_2A\right]}{\left[H^+\right]^2} \quad \text{(3.15)}$$

Now let us denote the molecules with $\sim NH_2$ group protonation as $\left[R-H^+\right]$ and remaining molecules as $\left[R-H\right]$, then we have,

$$\left[R-H\right]+\left[R-H^+\right]=\left[H_2A\right]^0=C^0 \quad \text{(3.16)}$$

Where $\left[R-H\right]$ denotes all the species $\left[H_2A\right]$, $\left[HA^-\right]$, $\left[A^{2-}\right]$ with the $\sim NH_2$ group unprotonated.

By definition, we have,

$$K_b=\frac{\left[R-H^+\right]\left[H^+\right]}{\left[R-H\right]} \quad \text{(3.17)}$$

$$\left[R-H\right]=\left[H_2A\right]+\left[HA^-\right]+\left[A^{2-}\right] \quad \text{(3.18)}$$

Eliminating $\left[R-H\right]$ using equation 3.17 we have after combining with equation 3.16,

$$\left[R-H\right]=\frac{C^0}{\left(1+K_b\left[H^+\right]\right)} \quad \text{(3.19)}$$

$$\left[R-H^+\right]=\frac{C^0K_b\left[H^+\right]}{\left(1+K_b\left[H^+\right]\right)} \quad \text{(3.20)}$$

All other species have to be expressed as function of the $\left[H_2A\right]$, $\left[H^+\right]$ using equation 3.11 to 3.15 and then written as a function of the C^0 - total concentration of aspartic acid, K_1, K_2, K_b and $\left[H^+\right]$ i.e. pH.

We give the final results:

$$\left[H_2A\right]=\frac{C^0}{\Delta} \quad \text{(3.21)}$$

$$\Delta = \frac{K_1 K_2}{\left[H^+\right]^2} + \frac{K_1}{\left[H^+\right]} + 1 \quad \text{.....(3.22)}$$

$$\left[HA^-\right] = \frac{\frac{C^0 K_1}{\left[H^+\right]}}{\Delta} \quad \text{..... (3.23)}$$

$$\left[A^{2-}\right] = \frac{\frac{C^0 K_1 K_2}{\left[H^+\right]^2}}{\Delta} \quad \text{.....(3.24)}$$

The important point to be noted is that the aspartic acid concentration is quite low initially, so as to affect the pH. As subsequent aliquots are added, the aspartic acid concentration rises and the pH fall. In order to determine the actual pH resulting from the interplay of all these equilibria, we employ in addition, the charge balance condition,

$$\left[H^+\right] + \left[R - H^+\right] = \left[HA^-\right] + 2\left[A^{2-}\right] \quad \text{.....(3.25)}$$

or after using equation 3.19,

$$\left[H^+\right] + \frac{C^0}{\left(1 + K_b\left[H^+\right]\right)} = \frac{\left[\frac{C^0 K_1}{\left[H^+\right]} + \frac{2C^0 K_1 K_2}{\left[H^+\right]^2}\right]}{\Delta} \quad \text{.....(3.26)}$$

This gives an implicit equation for the $\left[H^+\right]$, (equation 3.26) which has to be numerically solved for $\left[H^+\right]$ as a function of C^0, K_1, K_2, K_b. Dissociation constants of aspartic acid taken for calculations are K_1 = 7.94 x 10^{-3}, K_2 =1.3803 x 10^{-4} and K_b = 6.606 x 10^{-5}. Once the $\left[H^+\right]$ determined, it is a straightforward exercise to compute the fractions of $\left[R - H^+\right]$, $\left[HA^-\right]$, $\left[A^{2-}\right]$ using equation 3.19, 3.20 and 3.21 to 3.24.

We use a standard package employing Mueller's iteration method for the numerical computations [41]. Prime objective behind the detail calculations mentioned

previously was to show that the unprotonated NH_2 group concentration is appreciable and therefore gives rise to significant binding with gold nanoparticles.

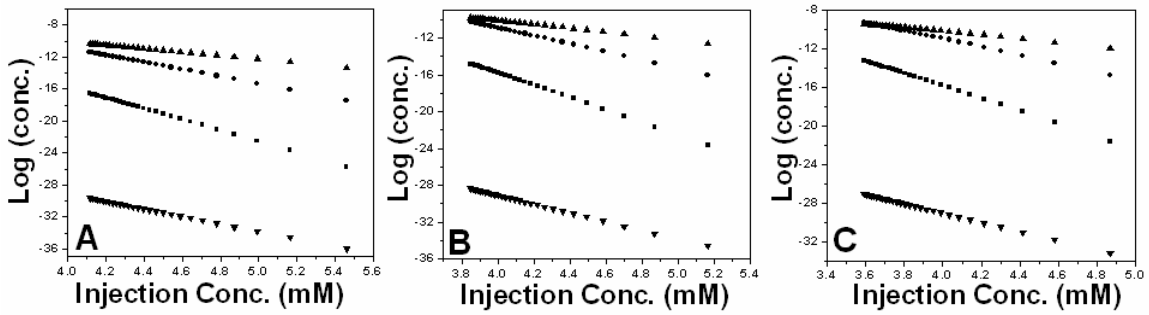

Figure 3.9: *The concentration of all the various ionic forms of aspartic acid of A) 0.25 x 10^{-3}M, B) 0.5x10^{-3} M, C)1 x 10^{-3}M in a blank experiment (without the gold nanoparticles solution) as function of the pH.* ▼$[H_2A]$ *aspartic acid,* ■$[HA^-]$ *singly ionized aspartic acid,* ●$[A^{2-}]$ *doubly ionized aspartic acid,* ▲ *zwitterionic form.*

Fig. 3.9 show how the concentration of all the ionic fractions of aspartic acid varies as function of aspartic acid concentration in the aqueous medium. We recall that with the progressive addition of aspartic acid results in considerable pH drop and theirby various ionic equilibria affected to a significant extent.

3.9.3 Determination of thermodynamic parameters

As mentioned above since the various ionic species exist simultaneously during the titration of aspartic acid with gold nanoparticles, it is necessary to understand the solvation effects of aspartic acid. The heat released or absorbed has to be corrected for in a blank experiment (without gold nanoparticles) involving the addition of aspartic acid to the ITC cell. The over all steps involved during the solvation can be visualized as follows:

$$H_2A + H_2O \xrightarrow{\Delta H_1} H_2A \cdot H_2O$$

$$H_2A \xleftrightarrow{K_1,\Delta H_2} HA^- + H^+$$

$$[HA^-] + [H^+] + H_2O \xrightarrow[\Delta H_3]{} [HA^-] \cdot nH_2O + [H^+] \cdot mH_2O$$

$$HA^- \xleftrightarrow{K_2,\Delta H_4} A^{2-} + [H^+]$$

$$A^{2-} + H^{+} + (r+s)H_2O \xrightarrow{\Delta H_5} \left[A^{2-}\right] \cdot rH_2O + \left[H^{+}\right] \cdot sH_2O$$

The enthalpy of the overall process will be given by the algebraic sum of all the individual enthalpies of the process,

$$\Delta H^{total\ soln} = \Delta H_1 + \Delta H_2 + \Delta H_3 + \Delta H_4 + \Delta H_5 \quad \text{.....(3.27)}$$

It is implied that the electrostatic interactions can also be included (viz.a simple Born hydration model [38] in these individual enthalpies. It is not possible to individually estimate the various ΔH_i, nor is it necessary. The experimental procedure gives the sum of the overall heats ΔH^{total} after every aliquot of aspartic acid has been added. Initially, a few additions can have $\Delta H^{total} < 0$, which can change sign as more and more aspartic acid is added. Besides on the basis of the ionic euqilibria discussed previously, the pH of the solution may drop appreciably, resulting in the redistribution of the various ionized species.

The Fig. 3.7.1 A- 3.7.3 A describes the evolution of heat as a function of the amount of aspartic acid added (in red), for various concentrations of aspartic acid. From the slope of the graph of the integral heat Vs solvated molar fraction (Fig. 3.10), we get the molar integral heat of solution (averaged overall additions) which is presented in table 3.1.

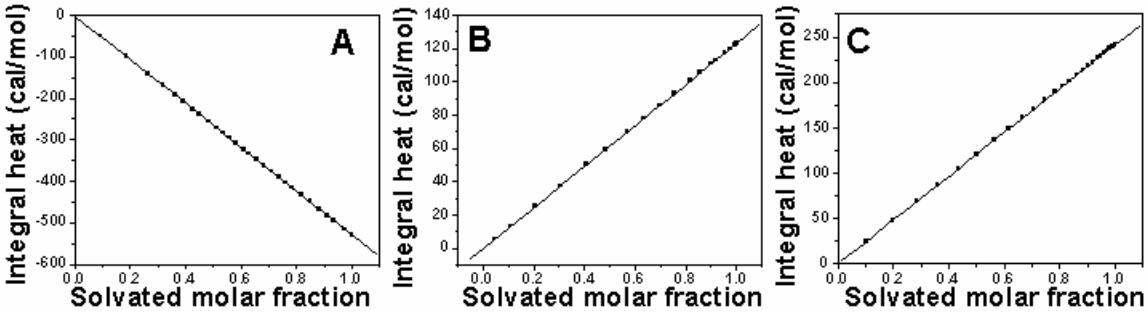

Figure 3.10: *Solvation enthalpies of aspartic acid of A) 0.25 x 10^{-3}M, B) 0.5x10^{-3} M and C) 1 x 10^{-3}M.*

At the lowest concentration of the aspartic acid, the heat of solution is largest and negative, signaling the full ionization of the aspartic acid and solvation. At higher

concentration, the heat becomes progressively endothermic, implying less ionization of the aspartic acid. It is not clear, as to why the change in sign of the solvation energy occurs at high concentrations.

Table 3.1: Molar integral heats of solution for aspartic acid

Conc. of aspartic acid mM	Heats of solution cal/mole *
0.25	-530
0.5	-123
1	242

* The uncertainties of the integral heat values are very small and ignored

Using the same procedure employed previously for calculating the molar integrals of solvation, the heats of binding of aspartic acid to gold nanoparticles can be estimated. The integral heat is found out by summing overall, the individual heats, till the heat evolved per i^{th} pulse is almost zero.

This obviously corresponds to saturation i.e. θ=1, and also equals the overall molar integral heat up to the last of the pulses. The fractional loading at any i^{th} pulse can be estimated as the ratio of the heat summed up to the i^{th} pulse divided by the total integral heat.

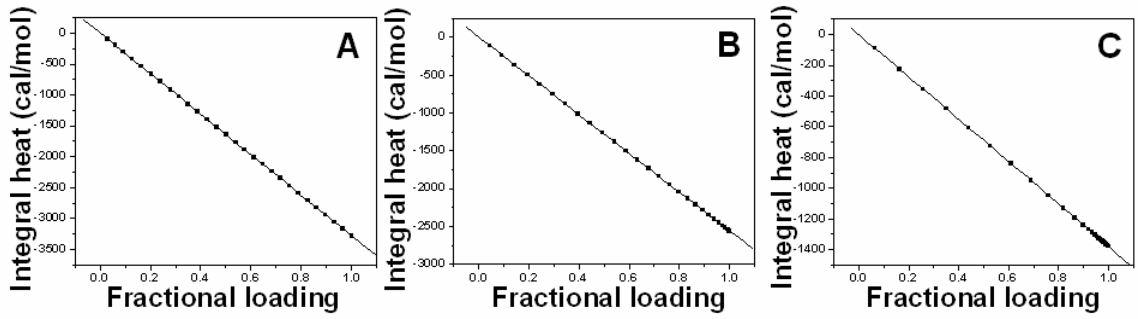

Figure 3.11: *Heat evolved during fractional loading of gold nanoparticles by A) 0.25 x 10^{-3}M, B) 0.5x10^{-3} M C)1 x 10^{-3}M concentration of aspartic acid (since exact surface area is not known surface coverage units are arbitrary).*

Fig. 3.11 displays the integrated heat evolved during the binding of aspartic acid to the gold nanoparticles. Since the graph is a perfect straight line it is evident that the

binding isotherm is linear. The fractional loading and the free aspartic acid concentration have been evaluated using equation 3.4. An examination of Fig. 3.12 further shows that the binding isotherm is indeed linear and should be also reflected in the values of binding constants. The binding constants are computed by fitting a least square line to the surface coverage versus ligand concentration plot and using relation given in equation 3.6 b. An analysis of Table 3.2 shows that binding constants are of the order of 10^4 which further confirm our hypothesis. In all these cases, the residuals are very small, suggesting an excellent linear fit over four fold concentration variation of the aspartic acid.

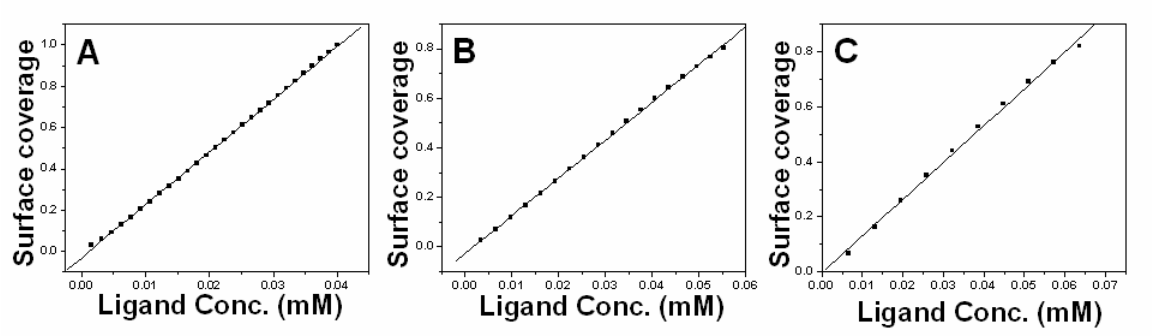

Figure 3.12: *Surface coverage of nanoparticles by A) 0.25 x 10^{-3}M, B) 0.5x10^{-3} M C)1 x 10^{-3}M concentration of aspartic acid. Notice the excellent linear fits implying a linear isotherm.*

From Table 3.2, it is described that as the pH decrease, the extent of protonation of the NH_2 group proportionally increases, as a result of which, the binding progressively decreases.

Table 3.2: Binding constants for the linear isotherm for the aspartic acid-gold nanoparticles system at 277 K

Conc. of aspartic acid mM	K_A mol/litre	Residual
0.25	(24.5±0.127) x 10^3	0.0163
0.5	(15.3±0.0853) x 10^3	0.0141
1	(13.3±0.12) x 10^3	0.0151

This is also reflected in the binding constants. Thermodynamic parameters such as entropy and free energy were calculated with the help of equations given below.

$$\Delta G^0 = -RT \ln K_A \quad \text{.....(3.28)}$$

$$\Delta G^0 = \Delta H^0 - T\Delta S^0 \quad \text{.....(3.29)}$$

where, $\Delta G^0, \Delta H^0, \Delta S^0$ denote the standard free energy change, enthalpy and entropy respectively.

Table 3.3: Thermodynamic parameters of the binding aspartic acid with gold nanoparticles system at T=277 K

Conc. Of aspartic acid (mM)	ΔG **kcal/mol**	ΔH **kcal/mol**	$\Delta S / R$ **e.u.**
0.25	-5.56±0.03	-3.281±1e^{-3}	4.145±0.0005
0.5	-5.303±0.003	-2.467±1e^{-3}	5.15±0.0001
1	-5.226±0.005	-1.379±1e^{-3}	6.99±0.007

We also recall that with the successive additions, the pH of the solution drops appreciably, and then zwitterions may be present. Since the isoelectric point of aspartic acid is $\approx$ 2.77. We would expect significant protonation of aspartic acid only below this pH.

Table 3.2 and 3.3 give the relevant heats and other thermodynamic parameters of the systems. Even though the binding constants differ by 50%, the free energies of binding (affinities) at the best differ only by a few percent. The heats of binding, which progressively become less negative has a direct correlation with the magnitude and sign of the heats of solution (Table 3.1).

The entropies of binding are all positive and increases substantially as aspartic acid concentrations are increased. There is a difference of almost ($\Delta S^0 \cong 3$ cal /deg/mole) between the entropies of the binding at the lowest and highest

concentrations. This may be qualitatively interpreted as effects of desolvation on binding of Aspartic acid to gold nanoparticles. A plausible explanation is as follows: At increasing concentrations of aspartic acid, the fraction of charged species increases. These will have coordinated water molecules associated with them, which themselves form a network of hydrogen bonds. Upon binding to gold nanoparticles these hydrogen bonds of aspartic acid are broken resulting in a large release of entropy. Due to the restriction of the hydrogen bond, we accept that, this is a tacit explanation in the absence of direct spectroscopic information on the charged species of the aspartic acid and gold nanoparticles complex, no other interpretation is available.

A DFT calculation is reported for the solvation of L-aspartic acid with water, and other protic solvents, [41] but quantitative comparison are strictly not possible, as energies of solvation are not presented.

3.10 Conclusion

The study of the binding of lysine and aspartic acid as a function of solution pH indicates that the amino acids bind to the gold particles strongly, provided the amine groups are unprotonated. Lack of ITC signatures in the binding of the ligand to the gold surface should not be construed to indicate lack of binding of the ligand to the surface. Weak electrostatic interactions between lysine and the gold nanoparticles at pH 7 (not detected by ITC) resulted in significant coverage of the nanoparticle surface by the amino acid. An ITC study of aspartic acid with gold nanoparticles shows that aspartic acid binds with binding constants of the order $\approx 1.4 - 2 \times 10^4$. The entropies of binding are large and positive and contribute a significant component to the binding free energy. Energy changes due to solvation are considerable; the entropy changes are more significant. This is especially evident at higher aspartic acid concentrations. The large positive entropies of binding suggest that desolvation processes are important.

References

[1] Daniel, M.; Astruc, D. "Gold nanoparticles: assembly, supramolecular chemistry, quantum-size-related properties, and applications toward biology, catalysis, and nanotechnology" *Chem. Rev.*, **2004**, *104,* 293.

[2] Faraday, M. "Experimental relations of gold (and other Metals) to light" *Philos. Trans.,* **1857**, *147*, 145.

[3] Jana, N. R.; Gearheart, L.; Murphy, C. J. " Seeding growth for size control of 5-40 nm diameter gold nanoparticles." *Langmuir,* **2001**, *17*, 6782.

[4] Shankar, S. S.; Rai, A.; Ankamwar, B.; Singh, A.; Ahmad, A.; Sastry, M. "Biological synthesis of triangular gold nanoprisms" *Nat. Mat.*, **2004,** *3***,** 482.

[5] Savage, G. "Glass and Glassware*"* Octopus Book: London, **1975**.

[6] Haruta, M.; Kobayashi, T.; Sano, H.; Yamada, N. "Novel gold catalysts for the oxidation of carbon monoxide at a temperature far below 0 °C" *Chem. Lett.,* **1987**, 405.

[7] Joshi, H. M.; Bhumkar, D.R.; Joshi, K.; Pokharkar, V.; Sastry, M. "Gold nanoparticles as carriers for efficient transmucosal insulin delivery" *Langmuir,* **2006,** *22,* 300.

[8] Liu, J.; Lu, Y. "A Colorimetric lead biosensor using DNAzyme-directed assembly of gold nanoparticles**"** *J. Am. Chem. Soc***.**, **2003,** *125*, 6642.

[9] Gole, A.; Dash, C.; Ramakrishnan, V.; Sainkar, S. R.; Mandale, A. B.; Rao, M.; Sastry, M. "Pepsin-gold colloid conjugates: preparation, characterization, and enzymatic activity" *Langmuir,* **2001**, *17,* 1674.

[10] Alivisatos, A. P.; Johnsson, K. P.; Peng, X.; Wislon, T. E.; Loweth, C. J.; Bruchez, M. P., Jr.; Schultz, P. G. "Organization of nanocrystal molecules using DNA" *Nature,* **1996**, *382*, 609.

[11] Niemeyer, C. M. "Nanoparticles, proteins, and nucleic acids: biotechnology meets materials science" *Angew. Chem. Int. Ed.,* **2001**, *40*, 4128.

[12] Tzhayik, O.; Sawant, P.; Efrima, S.; Kovalev, E.; Klug, J. T. "Xanthate capping of silver, copper, and gold colloids." *Langmuir,* **2002**, *18*, 3364.

[13] Porter, L. A., Jr.; Ji, D.; Westcott, S. L.; Graupe, M.; Czernuszewicz, R. S.; Halas, N. J.; Lee, T. R. "Gold and silver nanoparticles functionalized by the adsorption of dialkyl disulfides." *Langmuir,* **1998**, *14*, 7378.

[14] Resch, R.; Baur, C.; Bugacov, A.; Koel, B. E.; Echternach, P. M.; Madhukar, A.; Montoya, N.; Requicha, A. A. G.; Will, P. "Linking and manipulation of gold multinanoparticle structures using dithiols and scanning force mircroscopy." *J. Phys. Chem. B,* **1999**, *103*, 3647.

[15] Sarathy, K. V.; Kulkarni, G. U.; Rao, C. N. R. "A novel method of preparing thiol-derivatised nanoparticles of gold, platinum and silver forming superstructures" *Chem. Commun,* **1997**, 537.

[16] Heath, J. R.; Brandt, L.; Leff, D. V. "Synthesis and characterization of hydrophobic, organically-soluble gold nanocrystals functionalized with primary amines." *Langmuir,* **1996**, *12*, 4723.

[17] Sastry, M.; Kumar, A.; Mukherjee, P. "Phase transfer of aqueous colloidal gold particles into organic solutions containing fatty amine molecules" *Colloids Surf. A,* **2001**, *181,* 255.

[18] Kim, H. S.; Lee, S. J.; Kim, N. H.; Yoon, J. K.; Park, H. K.; Kim, K. "Adsorption Characteristics of 1,4- Phenylene Diisocyanide on Gold Nanoparticles: Infrared and Raman Spectroscopy Study." *Langmuir,* **2003**, *19*, 6701.

[19] Li, G.; Lauer, M.; Schulz, A.; Boettcher, C.; Li, F.; Fuhrhop, J.-H. "Spherical and Planar Gold (0) Nanoparticles with a Rigid Gold(I)-Anion or a Fluid Gold- (0)-Acetone Surface." *Langmuir,* **2003**, *19*, 6483.

[20] Cheng, W.; Dong, S.; Wang, E. "Iodine-induced gold nanoparticle fusion/ fragmentation/aggregation and iodine-linked nanostructured assemblies on a glass substrate." *Angew. Chem. Int. Ed.,* **2003**, *42*, 449.

[21] Sellers, H.; Ulman, A.; Shnidman, Y.; Eilers, J. E. "Structure and binding of alkanethiolates on gold and silver surfaces: implications for self-assembled monolayers" *J. Am. Chem. Soc.,* **1993**, *115,* 9389.

[22] Ulman, A. "Formation and structure of self- assembled monolayers" *Chem. Rev.*, **1996**, *96*, 1533.

[23] Selvakannan, PR.; Mandal, S.; Phadtare, S.; Pasricha, R.; Sastry, M. "Capping of gold nanoparticles by the amino acid lysine renders them water-dispersible" *Langmuir,* **2003,** *19,* 3545.

[24] Selvakannan, PR.; Mandal, S.; Phadtare, S.; Gole, A.; Pasricha, R.; Adyanthaya S. D.; Sastry, M. "Water-dispersible tryptophan-protected gold nanoparticles prepared by the spontaneous reduction of aqueous chloroaurate ions by the amino acid" *J. Colloid Interface Sci.*, **2004**, *269*, 97.

[25] Selvakannan, PR.; Swami, A.; Srisathiyanarayanan, D.; Shirude, P. S.; Pasricha, R.; Mandale, A. B.; Sastry, M. "Synthesis of aqueous Au core-Ag shell nanoparticles using tyrosine as a pH-dependent reducing agent and assembling phase-transferred silver nanoparticles at the air-water interface" *Langmuir,* **2004**, *20*, 7825.

[26] Mandal, S.; Selvakannan PR.; Phadtare, S.; Pasricha, R.; Sastry, M "Synthesis of a stable gold hydrosol by the reduction of chloroaurate ions by the amino acid, aspartic acid" *Proc. Indian Acad. Sci.* (*Chem. Sci.*), **2002**, *114*, 513.

[27] Patil, V.; Malvankar, R. B.; Sastry, M. "Role of particle size in individual and competitive diffusion of carboxylic acid derivatized colloidal gold particles in thermally evaporated fatty amine films" *Langmuir,* **1999**, *15*, 8197.

[28] Zhang, Y.; Akilesh, S.; Wilcox, D. E. "Isothermal titration calorimetry measurements of Ni(II) and Cu(II) binding to His, GlyGlyHis, HisGlyHis, and bovine serum albumin: A critical evaluation" *Inorg. Chem.*, **2000**, *39*, 3057.

[29] Kumar, A.; Mandal, S.; Selvakannan, P.R.; Pasricha, R.; Mandale, A. B.; Sastry, M. "Investigation into the interaction between surface-bound alkylamines and gold nanoparticles" *Langmuir,* **2003**, *19,* 6277.

[30] Shirley, D. A. "High-Resolution X-Ray photoemission spectrum of the valence bands of gold" *Phys. Rev. B.,* **1972**, *5*, 4709.

[31] Sandstrom, P.; Boncheva, M.; Akerman, B. **"**Nonspecific and Thiol-Specific Binding of DNA to Gold Nanoparticles**"** *Langmuir,* **2003,** *19*, 7537.

[32] Hong, R.; Fischer, N.O.; Verma, A.; Goodman, C.M.; Emrick, T.; Rotello, V.M. "Control of Protein Structure and Function through Surface Recognition by Tailored Nanoparticle Scaffolds**"** *J. Am. Chem. Soc,.* **2004**, *126*, 739.

[33] Luque, I.; Todd, M. J.; Gomez, J.; Semo, N.; Freire, E. "Molecular basis of resistance to HIV-1 protease inhibition: A plausible hypothesis" *Biochemistry,* **1998**, *37*, 5791.

[34] Thompson, G.; Owen, D.; Chalk, P. A.; Lowe, P. N. **"**Delineation of the Cdc42/Rac-binding domain of p21-activated kinase" *Biochemistry,* **1998**, *37*, 7885.

[35] Qin, K.; Srivastava, D. K. "Energetics of two-step binding of a chromophoric reaction product, *trans*-3-Indoleacryloyl-CoA, to medium-chain acyl-coenzyme-A dehydrogenase" *Biochemistry,* **1998**, *37*, 3499.

[36] Tellez-Sanz, R.; Garcia-Fuentes, L.; Baron, C. "Calorimetric analysis of lisinopril binding to angiotensin I-converting enzyme" *FEBS Lett.,* **1998**, *423*, 75.

[37] Jelesarov, I.; Bosshard, H. R. "Isothermal titration calorimetry and differential scanning calorimetry as complementary tools to investigate the energetics of biomolecular recognition" *J. Mol. Recognit.,* **1999**, *12*, 3.

[38] Prasad, S. D. "Looking for gold in langmuir's data: surface heterogeneity identification through pressure derivatives" *Langmuir,* **1999**, *15*, 5722.

[39] Prasad, S. D. "A Novel Two-parameter biexponential distribution to map surface heterogeneity: genesis of common distributions and isotherms" *Langmuir*, **1997**, *13,* 1307.

[40] Chellani, M. Application Notes (ITC instrument manual) **1999**, 14.

[41] Paxton, A.T.; Harper, J.B. "On the solvation of L-aspartic acid" *Mol. Phys.*, **2004**, *102*, 953.

CHAPTER IV

Gold Nanoparticles for Efficient Transmucosal Insulin Delivery

The binding of the hormone insulin to gold nanoparticles and its application in transmucosal delivery for the therapeutic treatment of diabetes mellitus is discussed. Insulin was loaded onto bare gold nanoparticles as well as aspartic acid-capped gold nanoparticles and delivered by both oral and intranasal routes. Our principle observations suggest that there is a significant reduction of blood glucose level (postprandial hyperglycemia) when insulin is delivered using gold nanoparticles as a carrier by the transmucosal route in diabetic rats. Furthermore, control of postprandial hyperglycemia by the intranasal delivery protocol is comparable to that achieved using standard subcutaneous administration used for type I diabetes mellitus.

Part of the work presented in this chapter has been published in the following article:

1. Joshi, H. M.; Bhumkar, D. R.; Joshi, K.; Pokharkar, V.; Sastry, M. "Gold Nanoparticles as Carriers for Efficient Transmucosal Insulin Delivery" *Langmuir* **2006,** *22,* 300.

4.1 Introduction

Gold is one of the most ancient metals known to humans. Ornaments are made using gold because of its majestic metallic golden luster. Gold is also found to be of great importance to mankind due to its medicinal properties. It has been used in the field of medicine since 2500 B.C. Use of gold in bhasmas [1] (mixture of medicinal plants and metals in powder form) is very well known in Indian ayurvedic therapies; gold sodium thiomalate has been utilized in the treatment of rheumatoid arthritis [2] and gold compounds have also been investigated for their anti-tumor activity [3]. These properties are mainly due to various oxidation states of gold or compound themselves, in which gold can exist in the +3 or +1 oxidation state, which might be toxic for cells [4, 5]. Recent advances in nanoscience have shown that gold particles at nanoscale dimensions could also be used for medicinal treatments in which gold is in the '0' oxidation state [6]. Ease of preparation, stability, comparable size with biomolecules, shape and size tuning ability, well studied chemistry, binding ability to various molecules, excellent biocompatibility, nontoxic nature, and optical properties (SPR) in the visible and NIR regions make gold nanoparticles potential candidates for chemical as well as biological applications [7]. Developments in the field of nanotechnology encompass the use of gold nanoparticles for numerous applications such as organic reactions [8, 9], sensors [10, 11], drug delivery [12], plasmon wave-guides [13] etc. Sastry and co-workers have used gold nanotriangles for optical coatings, which absorb solar radiation in NIR region and maintain the indoor temperature [14]. Recently SiO_2 core and Au shell nanoparticles designed to absorb in near infrared region, have been shown to be applicable in hyperthermia [15]. Shah et al. used gold nanoparticles as a marker, in which insulin is cross-linked with gold nanoparticles that could assist in visualizing intracellular translocation of insulin and confirmed that insulin enters into cytoplasm of the cell [16]. Gu et al. have shown that gold nanoparticles in toluene react with bis (vancomycine) cystamide in water under vigorous stirring conditions to form vancomycin-capped gold nanoparticles. These antibiotics-capped gold nanoparticles showed enhanced antibacterial activity against *E.*

coli strains [17]. Similarly in another report, capping and release of antibacterial molecule, ciprofloxacin from the surface of gold nanoparticles has been studied [18]. Branched polyethylenimine, covalently attached to gold nanoparticles has been investigated for the delivery of plasmid [19]. Rotello et al. showed the glutathione mediated release of biomolecules from monolayer protected gold nanoparticle surfaces and in vitro manipulation of their bioactivities [20]. Hillyer et al. demonstrated that gold nanoparticles uptake in cells depends on size. When gold nanoparticles are administered orally, the smaller particles cross the gastrointestinal tract more efficiently than the bigger ones [21]. Thus, the above discussion indicates that gold nanoparticles can be used as drug carriers for effective administration of drugs.

Insulin is a very important biomolecule and controls glucose levels (glycimia) in the blood. The destruction of insulin secreting β cells of the pancreatic islets of Langerhans (β cells of pancreas) causes insulin-dependent Diabetes Mellitus (type 1 diabetes, IDDM). Type 1 diabetes affects 0.3 percent of the world population every year. In a normal human being, pancreatic human insulin response is described as an early burst of insulin release followed by a gradual increasing phase of insulin secretion lasting for several hours. In the postprandial hyperglycemia (PPHG) there is a loss in this first phase of insulin secretion, which may contribute to a reduced suppression of hepatic glucose levels, leading to higher glucose appearance in blood [22]. Epidemiological studies have shown that PPHG is an independent risk factor in the development of macrovesicular complications of Diabetes Mellitus. It also has stronger association with fatal and non-fatal cardiovascular diseases than with higher insulinemia [23]. The main challenge in the management of patients with diabetes mellitus is to maintain blood glucose levels as close to normal as possible. Hence, it is important that the delivery systems provide this first phase of insulin to treat the PPHG.

There are many ways by which insulin can be delivered in the body. At present, subcutaneous delivery by injections is one of the popular ways to deliver insulin. Single or multiple injections per day are required to maintain low serum glucose levels. Insulin absorption via subcutaneous route is sustained, thus it does not mimic the normal

pattern of endogenous insulin secretion. However, due to the sustained absorption, insulin concentrations between meals sometimes may be inappropriately high which commonly results in episodes of hypoglycemia. It fails to retain physiological pattern of insulin due to adverse insulin pharmacokinetics and normoglycaemia cannot be achieved [24, 25]. This may result in peripheral hyperinsulinemia, leading to exacerbation of the macrovascular complications of diabetes. Such therapies might be uncomfortable during self-injection, particularly when daily injections are required [26]. There is also a risk of HIV contaminated syringes in developing countries. Difficulties in achieving a normal physiological profile of insulin by injectable therapy has led to the investigation of alternative, non-parenteral routes for the delivery of insulin in an attempt to provide the peak post-prandial insulin concentrations and improve glycemic control.

Generally, oral route is used for administration of drugs particularly required for chronic therapies. The enzymatic barrier of the intestinal tract and the physical barrier made up of the intestinal epithelium are the two major obstacles for successful oral administration of insulin [27]. Furthermore, bioavailability of insulin is extremely low due to poor membrane permeability [28]. Thus, oral administration of insulin remains a significant challenge. Insulin administration could be made much less traumatic and more efficient if other delivery routes could be identified. Other approaches for insulin delivery have also been investigated for systematic administration of insulin viz. nasal [27], transdermal [28], buccal [29], rectal [30], and pulmonary routes [31]. Among all the above routes, the nasal cavity has relatively large absorptive surface area. The high vascularity of nasal mucosa ensures that absorbed compounds are rapidly removed. Drugs absorbed into rich network of blood vessels pass directly into the systemic circulation thereby avoiding hepato-gastrointestinal first pass metabolism [32,33], which makes intranasal route most viable and favorable for chronic system medication of such drugs.

Polymeric nanoparticles are already in practice for drug delivery applications but have their own limitations. By-product of biodegradable polymeric nanoparticles,

themselves degrade drug molecules and thus reduces the effect of drug [34, 35]. These might be the primary reasons for the design of alternative biocompatible non-toxic metal nanoparticle based drug delivery systems. In spite of the large number of studies that have demonstrated that gold nanoparticles are non-toxic to living cells [6], biocompatible and can be conjugated with a spectrum of biological ligands, reports on their application in vivo drug delivery are rather limited. In this chapter, the study and comparison of oral and nasal administration of insulin with gold nanoparticles as carrier is demonstrated.

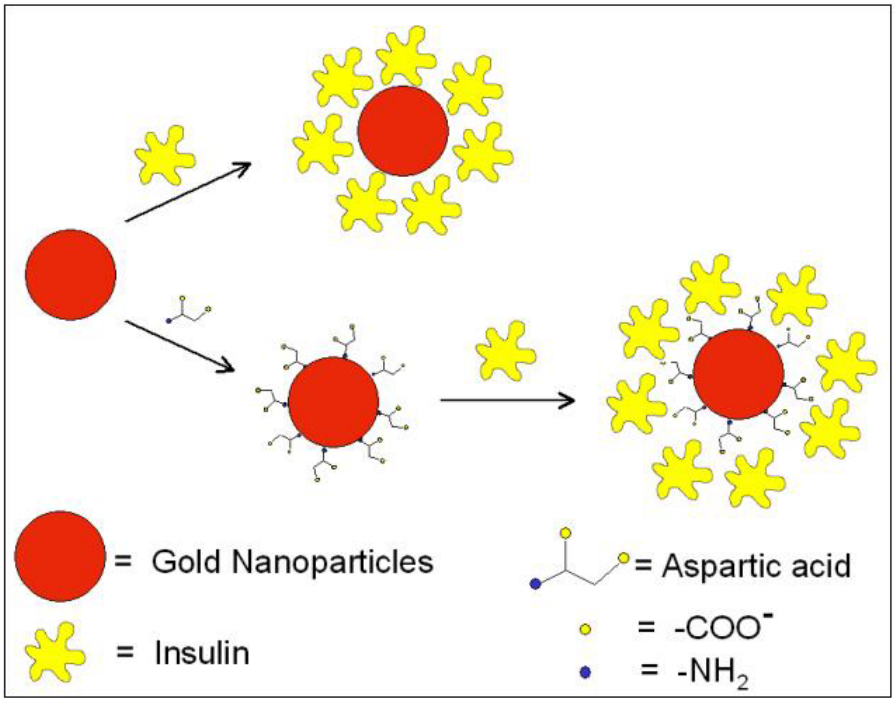

Figure 4.1: *Scheme illustrating insulin loading on bare gold nanoparticles and aspartic acid capped gold nanoparticles (not to the scale).*

The nature of binding interaction between insulin and gold nanoparticles is an important parameter that would influence the stability of the formulation as well as determine the facility with which insulin is released from the gold particles. We have already seen in the previous chapter that gold nanoparticles surface, modified with aspartic acid behave differently than without surface modification and that the charge on the aspartic acid contributes to the overall charge of gold nanoparticles which leads

to higher mobility between two electrodes. In this chapter, bare gold nanoparticles and aspartic acid capped gold nanoparticles have been used, in which bare gold nanoparticles provide stronger interactions [36] while the modification of gold nanoparticles by aspartic acid facilitate weaker interaction with insulin. Aspartic acid renders the surface of nanoparticles more biocompatible since it is one of the building blocks of biomolecules (proteins and enzymes). As shown in Fig. 4.1, a methodology has been developed, in which insulin is loaded on gold nanoparticles as well as on aspartic acid capped gold nanoparticles and then administered orally as well as nasally to diabetic rats. Animal trials show that there is major nasal uptake which is confirmed by significant fall in their blood glucose levels.

4.2 Synthesis and surface modification of nanoparticles

4.2.1 Synthesis of gold nanoparticles

In a typical experiment, 100 mL of 1.25 x 10^{-4} M concentration of aqueous solution of chloroauric acid ($HAuCl_4$) was reduced by 0.01 g of sodium borohydride ($NaBH_4$) at room temperature to yield a ruby-red solution containing 70 ± 20 Å diameter gold nanoparticles [37]. The ruby red colored solution yielded an absorbance maximum at 520 nm. The gold nanoparticle solution was thoroughly dialyzed (Dialysis tubing 12 kDa cutoff) for 12 h to remove excess unreacted ions of the reaction. After dialysis, the pH of the gold nanoparticles solution was measured to be ~ 7.

4.2.2 Surface modification of gold nanoparticles by aspartic acid

Aspartic acid was added to the sodium borohydride reduced gold nanoparticle solution to yield an overall amino acid concentration of 1 x 10^{-4} M in solution. This solution was incubated for 12 h and then thoroughly dialyzed for 24 h to remove uncoordinated aspartic acid. The pH of the solution was 7.

4.2.3 Quantification of insulin onto gold nanoparticles surface

A calculated amount of insulin was added to solutions of uncapped and aspartic acid capped gold nanoparticles to yield an insulin concentration of 0.063 mg/mL in

solution. These solutions were then incubated for 16 h at 2-8 $^{\circ}$C and centrifuged at 30,000 rpm for 30 minutes. The pellets thus obtained were separated from the supernatant solution and redispersed in milli Q water prior to further characterization. The free insulin present in the supernatant was determined by standard method of ELISA protocol. The free insulin in supernatant binds specifically to antibodies coated on the plate, which is a specific reaction. To this complex, anti-antibodies conjugated with peroxidase were added. The substrate, when added, gives a colour, the intensity of which is directly proportional to the antigen present in the supernatant. The percentage loading of insulin on the nanoparticles was determined by the following formula:

$$\%\text{age loading} = \frac{\text{Total loading of insulin added} - \text{Amount of insulin in supernatent}}{\text{Total amount of insulin added}} \text{ X } 100$$

The loading of insulin on bare and aspartic acid capped gold nanoparticles was determined as 86% and 95 % respectively.

4.3 UV-Visible spectroscopy measurements

The binding of insulin to bare gold nanoparticles and to aspartic acid capped gold nanoparticles was monitored by UV-visible spectroscopy measurements. Curves 1 and 2 in Fig. 4.2 A correspond to UV-visible absorption spectra recorded from the dialyzed gold nanoparticle solutions before and after loading of insulin directly onto the gold surface.

In the case of the as-prepared solution, a prominent absorption at 520 nm is observed that arises due to excitation of surface plasmon (SP) vibrations in the gold nanoparticles. Consequent to exposure to insulin, the SP band shifts to 534 nm (curve 2 Fig. 4.2 A) indicating binding of insulin to the gold nanoparticles. After surface modification of the gold nanoparticles with aspartic acid, the SP band shifts to 522 nm (curve 1, Fig. 4.2 B). Further complexation with insulin results in an additional shift to 535 nm indicating surface complexation of Au-asp with insulin (curve 2, Fig. 4.2 B).

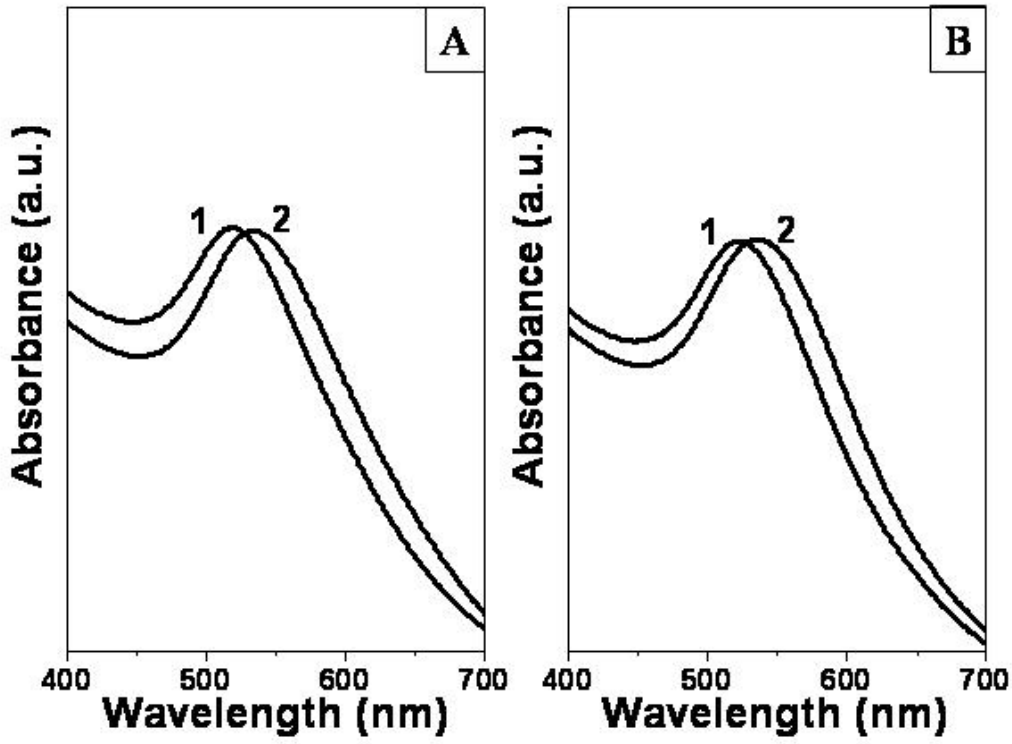

Figure 4.2: *A-UV-Vis absorption spectra recorded from the gold nanoparticle solutions before (curve 1) and after loading of insulin (curve 2). B - UV-vis absorption spectra recorded from the aspartic acid capped gold nanoparticle solutions before (curve 1) and after loading with insulin (curve 2).*

In both cases (insulin loaded onto bare gold and aspartic acid capped gold nanoparticles), we do not observe a broadening of the SP band suggesting that the particles are not aggregating. The shifts in the SP band of the gold nanoparticles after loading of insulin (Figs. 4.2 A and B) therefore may be attributed to the surface complexation of insulin and not due to secondary effects such as aggregation of the nanoparticles.

4.4 Fourier transform infrared spectroscopy measurements and analysis

FTIR spectroscopy was used to study the secondary structure of insulin after binding with bare gold and aspartic acid capped gold nanoparticles. FTIR spectra of pure insulin (curve a, Fig. 4.3), insulin bound to (i) gold nanoparticles (curve b, Fig. 4.3) and (ii) aspartic acid capped gold nanoparticles (curve c, Fig. 4.3) were recorded in the HATR mode at a resolution of 4 cm^{-1} in the range 650 – 4000 cm^{-1}.

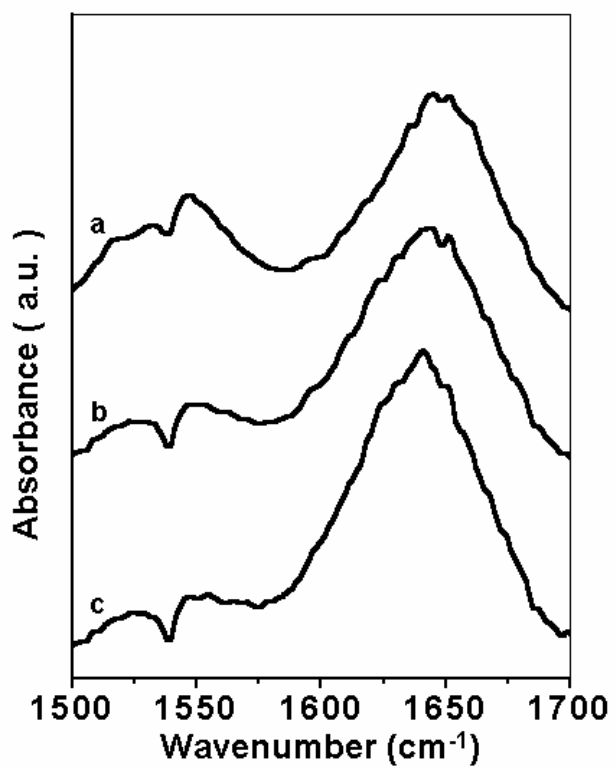

Figure 4.3: *FTIR spectra of (a) Insulin solution; (b) Au-insulin nanoparticles; and (c) Au-asp-insulin nanoparticles.*

A comparison of these two spectra with that recorded from insulin solution reveals the presence of two prominent resonances at 1644 cm^{-1} and 1546 cm^{-1}. These two absorption bands are identified as the amide I and II vibrational modes [38] respectively and can only arise from the insulin bound to the surface of the nanoparticles. The position of the amide I and II bands also indicates that the secondary structure of insulin, which is important for the biological activity of insulin, is not perturbed after complexation with the gold nanoparticles. These bands were absent in FTIR spectra recorded from the bare gold and aspartic acid capped gold nanoparticle samples (data not shown for brevity).

4.5 Transmission electron microscopy measurements

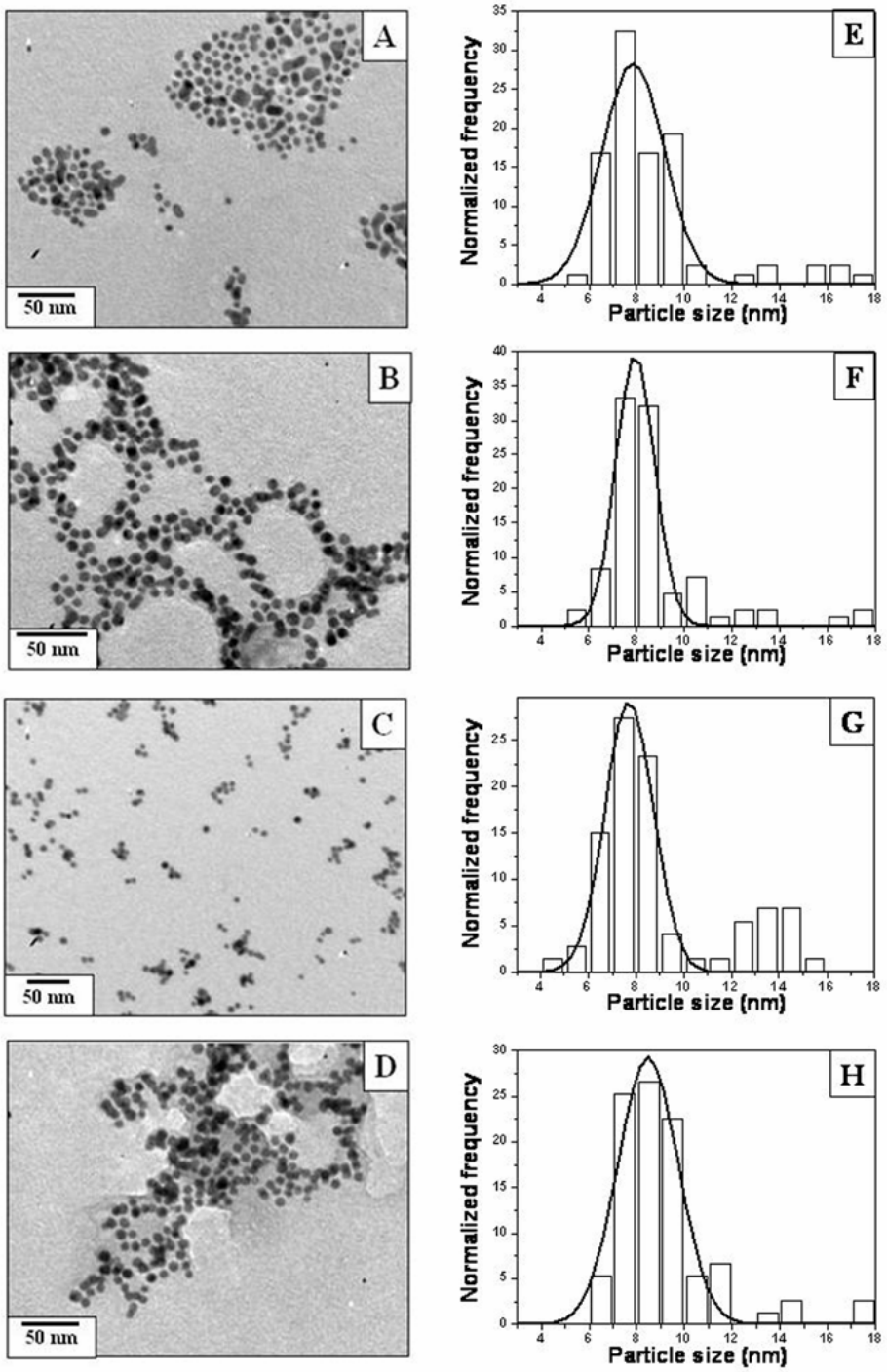

Figure 4.4: *Representative TEM images recorded from: (A) Dialyzed gold nanoparticles; (B) Au-ins nanoparticles; C) Au-asp nanoparticles; (D) Au-asp-ins nanoparticles while E to H shows particle size distribution histograms of TEM images A to D respectively.*

TEM measurements of the gold nanoparticles at various stages of surface treatment were performed at an accelerating voltage of 120 kV. Samples for TEM analysis were prepared in same manner as mentioned in the previous chapter. The TEM images recorded from the as-prepared dialyzed borohydride reduced gold nanoparticles (Fig. 4.4 A), insulin loaded gold nanoparticles (Au-ins) i.e. formulation A (Fig. 4.4 B), aspartic acid capped gold nanoparticles (Fig. 4.4 C) and insulin loaded aspartic acid capped gold nanoparticles (Au-asp-ins) i.e. formulation B (Fig. 4.4 D) indicate that the overall structure of the nanoparticles and their assemblies are not significantly different in each case. Fig. 4.4 E to 4.4 H indicate particles size distribution histogram of gold nano particles, insulin loaded gold nanoparticles, aspartic acid capped gold nanoparticles and insulin loaded aspartic acid capped gold nanoparticles respectively. Form the Fig. 4.4 E to 4.4 H, the nanoparticles range in size was 7 ± 2 nm. TEM images do not show any significant change in the particle size before and after loading of insulin on dialyzed gold nanoparticles as well as aspartic acid capped gold nanoparticles. This suggests that modification of the gold nanoparticles either with aspartic acid and insulin does not lead to nanoparticles aggregation.

4.6 In-vivo insulin delivery studies

The insulin-gold nanoparticle formulations were tested for oral and nasal administration on diabetic rats. Twelve to thirteen weeks old Wistar male rats weighing 180-200 g each were provided by National Toxicology Centre, Pune, India. The animals were housed under standard conditions of temperature (25 $^{\circ}$C), in 12h/12h light and dark cycles and fed with standard pellet diet and water *ad libitum.* Animal handling was performed according to good laboratory practice (GLP). The Wistar male and female rats were rendered diabetic prior to the study by intravenous injection dose of 70-mg/kg alloxan in distilled water [39]. The animals were divided in groups containing six animals each. They were considered to be diabetic when the baseline glucose levels were above 200 mg/dl. The diabetic rats were fasted for 12 h before the experiments. Dose was given in IU/Kg where 1 IU = 45.5 μg.

The formulations administered to the rats were as follows:

(1) Insulin solution administered per orally (p.o.) (50 IU/Kg), intra nasally (i.n.) (20 IU/Kg) and subcutaneously (5 IU/Kg)

(2) Bare (uncapped) gold nanoparticles administered p.o. and i.n

(3) Aspartic acid capped gold nanoparticles administered p.o. and i.n.

(4) Insulin loaded gold nanoparticles (Au-ins, formulation A) administered p.o. (50 IU/Kg) and i.n. (20 IU/Kg)

(5) Insulin loaded aspartic acid capped gold nanoparticles (Au-asp-ins, formulation B) administered p.o. (50 IU/Kg) and i.n. (20 IU/Kg)

In the animal studies mentioned below, glycemia was determined in the serum samples by the standard glucose oxidase- peroxidase method. Glucose oxidase (GOD) converts glucose to gluconic acid and hydrogen peroxide. Hydrogen peroxide formed in this reaction, in the presence of peroxidase (POD), oxidatively couples with 4-aminoantipyrine/phenol to produce red quinoeimine dye. This dye has absorbance maximum at 505 nm. The intensity of colour complex is directly proportional to glucose in the serum sample (reaction) [40, 41]. Serum insulin levels were determined by ELISA tests. The results shown are the mean values of serum glucose levels and insulin levels in the blood serum of animals in each group (six each). The research proposals for these studies were prepared according to form B of the guidelines of the committee for the purpose of control and supervision of experiments on animals (CPCSEA). The institutional animal ethics committee (IAEC) of the Poona College of Pharmacy approved the proposal.

For intranasal administration, the rats were anaesthetized to prevent sneezing during administration. The sedation lasted for about 3 min. The rats were placed in supine position and the samples were delivered using PVC tube connected to a micro litre syringe. In both cases i.e. oral and intranasal administrations, blood samples were collected from the retro-orbital plexus of the rats prior to administration of the

formulations to establish baseline glucose levels and for determination of insulin and gold concentration levels in the blood serum. Similarly, after dosing the animals with the various insulin formulations, blood samples were collected at different time intervals over a period of 5 hours.

After administering the dose to the diabetic rats with the different insulin formulations, the percentage of blood glucose levels relative to the baseline (taken as 100 %) at each time interval was measured. The mean percentage of blood glucose level versus time profile obtained after subcutaneous administration of insulin is plotted in Fig. 4.5, which is considered as a reference for subsequent studies using the nanoparticle based insulin formulations.

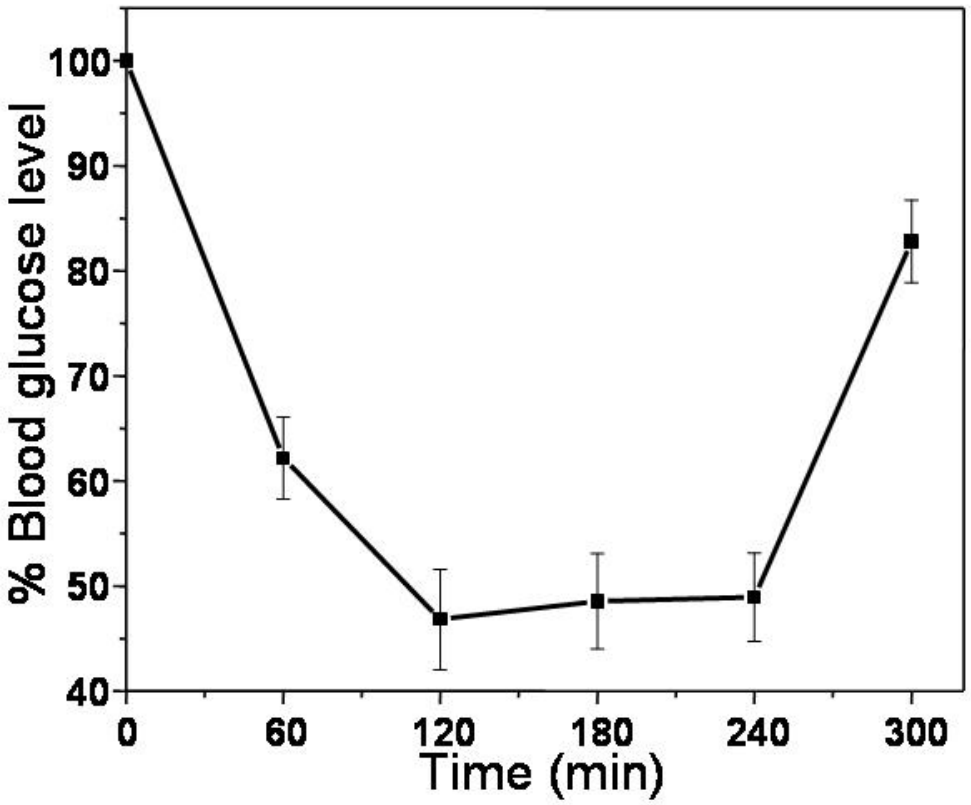

Figure 4.5: *Plot of the time variation of the blood glucose level (expressed in %) in diabetic rats after subcutaneous administration of insulin; dose 5 IU/Kg. The solid lines in all the cases are aid to the eye and have no physical significance.*

In the case of subcutaneous administration of insulin solution (dose 5 IU/Kg), a rapid decrease in the blood glucose level in diabetic rats was observed. This reduction

was about 38 and 53 % within 1 and 2 h post administration respectively (Fig. 4.5). The depression in the blood glucose levels is sustained over a period of ca. 4 h.

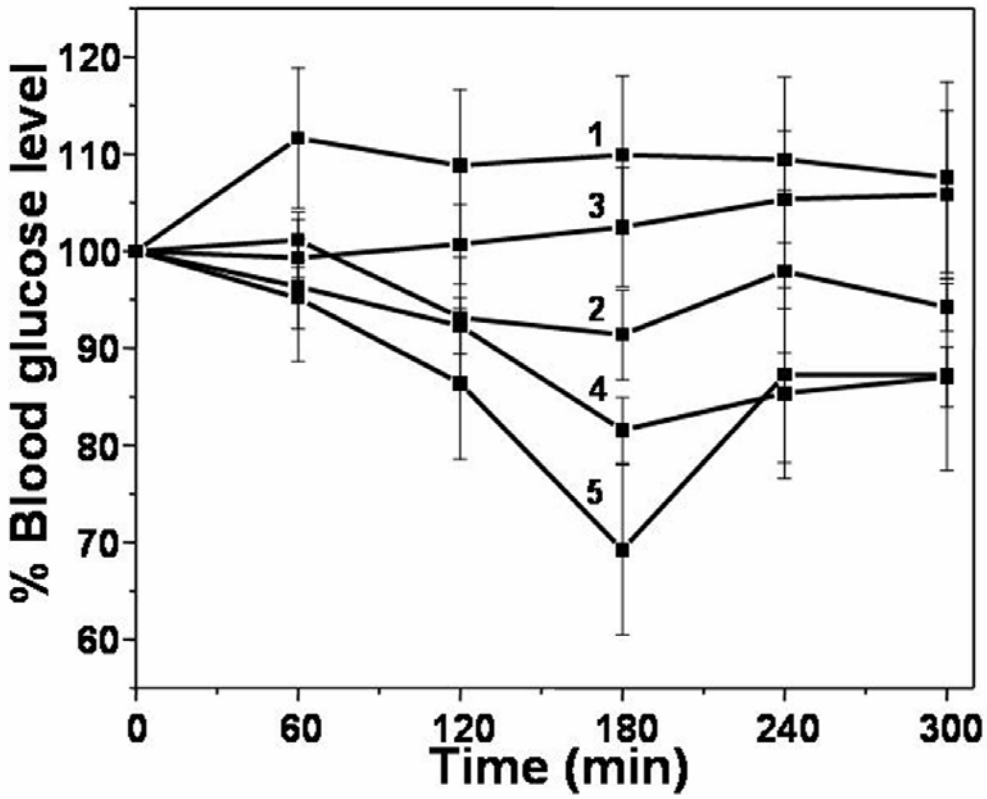

Figure 4.6: *Plot of time variation of the blood glucose levels (expressed in %) in diabetic rats after per oral administration of insulin. control insulin, dose 50 IU/Kg (curve 1); bare Au nanoparticles, 1 mL (curve 2); Au-asp nanoparticles, 1 mL (curve 3); Au-ins nanoparticles, dose 50 IU/Kg (curve 4) and Au-asp-ins nanoparticles, dose 50 IU/Kg (curve 5). The solid lines in all the cases are aid to the eye and have no physical significance.*

The time dependent variation in blood glucose levels in diabetic rats, those were administered with different insulin formulations per orally (p.o) and intranasally (i.n.) is plotted in Fig. 4.6 and 4.7 respectively. In some of the experiments, a small increase in blood glucose levels above the baseline is observed (curve 1, Fig. 4.6 and curves 2 & 4 in Fig. 4.7). This increase may be attributed to metabolic changes and endogenous secretion of glucagon in the diabetic rats due to stress in the animals during blood sampling [42]. In both the p.o. (Fig. 4.6) and i.n. administration protocols (Fig. 4.7), we observed that bare gold nanoparticles (curve 2) and aspartic acid capped gold nanoparticles (curve 3) do not result in lowering of blood glucose level in the diabetic

rats. Oral administration of insulin solution (curve 1, Fig. 4.6) did not result in a detectable reduction of blood glucose levels even after 5 h of dosage which could be mainly attributed to poor uptake and enzymatic degradation of insulin in the gastrointestinal tract (g.i. tract).

On the other hand, oral administration of both formulation A; Au-ins (curve 4, Fig 4.6) and formulation B; Au-asp-ins (Curve 5, Fig. 4.6) resulted in a detectable reduction in blood glucose levels of up to 19 % and 31 % respectively. This result indicates that in both cases, the gold nanoparticle surface bound insulin was bioactive and that the absorption of insulin was enhanced in the formulation where insulin was bound to the aspartic acid modified gold nanoparticles surface.

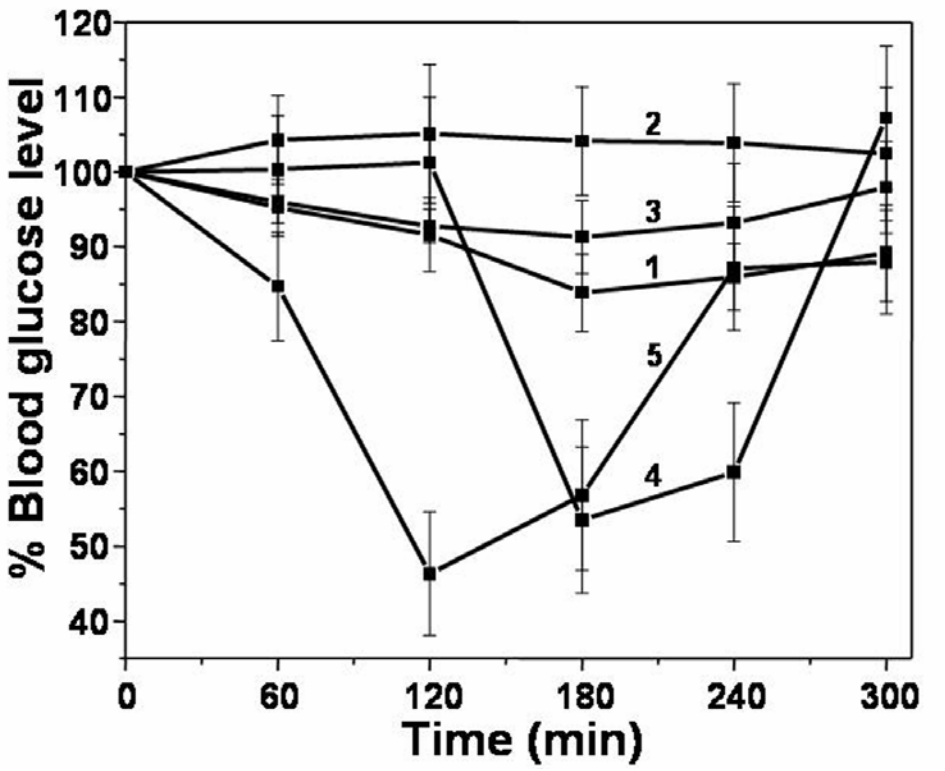

Figure 4.7: *Plot of time variation of the blood glucose levels (expressed in %) in diabetic rats after intranasal administration of insulin. control insulin, dose 20 IU/Kg, (curve 1); bare Au nanoparticles, 1 mL (curve 2); Au-asp nanoparticles, 1mL (curve 3); Au-ins nanoparticles, dose 20 IU/Kg (curve 4) and Au-asp-ins nanoparticles, dose 20 IU/Kg (curve 5). The solid lines in all the cases are aid to the eye and have no physical significance.*

In both these experiments, the maximum decrease in blood glucose level occurred at 180 min after administration of the respective formulations. As expected and observed above, nasal administration of both bare gold nanoparticles and aspartic acid capped gold nanoparticles did not show positive results. In contrast with oral administration of insulin solutions where significant drop in blood glucose levels was not observed, nasal administration of insulin solutions resulted in a small drop in blood glucose levels in diabetic rats (curve 1, Fig. 4.7). The average blood glucose level fell by ca. 18 % in this experiment. The nasal administration experiment results with Au-ins (curve 4, Fig. 4.7) and Au-asp-ins (curve 5, Fig. 4.7) are much more interesting. The decrease in blood glucose level in both experiments is quite significant and reached a maximum reduction of 50 and 55 % for Au-ins and Au-asp-ins respectively. The rate of release of insulin and consequent uptake in both cases is quite different; maximum blood glucose reduction occurs at 180 min after administration of the Au-ins formulation while corresponding time period is ca. 120 min the case of Au-asp-ins. This result clearly shows that insulin uptake during intranasal administration is more in case of insulin bound to Au-asp than to insulin bound to bare gold nanoparticles.

Furthermore, comparison of the maximum blood glucose reduction values in the two formulations administered p.o. and i.n. indicates that the insulin uptake is much higher in the i.n. delivery protocol. Clearly, membrane permeability of the gold nanoparticles-insulin formulations across nasal mucosal cells is much better than across g.i. mucosa. This result is particularly gratifying considering that the insulin-gold nanoparticles dosage administered to the diabetic rats in the i.n. experiment (20 IU/Kg) is smaller than that in the p.o. administration (50 IU/Kg). The maximum blood glucose level reduction in the case of the Au-asp-ins i.n. administration (55 %) is also comparable to that observed in the subcutaneous administration (53 %, Fig. 4.5). This is an important result and indicates that the transmucosal delivery of insulin by gold nanoparticles could be an exciting alternative to the painful and traumatic subcutaneous delivery.

The nature of interaction between insulin and gold nanoparticles is expected to play a major role in the release of insulin. The formulation Au-ins consists of covalently linked insulin to gold nanoparticles. The release of insulin from this formulation is observed to be slower and less intense in comparison with insulin in the Au-asp-ins formulation. In the later case, insulin is believed to be linked to the aspartic acid capped gold nanoparticle via much weaker hydrogen bonding and electrostatic interactions. This weak interaction may be responsible for the faster and larger release of insulin.

4.7 Inductively coupled plasmon (ICP) measurements and insulin levels in the blood

Inductive coupled plasmon technique was used to determine the gold concentration in the blood serum after administration of different gold nanoparticle formulations in diabetic rats. Samples were prepared by adding 0.3 mL of 35% 36 N HCl, and 0.1 mL of 55% , 12 N HNO_3 to weighed amount of blood plasma and diluting it up to 2 mL. Gold concentrations in the above samples were determined with the help of inductive coupled plasmon technique, while ELISA was performed on AxSYM/Imx Fully Automated Immunoassay System.

Insulin and gold concentrations in blood serum of diabetic rats were monitored at different times after administrating the doses as discussed above with the various insulin-gold nanoparticles formulations. The data obtained is shown in Table 4.1 (serum insulin levels) and 4.2 (serum gold levels).

When the gold nanoparticles-insulin formulations were used either in the oral or nasal protocol, it was observed that the blood insulin levels were, consistently higher in those experiments where insulin solutions were administered per orally and intra nasally (Table 4.1). This clearly indicates that the insulin uptake is enhanced when administered as Au-ins and Au-asp-ins nanoparticles resulting in the lowering of blood glucose levels as observed and discussed earlier (Fig. 4.6, 4.7).

Table 4.1: Levels of insulin in blood serum

Time (min)	Au-insulin (mIU/mL)		Au-asp-insulin (mIU/mL)		Control (mIU/mL)		Subcut-aneous (mIU/mL)
	Oral	Nasal	Oral	Nasal	Oral	Nasal	
120	1.7	1.2	0.9	1.9	--	0.90	2.50
240	1.2	2.0	0.9	1.6	0.60	0.20	1.60
360	0.9	--	0.8	1.9	0.50	0.60	1.60

Table 4.2: Levels of Au in blood serum determined by ICP analysis

Time (min)	Au-insulin (in ppm)		Au-asp-insulin (in ppm)	
	Oral	Nasal	Oral	Nasal
120	0.031	0.024	0.030	0.020
240	0.031	0.021	0.025	0.026
360	0.029	0.032	0.029	0.022

A comparison of the blood insulin levels at a particular time for a given formulation in the per oral and intranasal protocols shows that the levels were, in general, higher for the intranasal administration (Table 4.1). This result is also in agreement with our observations of the lower blood glucose levels when insulin bound to gold nanoparticles is administered intranasally (Fig. 4.6 and 4.7). The blood insulin levels in a subcutaneous administration experiment vis-à-vis intranasal administration of Au-ins and Au-asp-ins formulation are not significantly different (Table 4.1) and result in similar depression of blood glucose levels. The gold concentration levels in the blood at different times after administration of the Au-ins and Au-asp-ins formulations in the oral and nasal forms are almost constant over the time interval studied (Table 4.2). This suggests that while the overall uptake of the nanoparticles in both modes of administration is of the same order of magnitude, the quantum of insulin absorbed across nasal mucosa and g.i. mucosa is significantly different; insulin absorption is much higher for the nasal mucosa.

As briefly mentioned earlier, the relatively poor blood glucose level reduction in the per oral administration protocol now may be ascribed with better confidence limits to either poor membrane permeability of insulin in the gastrointestinal tract or degradation of insulin by gastric juices. Clearly poor uptake of the carrier nanoparticles may not be the cause for the difference between per oral and intranasal administrations.

4.8 Conclusion

Gold nanoparticles could serve as an excellent carrier for insulin in treatment of diabetes mellitus. The dose changes with different delivery routes. These studies indicate that, insulin absorption via the nasal route is more effective than the oral route in terms of dose requirement, time required for blood glucose reduction and percentage blood glucose reduction. It leads to reduction of blood glucose level (postprandial hyperglycemia) that is comparable to subcutaneous administration of insulin. The presence of an amino acid layer between insulin and the gold nanoparticle is observed to promote the uptake of insulin. Thus, this approach has been demonstrated to be of considerable promise for development of non-parenteral delivery system for insulin. It also possesses the potential to alleviate the pain and trauma associated with subcutaneous administration of insulin.

References:

[1] *Rasaratnasamuchchay*, **1995,** adhyay *5*, shloka *15*, 97.

[2] Mangalam, A. K.; Aggarwal, A.; Naik, S. "Mechanism of action of disease modifying anti-rheumatic agent, gold sodium thiomalate (GSTM)", *International Immunopharmacology,* **2001**, *1*, 1165.

[3] Tiekink, E. R. T. "Gold derivatives for the treatment of cancer", *Crit. Rev. Oncol. Hematol.,* **2002**, *42,* 225.

[4] Gleichmann, E.; Kubicka-Muranyi, M.; Kind, P.; Goldermann, R.; Goerz, G.; Merk, H.; Rau R. "Insights into the mechanism of gold action provided by

immunotoxicology: biooxidation of gold(I) to gold(III) detected by sensitized T-cells" *Rheumatol. Int.,* **1991**, *11*, 219.

[5] Mirabelli, C. K.; Johnson, R. K.; Sung, C. M.; Faucette, L.; Muirhead, K.; Crooke, S. T., "Evaluation of the in vivo antitumor activity and in vitro cytotoxic properties of auranofin, a coordinated gold compound, in murine tumor models" *Cancer Res.,* **1985**, *45*, 32.

[6] Shukla, R.; Bansal, V.; Chaudhary, M.; Basu, A.; Bhonde, R. R.; Sastry, M. "Biocompatibility of gold nanoparticles and their endocytotic fate inside the cellular compartment: A microscopic overview" *Langmuir,* **2005**, *21,* 10644.

[7] Daniel, M. C.; Astruc, D., "Gold Nanoparticles: Assembly, supramolecular chemistry, quantum-size-related properties, and applications toward biology, catalysis, and nanotechnology" *Chem. Rev.,* **2004,** *104*, 293.

[8] Haruta, M.; Kobayashi, T.; Sano, H.; Yamada, N. "Novel gold catalysts for the oxidation of carbon monoxide at a temperature far below 0 °C." *Chem. Lett.,* **1987**, 405.

[9] Ueda, A.; Oshima, T.; Haruta, M. "Reduction of nitrogen monoxide with propene in the presence of oxygen and moisture over gold supported on metal oxides." *Appl. Catal. B,* **1997**, *12*, 81.

[10] Obare, S. O.; Hollowell, R. E.; Murphy, C. J. "Sensing strategy for lithium ion based on gold nanoparticles." *Langmuir,* **2002**, *18*, 10407.

[11] Singh, A.; Chaudhari, M.; Sastry, M. "Construction of conductive multilayer films of biogenic triangular gold nanoparticles and their application in chemical vapour sensing" *Nanotechnology* (in press).

[12] Paciotti, G. F.; Myer, L., Kingston, D. G. I., Ganesh, T.; Tamarkin, L.; "Colloidal gold nanoparticles: a versatile platform for developing tumor targeted cancer therapies" *NSTI-Nanotech 2005*, **2005,** Vol. 1, www.nsti.org.

[13] Maier, S. A.; Brongersma, M. L.; Kik, P. G.; Meltzer, S.; Requicha, A. A. G.; Atwater, H. A. **"**Plasmonics - A route to nanoscale optical devices" *Adv. Mater.,* **2001**, *13,* 1501.

[14] Shankar, S. S.; Rai, A.; Ahmad, A.; Sastry, M. "Controlling the optical properties of lemongrass extract synthesized gold nanotriangles and potential application in infrared-absorbing optical coatings" *Chem. Mater.,* **2005**, *17*, 566.

[15] Hirsch, L. R.; Stafford, R. J.; Bankson, J. A.; Sershen, S. R.; Rivera, B.; Price, R. E.; Hazle, J. D.; Halas, N. J.; West, J. L. "Nanoshell-mediated near-infrared thermal therapy of tumors under magnetic resonance guidance" *Proc. Natl. Acad. Sci.,* **2003**, *100*, 13549.

[16] Shah, N.; Zhang, S.; Harada, S.; Smith, S. M.; Jarett, L. "Electron microscopic visualization of insulin translocation into the cytoplasm and nuclei of intact H35 hepatoma cells using covalently linked nanogold-insulin" *Endo*., **1995,** *136*, 2825.

[17] Gu, H.; Ho, P. L.; Tong, E.; Wang, L.; Xu, B. "Presenting vancomycin on nanoparticles to enhance antimicrobial activities" *Nano Lett.,* **2003**, *3*, 1261.

[18] Tom, T. R.; Suryanarayanan, V.; Reddy, P. G.; Baskaran, S.; Pradeep, T. "Ciprofloxacin-protected gold nanoparticles" *Langmuir,* **2004**, *20,* 1909.

[19] Thomas, M.; Klibanov, A. M. "Conjugation to gold nanoparticles enhances polyethylenimine's transfer of plasmid DNA into mammalian cells" *Proc. Natl. Acad. Sci.,* **2003**, *100*, 9138.

[20] Verma, A.; Simard, J. M.; Worrall, J. W. E.; Rotello, V. M. "Tunable reactivation of nanoparticle-inhibited β-galactosidase by glutathione at intracellular concentrations" *J. Am. Chem. Soc.,* **2004**, *126*, 13987.

[21] Hillyer, J. F.; Albrech, R. M. "Gastrointestinal persorption and tissue distribution of differently sized colloidal gold nanoparticles", *J. Pharma. Sci*., **2001**, *90*, 1927.

[22] Gin, H.; Rigalleau, V. **"**Post-prandial hyperglycemia post-prandial hyperglycemia and diabetes" *Diabetes Metab.,* **2000**, *26*, 265.

[23] Pyörälä K.; Savolainen E.; Kaukola S.; Haapakoski, J. "Plasma insulin as coronary heart disease risk factor: relationship to other risk factors and predictive value during 9 1/2 years follow-up of the Helsinki policemen study population." *Acta Med. Scand. Suppl.,* **1985**, *701,* 38.

[24] Kennedy, F.P. "Recent developments in insulin delivery techniques" *Drugs,* **1991**, *42*, 213.

[25] Pickup, J.C. "An introduction to the problems of insulin delivery, in: J.C. Pickup (Ed.), biotechnology of insulin therapy", Blackwell Scientific, Oxford, **1991**, 1.

[26] Carino, G. P.; Jacob, J. S.; Mathiowitz, E. "Nanosphere based oral insulin delivery" *J. Control. Release,* **2000**, *65*, 261.

[27] Hinchcliffe, M. Illum, L. "Intranasal insulin delivery and therapy" *Adv. Drug Deliv. Rev.*, **1999**, *35*, 199.

[28] Pillai, O.; Borkute, S. D.; Sivaprasad, N.; Panchagnula, R. "Transdermal iontophoresis of insulin II. physicochemical considerations" *Int. J. Pharma.,* **2003**, *254*, 271.

[29] Aungst, B. J.; Rogers, N. J. "Site dependence of absorption-promoting actions of laureth-9, Na salicylate, Na2EDTA, and aprotinin on rectal, nasal, and buccal insulin delivery" *Pharm. Res.,* **1988**, *5*, 305.

[30] Yamamoto, A.; Muranishi, S. "Rectal drug delivery systems Improvement of rectal peptide absorption by absorption enhancers, protease inhibitors and chemical modification" *Adv. Drug Deliv. Rev.,* **1997,** *28*, 275.

[31] Kawashima, Y.; Yamamoto, H.; Takeuchi, H.; Fujioka, S.; Hino, T. "Pulmonary delivery of insulin with nebulized DL-lactide / glycolide copolymer (PLGA) nanospheres to prolong hypoglycemic effect" *J. Control Release,* **1999**, *62*, 279.

[32] Chien, Y. W.; Chang, Y. "Historical developments of transnasal systemic medications, in: Y.W. Chien (Ed.), Transnasal systemic medications: fundamentals, developmental concepts and biomedical assessments" Elsevier, Amsterdam, **1985**, 1.

[33] Chang, S. F.; Chien, Y. W. "Intranasal drug administration for systemic medication" *Pharm. Int.,* **1984**, *5*, 287.

[34] O'Hagan, D. T. "Microparticles and polymers for the mucosal delivery of vaccines" *Adv. Drug. Deliv. Rev.,* **1998**, *34*, 305.

[35] Yeh, I. Y; Ellens, H.; Smith, P. L. "Physiological considerations in the design of particulate dosage forms for oral vaccine delivery" *Adv. Drug. Deliv. Rev.,* **1998**, *34*, 123.

[36] Joshi, H.; Shirude, P.; Bansal, V.; Ganesh, K. N.; Sastry, M. "Isothermal titration calorimetry studies on the binding of amino acids to gold nanoparticles" *J. Phys.Chem. B,* **2004**, *108,* 11535.

[37] Patil, V.; Malvankar, R. B.; Sastry, M. **"**Role of particle size in individual and competitive diffusion of carboxylic acid derivatized colloidal gold particles in thermally Evaporated Fatty Amine Films" *Langmuir,* **1999,** *15***,** 8197**.**

[38] Dzwolak, W.; Ravindra, R.; Lendermann, J.; Winter, R "Aggregation of bovine insulin probed by DSC/PPC calorimetry and FTIR Spectroscopy" *Biochemistry*, **2003**, *42*, 11347.

[39] Rameshkumar, K.; Shah, S. N.; Goswami, D. B.; Mohan, V.; Bodhankar, S. L. "Efficacy and toxicity of vanadium nicotinate in diabetic rats" *Toxicol. Int*., **2004**, *11*, 75.

[40] Takenaga, M.; Yamaguchi, Y.; Kitagawa, A.; Ogawa, Y.; Mizushima, Y.; Igarashi, R. "A novel sustained-release formulation of insulin with dramatic reduction in initial rapid release" *J. Control Release,* **2002**, *79*, 81.

[41] Hosny, E. A.; Al-Shora, H. I.; Elmazar, M. A. "Oral delivery of insulin from enteric-coated capsules containing sodium salicylate: effect on relative hypoglycemia of diabetic beagle dogs" *Int. J. Pharm*., **2002**, *237*, 71.

[42] Dorkoosh, F. A.; Verhoef, J. C.; Borchard, G.; Rafiee-Tehrani, M.; Verheijden, J. H. M.; Junginger, H. E. "Intestinal absorption of human insulin in pigs using delivery systems based on superporous hydrogel polymers" *Int. J. Pharm.,* **2002**, *247*, 47.

CHAPTER V

Phase Transfer of Platinum Nanoparticles from Aqueous to Organic Medium and its Catalytic Applications

In this chapter, the phase transfer of platinum nanoparticles from aqueous to organic media is discussed. The phase transfer is accomplished by vigorous stirring of a biphasic mixture of platinum nanoparticles synthesized in an aqueous medium and octadecylamine (ODA) in hexane. During shaking of the biphasic mixture, the aqueous platinum nanoparticles interact with the ODA molecules present in the organic phase. This process renders the nanoparticles sufficiently hydrophobic and dispersible in the organic phase. The ODA-capped platinum nanoparticles show high catalytic activity in hydrogenation reactions, which is demonstrated in the efficient conversion of styrene to ethyl benzene and cyclohexene to cyclohexane. The nature of binding of ODA molecules to the platinum nanoparticle surface was characterized by FTIR, TGA and XPS studies.

Part of the work presented in this chapter has been published in the following article:

1. Kumar, A.; Joshi, H. M.; Mandale, A. B.; Srivastava, R.; Adyanthaya, S. D.; Pasricha, R.; Sastry, M. "Phase transfer of platinum nanoparticles from aqueous to organic solutions using fatty amine molecules" *J. Chem. Sci.*, **2004**, *116,* 293.

5.1 Introduction

Nanoparticles are very attractive candidates in caralysis in different chemical reactions, since they provide large surface to volume ratios than bulk materials. Synthesis of metal nanoparticles for catalytic application is an active area of research mainly due to the difficulties in synthesis and stability of nanoparticles. There are many experimental protocols such as reduction of aqueous metal ions by electromagnetic radiation [1, 2], sonochemical methods [3] and conventional chemical reduction [4,5], by which nanoparticles can be synthesized. Nanoparticles in aqueous phase can be used in biological systems, which is a major advantage of aqueous medium based synthesis of nanoparticles. But poor control over size, shape and dispersibility of nanoparticles are major drawbacks in the water-based synthesis [6, 7]. Ionic effects present in aqueous medium also limit the concentration of metal nanoparticles in aqueous solutions [8].

Brust et al. have developed a method, which involves extraction of metal ions into toluene using a phase transfer molecule such as tetra octyl ammonium bromide. Phase transferred metal ions were reduced by sodium borohydride in the presence of alkane thiols. This resulted in the formation of monodisperse nanoparticles [9]. Very high concentration of nanoparticles in a given solvent and the ability to obtain these nanoparticles in powder form without significant variation of particle size distribution are two major advantages of organic medium based synthesis. Nanoparticles thus obtained in powder form can be easily redispersed in a range of organic solvents thus overcoming the drawbacks of aqueous synthetic methodologies. However the use of two different molecules i.e., for phase transfer and for capping of nanoparticles, makes this process rather costly and laborious. Similar methods rapidly followed, in which alkane-thiols [10, 11], aromatic thiols [12, 13], dialkyl disulfides [14] and thiolated cyclodextrins [15, 16] molecules were used as capping agents. From the above discussion, it is clear that both protocols possess some merits and demerits. It should be possible to maximize the advantages by combining them in some way. This can be achieved by synthesizing nanoparticles in one medium and transferring them into the

other complimentary medium. Many groups developed similar protocols in which metal nanoparticles were synthesized in aqueous medium and phase transferred in non-polar or weakly polar organic medium [17-19].

Sarathy et al. have demonstrated acid facilitated phase transfer of gold, silver and platinum nanoparticles into organic solvents such as toluene [20, 21]. In these experiments, biphasic mixture consisting of aqueous noble metal nanoparticles and alkane thiol in toluene, were taken in reaction vessel and concentrated HCl was added to this solution under stirring conditions. Phase transfer of metal nanoparticles from aqueous phase to organic phase was observed during this process indicating capping of the metal nanoparticles by alkane thiol molecules. A similar method has also been applied to the acid-facilitated phase transfer of oleate-stabilised colloidal silver nanoparticles by Efrima [22]. Use of sulfur containing compounds in phase transfer protocols may affect the surface and catalytic properties of nanoparticles drastically because sulfur is known to act as poison for the metal catalyst and thus, is a major limitation of thiol based phase transfer protocols [23].

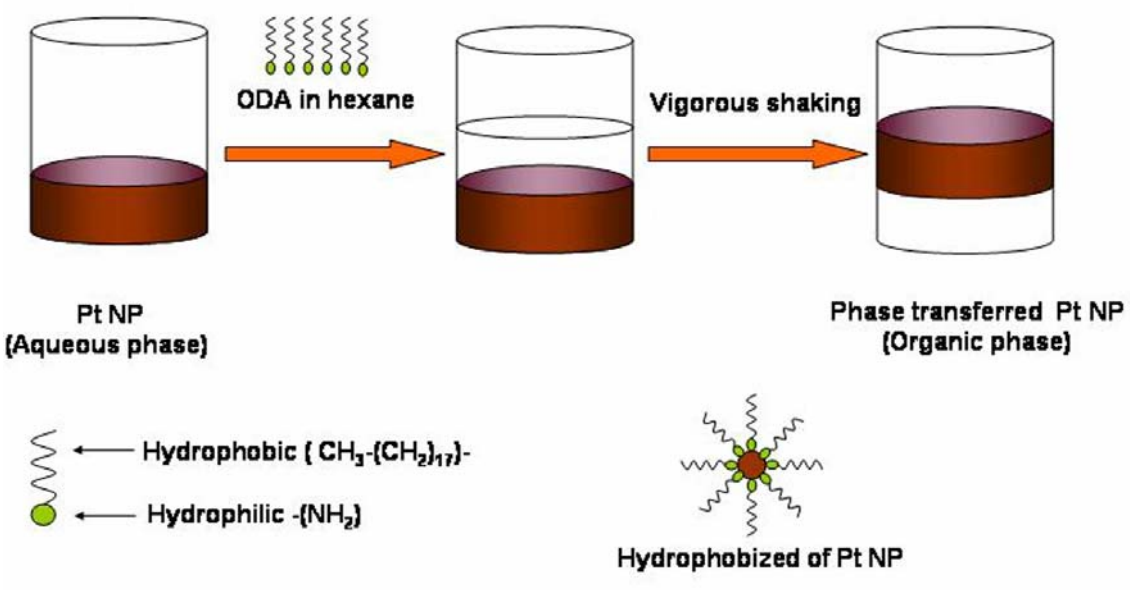

Figure 5.1: *Scheme of synthesis of platinum nanoparticles in aqueous phase followed by its phase transfer to organic phase (not to scale).*

Amine based phase transfer protocols can be a better alternative over these processes since amine is also known to bind strongly with metal. Very few reports have appeared in the literature demonstrating use of alkyl amine for phase transfer of nanoparticles from aqueous phase to organic phase and render them compatible for various applications [24, 25].

Keeping in mind advantages and limitations of amine and thiol based phase transfer protocols and its application in chemistry, Sastry and co-workers had developed phase transfer protocol for metal and semiconductor nanoparticles [26, 27]. In this chapter, the phase transfer of platinum nanoparticles from phase to organic phases (Fig. 5.1), and their high catalytic activity in hydrogenation reactions has been demonstrated. The phase transfer was accomplished by vigorous stirring of a biphasic mixture of platinum nanoparticles synthesized in an aqueous medium and octadecylamine (ODA) in hexane. During shaking of the biphasic mixture, the aqueous platinum nanoparticles interact with amine group of ODA molecules leading to transfer of platinum nanoparticles to organic phase. The ODA-capped platinum nanoparticles show high catalytic activity. The nature of binding of the ODA molecules to the platinum nanoparticle surface was characterized by thermogravimetry (TGA), transmission electron microscopy (TEM), X-ray photoemission spectroscopy (XPS) and Fourier transform infrared spectroscopy (FTIR).

5.2 Phase transfer of platinum nanoparticles from aqueous phase to organic phase

5.2.1 Synthesis of platinum nanoparticles

100 mL of 10^{-4} M aqueous solution of chloroplatinic acid (H_2PtCl_6) was reduced by 0.01 g sodium borohydride ($NaBH_4$) at room temperature to yield aqueous platinum nanoparticles. The resulting solution was clear brownish-black in color. pH of the solution was 9.

5.2.2 Hydrophobization of platinum nanoparticles

To 100 mL of the platinum nanoparticles solution, 100 mL of a 2 x 10^{-4} M solution of octadecylamine (ODA) in hexane was added to yield immiscible layer of the colorless organic solution on top of the brown-colored platinum nanoparticles (Fig. 5.2 A). Vigorous shaking of the mixture resulted in transfer of the platinum nanoparticles into the organic phase accompanied by the transfer of brown colour to the organic phase and a corresponding loss of color from the aqueous phase (Fig. 5.2 B). The ODA-capped platinum nanoparticles were separated from hexane by rotavapping. Free ODA molecules were removed by repeated washing with ethanol. The purified ODA capped Pt nanoparticles were redispersed in chloroform and characterized as mentioned above.

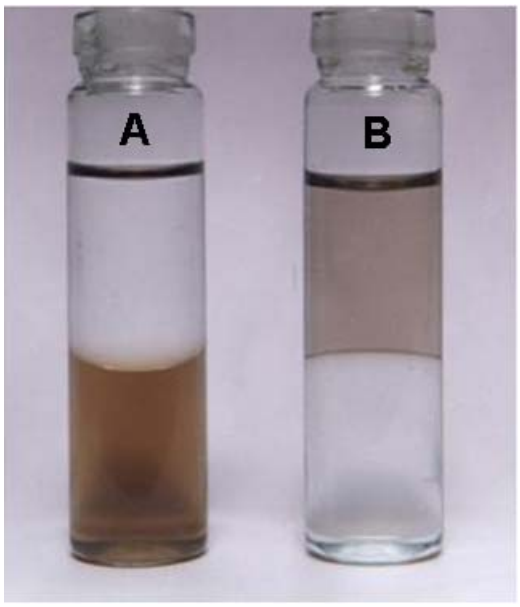

Figure 5.2: *Shows A) immiscible layers of the platinum nanoparticles (bottom layer) and the clear hexane solution containing ODA (on top) before shaking and B) ODA capped Pt nanoparticles in hexane (layer on top) and the clear aqueous solution at the bottom after the phase transfer by shaking the biphasic mixture.*

5.3 Thermo gravimetric studies

In order to understand the nature and strength of bond between platinum nanoparticles and ODA, TGA analysis of the purified powder of ODA-capped platinum

nanoparticles and only ODA powder were carried out. TGA analysis of above samples were done in the temperature range 25 – 800°C at a rate of 10°C/min. Fig. 5.3 shows the TGA data obtained from purified powder of ODA capped platinum nanoparticles (curve 1) and from pure ODA (curve 2). In the case of pure ODA, it is observed that there is 40% weight loss upto 260°C, which is followed by complete loss of the powder in the heating crucible by 600°C and indicates complete desorption/decomposition within this temperature interval. The ODA-Pt nanoparticles shows weight loss of 20% at 325 °C followed by negligible weight loss in the temperature range 434–800°C.

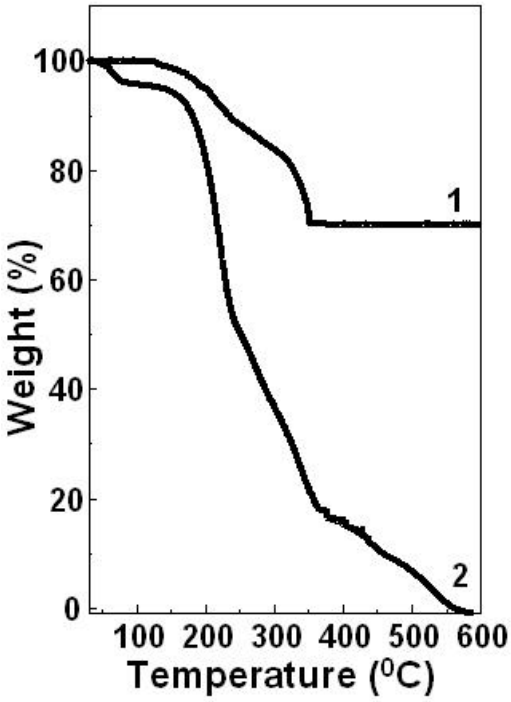

Figure 5.3: *TGA curves of purified powder of ODA-capped platinum nanoparticles (curve 1) and pure ODA powder (curve 2, see text for details).*

The weight loss at 325 °C is due to desorption/ decomposition of the ODA molecules bound to the platinum nanoparticles. The increase in the desorption/decomposition temperature of the ODA molecules bound to platinum nanoparticles relative to free ODA molecules indicates that the interaction between the ODA and platinum nanoparticles is quite strong. This trend agrees reasonably well with the desorption temperature observed in TGA analysis of alkyl amine molecules bound

to gold nanoparticles indicating that the interaction of alkyl amines with platinum nanoparticles could be of similar strength [26]. The percentage weight contribution of the surface bound ODA molecules (20%) is in reasonable agreement with the theoretical estimate of 24% (assuming the area occupied by ODA molecules on the nanoparticles surface as 20 $Å^2$ and the diameter of platinum nanoparticles to be 100 Å). It is clear from the TGA data that the increase in desorption/decomposition temperature of ODA molecules from the surface of platinum nanoparticles is due to fairly strong interaction of amine group with the platinum nanoparticles. In order to understand the nature of this interaction, FTIR and XPS measurements were done on purified ODA-capped platinum nanoparticles.

5.4 Fourier transform infra red spectroscopic studies

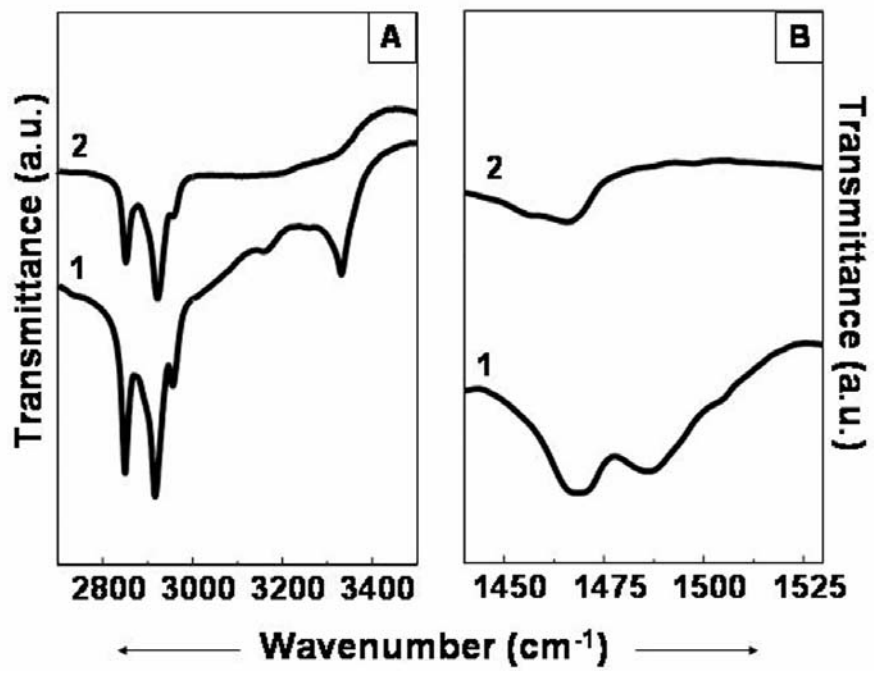

Figure 5.4: *FTIR spectra of drop-coated films of pure octadecylamine (curve 1) and ODA-capped platinum nanoparticles (curve 2) on Si (111) substrates in the spectral windows 2750-3500 (A) and 1400–1525 cm^{-1} (B).*

Fig. 5.4 A and B show the FTIR spectra recorded from drop coated films of pure ODA (curve 1) and ODA-capped platinum nanoparticles (curve 2) on Si (111) substrates in different spectral windows. A comparison of the spectra in Fig. 5.4 A

(curve 1 and 2) reveals the presence of three prominent features at 2850, 2920 and 3330 cm^{-1} in the bare ODA film (curve 1). The 3330 cm^{-1} band in the bare ODA film corresponds to N–H stretch vibration from ODA molecules which are significantly reduced in intensity of Pt-ODA complex.This significant reduction in intensity in the curve 2 may be due to binding of amine group in ODA with the surface of platinum nanoparticles. Similar effect in the N–H stretch vibration mode on formation of salts with anions such as $PtCl_6^{2-}$ has been observed in Langmuir–Blodgett films of ODA [28].

Interestingly in another important observation, the resonance peak at 1487 cm^{-1} (curve 1, Fig. 5.4 B) corresponding to the $–NH_2$ symmetric deformation band disappears after binding of the alkyl amine molecules with the platinum nanoparticles (curve 2, Fig. 5.4 B). Methylene scissoring band occurring at 1460 cm^{-1} (curves 1 and 2, Fig. 5.4 B) indicates that the hydrocarbon chain in the ODA monolayer surrounding the platinum particles are close-packed and in crystalline state [29]. The complete absence of N–H deformation vibration in ODA-capped nanoparticles at 1487 cm^{-1} and reduction in the relative intensity at 3330 cm^{-1} clearly indicates that the amine groups are interacting with platinum nanoparticles.

5.5 X-ray photoelectron spectroscopy studies

A solution-cast film of ODA-capped platinum nanoparticles formed on a Si (111) substrate was analyzed by XPS. The general scan spectrum of the film at room temperature showed the presence of C 1s, N 1s and Pt 4f core levels with no evidence of impurities. The film was sufficiently thick and therefore, no signal was measured from the substrate (Si 2p core level). Fig. 5.5 A shows the Pt 4f core level spectrum recorded from the Pt-ODA film formed by drop casting. The spectra have been background corrected using the Shirley algorithm [30] prior to curve resolution. The core levels were aligned with respect to the adventitious C 1s BE of 285 eV. The Pt 4f spectrum could be resolved into two spin-orbit pairs (splitting ~3.33 eV, identified in

Fig. 5.5 A) with the two chemically shifted components having $4f_{7/2}$ binding energies (BEs) of 71.4 and 74.0 eV respectively.

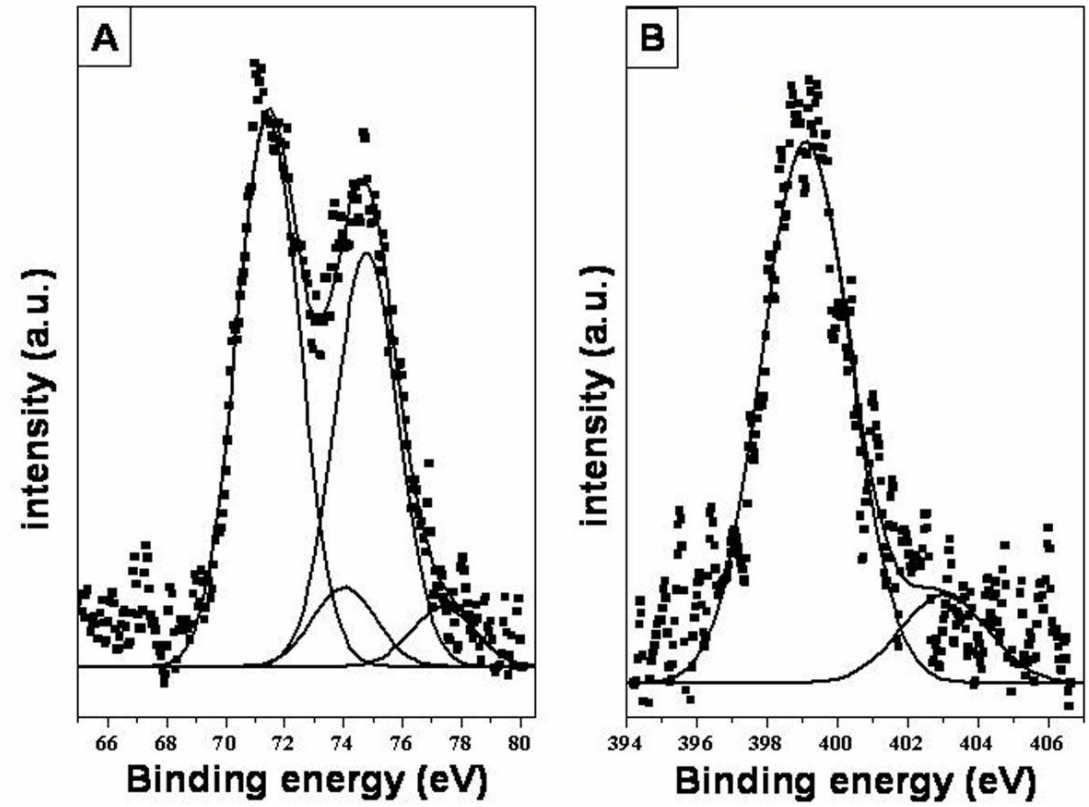

Figure 5.5: *Pt 4f (A) and N 1s (B) core level spectrum recorded from an ODA-stabilised platinum nanoparticles drop coated film on a Si (111) substrate. The resolved components are shown as solid lines in the figure.*

The low BE component may be assigned to electron emission from Pt(0) while the high BE component is assigned to Pt(II) [31]. The low BE component (BE = 71.4 eV) arises due to the metal core. The surface of the Pt nanoparticles appears to be different and is composed of a shell of Pt(II) ions. It is possible that partially reduced Pt ions ($PtCl_4^{2-}$) cap the surface of the metal core and interacts with amine group during phase transfer process. The N 1s spectrum recorded from the ODA-capped Pt nanoparticles showed the presence of two chemically distinct peaks centered at 399.1 eV and 403. 0 eV. The Peak at 399.1 eV may be assigned to HN_2/NH_3^+ groups, in which NH_3^+ group may be forming electrostatic bond with $PtCl_4^{2-}$ present on the surface of nanoparticles. The peak at 403.0 may be due to redistribution of charge on N

1s orbital electrons after donation of loan pair of electrons Pt (II) ions. The interaction of amine molecules with platinum is fairly well studied. Venand and coworkers have shown through NMR studies of platinum complexes such as *cis*-[$PtC1_2$ A_2], *trans*-[$PtCl_2$ A_2], *cis*-[$PtBr_2$ A_2], *trans*-[$PtBr_2$ A_2], *cis*-[$PtCl_4$ A_2], *cis*-[$PtBr_4$ A_2], [$PtBrA_3$]Br, [PtA_4]Br_2 where A = *n* dodecylamine [32] and the coupling constant (*J*) ^{195}Pt- ^{15}N is proportional to the *s* character involve in the bonding orbital. In another report, Romeo et al. have performed kinetic studies of the nucleophilic substitution of 5-aminoquinoline (5-Aq) and diethyl sulphide from the complexes *cis*-[$PtPh_2$(CO)(L)] (L = 5-Aq and SEt_2) by an extended series of aliphatic amines of comparable basicity (pK, = 10.6 ± 0.4) and of different steric hindrance [33]. These reports indicate the strong affinity of amine molecules for Pt (II) / Pt (IV). The above discussion indicates two modes of binding of the amine functionality with platinum nanoparticles. Electrostatic complexation is due to protonated amine group of ODA with $PtCl_4^{2-}$ ions while co-ordinate complexation appears to be due to unprotonated amine groups with Pt (II) / Pt (IV) ions present on the surface of platinum nanoparticles.

5.6 Catalytic activity studies

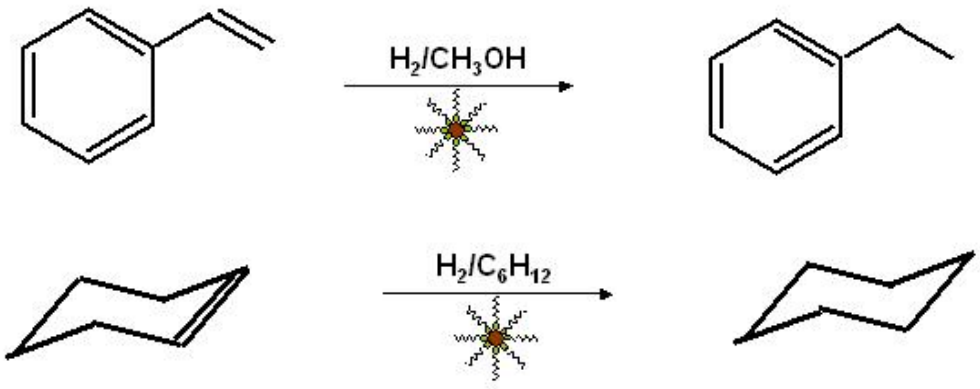

Figure 5.6: *Scheme showing hydrogenation of styrene to ethyl benzene (top) and cyclohexen to cyclohexane (bottom) where platinum nanoparticle acted as catalyst.*

Since platinum is known for its high catalytic activity, the catalytic activity of the hydrophobized platinum nanoparticles has been shown in simple hydrogenation reactions involving the conversion of styrene to ethyl benzene and cyclohexene to

cyclohexane (Fig. 5.6). These reactions were studied in a 100 mL reactor (supplied by Parr Instruments Company, USA). Analyses of the initial and final samples were done using gas chromatography (Varian 3400; CP-SIL 8CB Column; with a 30 m long and 0.53 mm inner diameter) with the experimental conditions: initial column temp. 80°C: 80–180°C at the rate of 3°C per min: 180–240°C at the rate of 10°C per min.

Reduction of styrene (10 mmol) to ethyl benzene and cyclohexene (10 mmol) to cyclohexane was carried out in methanol and hexane respectively. The GC analysis showed 87% conversion of styrene to ethyl benzene with 100% selectivity (TOF 19,683 h^{-1}).The platinum nanoparticle catalyst also worked excellently in the hydrogenation of a non-aromatic substrate such as cyclohexene giving 91% conversion from to cyclohexane with 98.8% selectivity (TOF 20,588 h^{-1}). Both the reactions were conducted at 200 psig hydrogen pressure for 2 h at 100°C.

5.7 Transmission electron microscopy studies

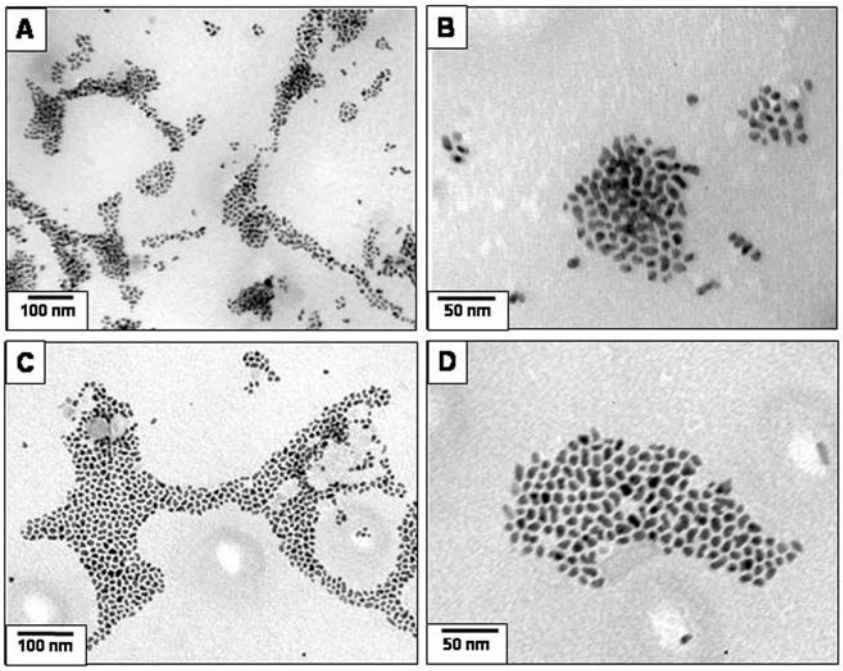

Figure 5.7: *TEM images of ODA-capped platinum nanoparticle films formed on carbon-coated grids by drop casting from the organic phase before (A and B) and after hydrogenation reaction (C and D).*

To understand the change in the particle size before and after reaction, TEM images (Fig. 5.7) of phase transferred platinum nanoparticles were taken in hexane before (A and B) and after the hydrogenation reaction of styrene to ethyl benzene (C and D).It is clear from the TEM images that the grid is uniformly covered with extremely large domains of platinum nanoparticles. The high magnification image revealed the close packing of the platinum nanoparticles (Fig. 5.7 B). While some degree of sintering of the particles is observed, the 2-D assembly are, to a large extent, well separated from one another. Comparison of the TEM images recorded from the ODA-capped Pt nanoparticles before (Fig. 5.7 A and B) and after hydrogenation reactions (Fig. 5.7 C and D) shows that nanoparticles are a little polydisperse before reaction while after reaction the polydispersity of nanoparticles decreases. This may be due to high pressure and temperature conditions applied during catalytic reactions resulting in a decrease in polydispersity, analogous to the digestive ripening process [34]. In spite of this, no detectable change in the average particle size after reaction was observed indicating the fact that the ODA monolayer surrounding the nanoparticles is intact.

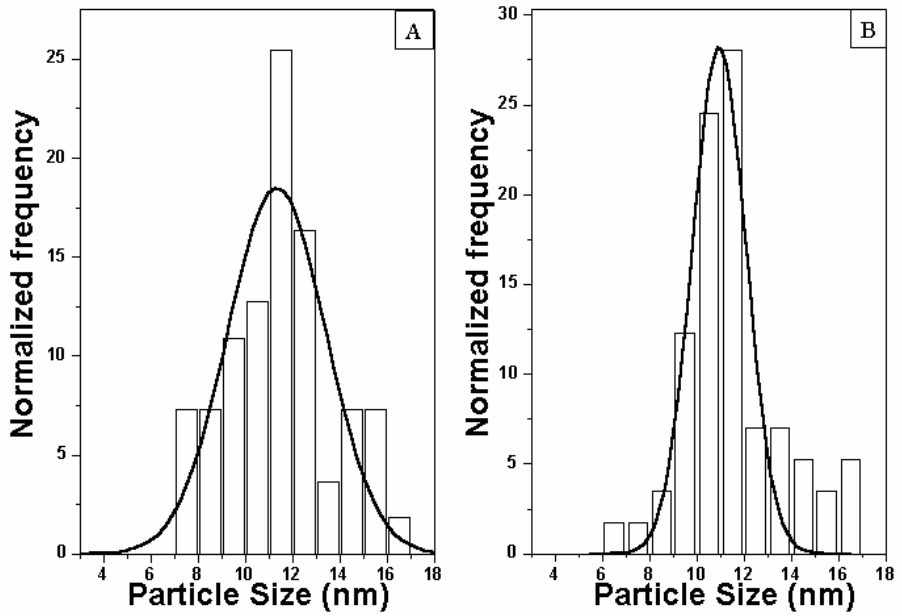

Figure 5.8: *Particle size distribution histogram of platinum nanoparticles (A) Before and (B) After hydrogenation reaction*

Fig. 5.8 A shows the histogram of the particle size distribution measured from different regions of TEM grid. Fig. 5.8 A and B shows Gaussian fit to the histogram of platinum nanoparticles before and after hydrogenation reaction respectively. Nature of Gaussian curve (FWHM) suggests the decrease in the polydispersity of nanoparticles after hydrogenation reaction, which matches the visual observation TEM micrographs. Narayan et al. reported similar observation in which change in the particle size was observed during catalytic reactions [32].

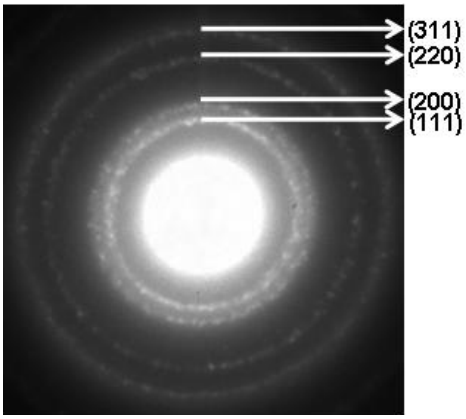

Figure 5.9: *Electron diffraction pattern of platinum nanoparticles*

Fig. 5.9 shows the electron diffraction pattern measured from the platinum nanoparticles of Fig. 5.7 B. It is clear from the electron diffraction pattern that the nanoparticles are crystalline; the diffraction rings could be indexed on the basis of the *fcc* structure of platinum.

5.8 Conclusion

The phase transfer of aqueous platinum nanoparticles into hexane using ODA molecules has been demonstrated. The amine groups of ODA molecules appear to interact with platinum nanoparticles in two ways. 1. Complex co-ordinate bond formation when the amine group is unprotonated, and 2. weak electrostatic bond formation when the amine group is protonated. The fatty amine-capped platinum particles are extremely stable, could be easily precipitated out of solution and

redissolved in different organic solvents. The hydrophobized Pt nanoparticles are highly stable and catalyze the hydrogenation of styrene to ethyl benzene and cyclohexene to cyclohexane with almost 98% selectivity. There was a slight change in the size of the nanoparticles during hydrogenation reaction.

References

[1] Henglein, A. "Radiolytic preparation of ultrafine colloidal gold particles in aqueous solution: optical spectrum, controlled growth, and some chemical reactions" *Langmuir,* **1999**, *15*, 6738.

[2] Gachard, E.; Remita, H.; Khatouri, J.; Keita, B.; Nadjo, L.; Belloni, J. "Radiation-induced and chemical formation of gold clusters" *New J. Chem.,* **1998,** *22*, 1257.

[3] Mizukoshi, Y.; Fujimoto, T.; Nagata, Y.; Oshima, R.; Maeda, Y. "Characterization and catalytic activity of core-shell structured gold/palladium bimetallic nanoparticles synthesized by the sonochemical Method" *J. Phys. Chem. B,* **2000,** *104*, 6028.

[4] Turkevich, J.; Garton, G.; Stevenson, P. C. "The color of colloidal gold" *J. Colloid Sci.,* **1954**, *9*, 26.

[5] Duff, D. G.; Baiker, A.; Edwards, P. P. "A new hydrosol of gold clusters. 1. formation and particle size variation" *Langmuir,* **1993**, *9*, 2301.

[6] Cliffel, D. E.; Zamborini, F. P.; Gross, S. M.; Murray, R. W. "Mercaptoamm-oniummonolayer-protected, water-soluble gold, silver, and palladium clusters" *Langmuir,* **2000**, *16*, 9699.

[7] Shon, Y. S.; Wuelfling, W. P.; Murray, R. W. "Water-soluble, sulfonic acid-functionalized, monolayer-protected nanoparticles and an ionically conductive molten salt containing them" *Langmuir,* **2001**, *17*, 1255.

[8] Elghanian, R.; Storhoff, J. J.; Mucic, R. C.; Letsinger, R. L.; Mirkin, C. A. "Selective colorimetric detection of polynucleotides based on the distance-dependent optical properties of gold nanoparticles" *Science,* **1997**, *277*, 1078.

[9] Brust, M.; Walker, M.; Bethell, D.; Schiffrin, D. J.; Whyman, R. "Synthesis of thiol derivatised gold nanoparticles in a two phase liquid/liquid system" *J. Chem. Soc.*, *Chem. Commun.,* **1994**, 801.

[10] Leaf, D. V.; Ohara, P. C.; Heath, J. R.; Gelbart, W. M. "Thermodynamic control of gold nanocrystal size: experiment and theory" *J. Phy. Chem.*, **1995**, *99*, 7036.

[11] Whetten, R. L.; Khoury, J. T.; Alvarez, M. M.; Murthy, S.; Vezmar, I.; Wang, Z. L. Stephens, P. W.; Cleveland, C. L.; Luedtke, W. D.; Landman, U. "Nanocrystal gold molecules" *Adv. Mater.,* **1996**, *8*, 428.

[12] Johnson, S. R.; Evans, S. D.; Mahan, S. W.; Ulman, A. "Alkanethiol molecules containing an aromatic moiety self-assembled onto gold clusters" *Langmuir*, **1997**, *13*, 51.

[13] Mayya, K. S.; Patil, V.; Sastry, M. "On the stability of carboxylic acid derivatized gold colloidal particles: the role of colloidal solution pH studied by optical absorption spectroscopy" *Langmuir*, **1997**, *13*, 3944.

[14] Porter, L. A., Jr.; Ji, D.; Westcott, S. L.; Graupe, M.; Czernuszewicz, R. S.; Halas, N. J.; Lee, T. R. "Gold and silver nanoparticles functionalized by the adsorption of dialkyl disulfides" *Langmuir,* **1998**, *14*, 7378.

[15] Liu, J.; Xu, R.; Kaifer, A. E. "In Situ modification of the surface of gold colloidal particles. preparation of cyclodextrin-based rotaxanes supported on gold nanospheres" *Langmuir,* **1998**, *14*, 7337.

[16] Liu, J.; Mendoza, S.; Roman, E.; Lynn, M. J.; Xu, R.; Kaifer, A. E. "Cyclodextrin-modified gold nanospheres. host-guest interactions at work to control colloidal properties" *J. Am. Chem. Soc.,* **1999**, *121*, 4304.

[17] Underwood, S.; Mulvaney, P. "Effect of the solution refractive index on the color of gold colloids" *Langmuir,* **1994**, *10*, 3427.

[18] Liz-Marzan, L. M.; Lado-Tourino, I. "Reduction and Stabilization of Silver Nanoparticles in Ethanol by Nonionic Surfactants" *Langmuir* **1996**, *12*, 3585.

[19] Lala, N.; Lalbegi, S. P.; Adyanthaya, S. D.; Sastry, M. "Phase Transfer of Aqueous Gold Colloidal Particles Capped with Inclusion Complexes of Cyclodextrin and Alkanethiol Molecules into Chloroform" *Langmuir,* **2001,** *17*, 3766.

[20] Sarathy, K. V.; Kulkarni, G. U.; Rao, C. N. R. "A novel method of preparing thiol-derivatised nanoparticles of gold, platinum and silver forming superstructures" *Chem. Commun.,* **1997**, 537.

[21] Sarathy, K. V.; Raina, G.; Yadav, R. T.; Kulkarni, G. U.; Rao, C. N. R. "Thiol-derivatized nanocrystalline arrays of Gold, Silver, and Platinum" *J. Phys. Chem.,* B **1997**, *101*, 9876.

[22] Wang, W.; Efrima, S.; Regev, O. "Directing oleate stabilized nanosized silver colloids into organic phases" *Langmuir,* **1998**, *14*, 602.

[23] Dunleavy, J. "Sulfur as a catalyst poison" *Platinum Metals Rev.*,**2006,** *50*,110.

[24] Leff, D. V.; Brandt, L.; Heath, J. R. "Synthesis and characterization of hydrophobic, organically-soluble gold nanocrystals functionalized with primary amines" *Langmuir,* **1996,** *12*, 4723.

[25] Brown, L. O.; Hutchison, J. E. "Controlled growth of gold nanoparticles during ligand exchange" *J. Am. Chem.Soc.,* **1999**, *121*, 882.

[26] Sastry, M.; Kumar, A.; Mukherjee, P. "Phase transfer of aqueous colloidal gold particles into organic solutions containing fatty amine molecules" *Coll. Surf. A.,* **2001,** *181*, 255.

[27] Kumar, A.; Mandale, A. B.; Sastry, M. "Phase transfer of aqueous CdS nanoparticles by co-ordination with octadecanethiol molecules present in nonpolar organic solvents" *Langmuir,* **2000**, *16*, 9299.

[28] Bardosava, M.; Tredgold, R. H.; Ali-Adib, Z. "Langmuir-Blodgett films of docosylamine" *Langmuir,* **1995**, *11*, 1273.

[29] Hostetler, M. J.; Stokes, J. J.; Murray, R. W. "Infrared spectroscopy of three-dimensional self-assembled monolayers: *N*-alkanethiolate monolayers on gold cluster compounds" *Langmuir,* **1996,** *12*, 3604.

[30] Shirley, D. A. "High-Rersolution X-Ray photoemission spectrum of the valence bands of gold" *Phys. Rev. B,* **1972**, *5*, 4709.

[31] Walter, J.; Nishioka, M.; Hara, S. "Ultrathin platinum nanoparticles encapsulated in a graphite lattice-prepared by a sonochemical approach" *Chem. Mater.*, **2001**, *13***,** 1828.

[32] Pregosin, P. S.; Omura, H.; Venand, L. M. " Use of 1[J^{195}Pt-^{15}N] as a probe into the electronic structure of some platinum(II)-amine complexes**"** *J. Am. Chem. Soc.*, **1973,** *95***,** 2047.

[33] Romeo, R.; Arena, G.; Scolaro, L. M.; Plutino, M. R.; Bruno, G.; Nicol, F. **"**Reactivity of aliphatic amines toward platinum(II) complexes" *Inorg. Chem.*, **1994,** *33***,** 4029.

[34] Lin, X. M.; Jaeger, H. M.; Sorensen, C. M.; Klabunde, K. J. "Formation of long-range-ordered nanocrystal superlattices on silicon nitride substrates**"** *J. Phys. Chem. B.,* **2001**, *105*, 3353.

CHAPTER VI

Conclusions

The important conclusions of the work detailed in the thesis and possible scope for future work are briefly discussed.

6.1 Summary of the work

In this thesis, an attempt has been made to understand the mode of binding of amino acids with gold nanoparticles. Surface functionalization of nanoparticles and its applications in drug delivery and catalysis have been demonstrated.

The study of the binding of lysine and aspartic acid indicates that the amino acid may be binding to the gold particles in one of the two modes. Amino acids form strong bonds with gold nanoparticles involving lone pair of nitrogen while they form electrostatic bond with gold nanoparticles when an amine group is protonated. An ITC study of aspartic acid with gold nanoparticles shows that the entropies of binding are large and positive and contributes a significant component of the binding free energy. Gold nanoparticles could also serve as excellent carrier for insulin delivery. Surface modification of nanoparticles promotes the insulin release from the nanoparticle surface. It can be delivered in different routes. The dose changes with different delivery routes. Insulin absorption via the nasal route is more promising than the oral route with respect to dose requirement, time required for blood glucose reduction and percentage blood glucose reduction.

The phase transfer of aqueous platinum nanoparticles into hexane using ODA molecules has been shown. The amine groups of ODA molecules interact with platinum nanoparticles in a similar way as that of amino acid with gold nanoparticles i.e. 1) complex co-ordinate bond formation when amine group is unprotonated, 2) weak electrostatic bond formation when amine group is protonated. The hydrophobized Pt nanoparticles in organic medium are highly stable and catalytically active. There is little difference in average particles size distribution before and after hydrogenation reaction. Hydrophobized nanoparticles can catalyze simple hydrogenation reactions with almost 98% selectivity.

6.2 Scope of the future work

In this thesis, we have seen that ITC is capable of determining heat changes occurring during biochemical reactions present in sample cell. It is also used to

understand the interaction of amino acid with gold nanoparticles. Interaction of proteins with gold nanoparticles will be different than just amino acid because of various nonspecific interactions of various functional moieties present on the proteins. Due to these interactions, proteins may change their structural features or configuration, when adsorbed on the surface of nanoparticles leading to a change in the biological activities. ITC can be effectively used to understand the changes in various thermodynamic parameters of proteins during the titration with its antibodies or substrates. This information can be utilized to understand drug action of these bioconjugates in in-vivo studies.

In this thesis, gold nanoparticles have been used for transmucosal delivery of insulin. In similar way, gold nanoparticles can be used as carrier for other hormones as well as drug molecules. Since these nanoparticles are of extremely small size, they can be used as carriers for different routes of drug administration for example ocular and transdermal delivery. In chronic diseases where regular uptake of drug formulations are necessary, the toxicity, immunological response and deposition of inorganic nanoparticles in various internal organs such as kidneys, liver etc. can be checked to determine the effect of these new classes of carriers on body. Surface modification of carrier nanoparticles is a very important aspect in drug delivery applications. Many other capping or surface modifying agents such as naturally occurring polymers can be used which will enhance the carrier properties of nanoparticles such as protection against hydrolyzing enzymes, controlled release of drug etc. It will also help in site specific drug administration.

In the case of catalytic application of nanoparticles, different chiral molecules can be used as capping agent which may be used for asymmetric synthesis of organic compounds. Few amino acids are known for their pH dependent optical activity. Capping of these amino acids on the surface of nanoparticles can be used for catalysis, where pH of the solution can be used as a switch to control the reaction in aqueous medium. Similar protocols can be used for synthesis of other transition metal nanoparticles. Since these protocols are relatively easy, cheap and do not use any sulfur containing molecules, it can

preserve surface properties of the nanoparticles and therefore large scale production of these nanoparticles can be feasible for industrial applications.

List of Publications

1) Bhumkar, D. R.; Joshi, H. M.; Sastry, M.; Pokharkar, V.B. "Polymer coated gold nanoparticles as novel carriers for transmucosal delivery of insulin" (communicated)

2) Joshi, H. M.; Bhumkar, D. R.; Joshi, K.; Pokharakar V.; Sastry, M. *"*Gold nanoparticles as carriers for efficient transmucosal insulin delivery*"* *Langmuir*, **2006**, *22* , 300.

3) Kumar, A.; Joshi, H.M.; Mandale A.B.; Srivastava, R.; Adhyanthaya, S. Pasricha, R. Sastry, M., "Phase transfer of platinum nanoparticles from aqueous to organic solutions using fatty amine molecules*"*, *J. Chem. Sci.*,**2004,** *116,* 293. (Cover page appearance on Journal of Chemical Sciences)

4) Joshi, H.; Shirude, P.S.; Bansal, V.; Ganesh, K.N.; Sastry, M."Isothermal Titration Calorimetry Studies on the Binding of Amino Acids to Gold Nanoparticles*"*, *J. Phys. Chem.. B,* **2004,** *108*, 11535.

5) Shankar, S.S.; Joshi, H.; Pasricha, R.; Pavaskar, N.R.; Mandale A. B., Sastry, M. **"**A. low-temperature, soft chemistry method for the synthesis of zirconia nanoparticles in thermally evaporated fatty amine thin films **"** *J. Colloid. Interface Sci*., **2004,** *269*, 126.

6) Kumar, A.; Joshi, H.; Pasricha, R.; Mandale A. B.; Sastry, M. **"**Phase transfer of Silver nanoparticles from aqueous to organic solutions using fatty amine molecules**",** *J. Colloid. Interface Sci*. **2003,** *264*, 396.

Erratum